DISSERTATION

MICROMETEOROLOGICAL STUDIES OF A BEEF FEEDLOT, DAIRY, AND GRASSLAND: MEASUREMENTS OF AMMONIA, METHANE, AND ENERGY BALANCE CLOSURE

Submitted by

Kira Brianne Shonkwiler

Department of Atmospheric Science

In partial fulfillment of the requirements

For the Degree of Doctor of Philosophy

Colorado State University

Fort Collins, Colorado

Spring 2018

Doctoral Committee:

Advisor: Jeffrey L. Collett, Jr.

Jay M. Ham
Sonia Kreidenweis
Russ Schumacher
Shawn Archibeque

ABSTRACT

MICROMETEOROLOGICAL STUDIES OF A BEEF FEEDLOT, DAIRY AND GRASSLAND: MEASUREMENTS OF AMMONIA, METHANE, AND ENERGY BALANCE CLOSURE

Ammonia emissions from concentrated animal feeding operations (CAFOs; most of which are beef feedlots) near the Colorado Front Range are suspected to be a large regional input of reactive nitrogen which has been found to accumulate and cause deleterious effects in nearby downwind Class I areas like Rocky Mountain National Park. Methane (CH_4) is a strong greenhouse gas (GHG) emitted in large amounts from dairy anaerobic lagoons used for liquid manure management. Lagoon systems account for over half of the manure management-based CH_4 emissions from agriculture in the US. There is a strong need for more emissions measurements from CAFOs like feedlots and dairies. For these data to be trusted, well-developed techniques must be utilized at emissions measurement sites and such techniques should be validated in ideal scenarios. Three micrometeorological studies were performed involving measurement of emissions using micrometeorological methods in the surface layer. The first study involved estimating summertime NH_3 emissions from a 25,000-head beef feedlot in Northern Colorado. Two different NH_3 sensors were used: a cavity ring down spectroscopy analyzer collected data at a single point while a long-path FTIR collected data along a 226-m long transect, both deployed along the same fenceline. Concentration data from these systems were used with two inverse dispersion models (FIDES, an inverse solution to the advection dispersion equation; and WindTrax, a backward Lagrangian stochastic model). Point sensor concentrations of NH_3 were similar to line-integrated sensor concentrations suggesting some spatial uniformity in emissions. Emissions had a diurnal pattern (i.e., afternoon peak with minimum in early morning) that was driven by temperature. Emissions predicted by WindTrax were 25.2% higher than those from FIDES. Point vs. long-path measurements of NH_3 had

minimal effect on predicted emissions. The mean NH_3 emission factor (EF) was 80 ± 39 g NH_3 hd^{-1} d^{-1}, with 40.0% of dietary-N emitted as NH_3.

The second study involved using eddy covariance and WindTrax to quantify CH_4 emissions from a 3.9-ha anaerobic lagoon serving a 1400-head dairy in northern Colorado. Methane emissions followed a strong seasonal pattern correlated with temperature of the organic sludge layer on the bottom of the lagoon. Fluxes started increasing in late spring (May; ~10°C), increased rapidly in Jun (10-15°C) peaked in the summer (Jul/Aug; ~18-20°C) and remained high until mid-autumn (late Oct/early Nov; ~10°C). Fluxes then decreased and remained consistently low (up to 10 times less than peak emissions) until microbial activity ramped up again in May. The EC signal was very dependent on wind direction, with highest concentrations and fluxes associated with the direction of the lagoon. Gap-filled data showed a slight diurnal pattern to all seasons, with tenfold increases in diurnal values for summer over winter. Additionally, EFs for the lagoon varied by season with lows in the winter and highs in the summer with an annual mean of 819 ± 774 g CH_4 hd^{-1} d^{-1}. WindTrax overestimated EC for the lagoon (1163 ± 1049 g CH_4 hd^{-1} d^{-1} versus 819 ± 774 g CH_4 hd^{-1} d^{-1}), but this difference may be attributable to differences in the sampling footprint and stability conditions. IPCC Tier 2-calculated EFs were extremely close to EC-based measurements and WT-based estimates.

The third study involved using eddy covariance in an ideal environment (tallgrass prairie in Kansas) to test the reasons behind the “energy balance (EB) closure problem” at two landscape positions. This problem can cast uncertainty on flux measurements made by EC. One upland and one lowland EC tower each were used to measure EB components (i.e., net radiation, R_n; soil heat flux, G; total change in heat storage, ΔS; and sensible and latent heat fluxes, H and λE) during the summers of 2007 and 2008. To maximize closure, special attention was given to reduce all forms of instrumentation error and account for heat storage and photosynthesis between the soil and the reference height. Landscape position had little effect

on G, H, and R_n; differences were ≤ 2% between sites. Lowland λE was 8% higher than upland λE because of greater biomass and soil moisture. On average, EB closure (i.e., $\Sigma[\lambda E+H] / \Sigma[R_n–G–\Delta S]$) was 0.88 and 0.94 at the upland and lowland sites, respectively. Closure was not correlated with friction velocity or the stability of the surface boundary layer. Given high confidence in R_n, G, and ΔS, turbulent fluxes depend directly on vertical velocity (*w*), and the fact that a systematic underestimation of w was recently found in literature, lack of closure may have resulted largely from anemometer-based underestimates of *w*.

ACKNOWLEDGEMENTS

The author would like to acknowledge the contributions from the National Science Foundation Experimental Program to Stimulate Competitive Research, Kansas Ecoforecasting Grant # GOBO600350. Guidance was given by J. Ham and this work was additionally contributed to by F.W. Caldwell, J. Blair, N. Brunsell, and C. Nash. Research was performed on the Konza Prairie Biological Station, a Long-Term Ecological Research station operated by Kansas State University. Additionally, funding was provided by the National Robotics Initiative via USDA-NIFA Award 2012-67021-19978 and from the USDA Award 2016-67021-24456. The cooperation and assistance provided by the commercial feedlot and dairy used for these studies was greatly appreciated.

Personally, I would like to extend my thanks to my co-advisors, Dr. Jay Ham and Dr. Jeffrey Collett, Jr., for the astounding research opportunities and advice. I truly feel like my time in graduate school was an adventure. Additionally, I would like to acknowledge the encouragement and support I received from colleagues at K-State: Kristen Baum, Fred Caldwell, and Jamey Duesterhaus; as well as Colorado State: Arsineh Hecobian, Andrea Clements, and Christina Nash for all their expertise, help, and for being excellent role models. Finally, for the ceaseless belief in my abilities I am greatly indebted to my friends and family.

DEDICATION

This document is the result of a great deal of personal effort and occurred during a time in my life where I endured immense mental and spiritual strain and growth. The adventures, lessons, and challenges I experienced will forever be dear to me and entangled in the foundation of my future. For the person who shared the most in all my joys and struggles during the writing of this dissertation, I dedicate the work and contents within to my endlessly astounding yet extraordinarily humble husband and best friend, Bryan Shaw. Thank you cannot describe how you helped keep me motivated, healthy, and happier than I've ever known during my memorable years at CSU.

TABLE OF CONTENTS

LIST OF TABLES

LIST OF FIGURES

CHAPTER 1 – INTRODUCTION

1.1 Livestock emissions

Animal agriculture and animal waste handling accounts for significant emissions of pollutants; chief among concern are emissions of reactive nitrogen products (i.e., ammonia (NH_3) gas) and greenhouse gases (GHG) such as methane (CH_4) (FAO, 2006). Concentrated animal feeding operations (CAFOs) such as cattle feedlots are a logical place to study and model NH_3 emissions because of their strong areal emissions source (i.e., the cattle pens) and typical deployment in flat terrain (and thus simpler dispersion characteristics). Additionally, CAFOs and other concentrated animal agriculture account for up to 64% of all anthropogenic NH_3 emissions (FAO, 2006). Dairies offer a unique location to study GHG emissions like CH_4. The strongest source over which to measure and model CH_4 emissions at dairies is near anaerobic lagoons, major GHG sources at many dairy operations. Dairy cattle in the US are outnumbered by cattle in feedlots by 17.5% (USDA, 2017a, 2017b), yet their associated manure management accounts for over half the US budget for CH_4 (32.2 out of 61.2 million metric tons of CO_2-equivalent emissions from all livestock in 2016; USEPA, 2016).

1.1.1 Ammonia and methane

Near the Colorado Front Range, for example, CAFOs have been identified as a major regional atmospheric source of ammonia contributing to measurable nitrogen deposition and environmental changes at Class I areas downwind such as Rocky Mountain National Park (Baron et al., 2000; Beem et al., 2010; Benedict et al., 2013a, 2013b; Malm et al., 2013, 2016; Wolfe et al., 2001, 2003). Ammonia is also associated with reduced local visibility from enhanced particulate matter formation (Arogo et al., 2006; Heald et al., 2012; Li et al., 2017).

Methane is a major component of the worldwide GHG budget, accounting for up to 17% of radiative forcing from all globally-mixed GHGs (Allen, 2016) and is emitted as a result of cattle digestive processes (enteric fermentation) as well as manure management, especially anaerobic manure lagoons (USEPA, 2016). There is much uncertainty in CH_4 estimates from manure management at dairies, specifically (Owen and Silver, 2015).

1.1.2 Measurements

Micrometeorological techniques are often recommended as the best way to quantify emissions from strong areal sources such as CAFOs (NRC, 2003). Methods such as eddy covariance (EC) and inverse dispersion modeling (backward Lagrangian stochastic; bLs) allow continuous undisturbed sampling of emissions over large source areas commonly associated with animal feeding operations (e.g., Flesch and Wilson, 2005; Shonkwiler and Ham, 2017). In livestock emissions research, the majority of emissions results are from dispersion modeling, with only some direct measurements like EC (Felber et al., 2015; Sun et al., 2015; Taylor et al., 2017). These inverse modeling efforts, with proper parameterization and groundwork, have much potential for practical applications such as real-time fenceline monitoring (Shonkwiler and Ham, 2017) and deposition measurements (Shen et al., 2016) or forecasting. Yet, even the most scientifically-viable results from direct measurement can be questioned.

One reason to question direct measurements is data quality and completeness. Micrometeorological datasets must undergo significant careful post-processing and quality control procedures including data correction, data filtering for non-ideal measurement conditions and/or wind directions (depending on measurement setup), and gap-filling for excluded or filtered data (to achieve final cumulative emissions for overall total emissions estimates). Ultimately, more field measurements are needed to achieve better confidence (reduce uncertainty) in the results, to quantify emissions at larger spatial and temporal scales, to develop and test process models of emissions, and for creation of science-based policy.

1.2 Energy Balance Closure

Eddy covariance is considered the most direct method for making measurements of surface-atmosphere exchange in the surface boundary layer (Baldocchi et al., 1988). However, the technique has issues resolving measurements of incoming and outgoing energy (deemed the "energy balance closure problem") (Foken et al., 2006; Foken, 2008), often considered a scale problem and an issue which can cast doubt on EC measurements. Closure of the energy balance, assuming the law of conservation of energy, means that turbulent fluxes or outgoing energy (measured by EC) of latent heat (λE) and sensible heat (H) fluxes are equal to the incoming energy component of net radiation (R_n) and storage within the soil (G), or (R_n – G) = (H + λE). Unfortunately with EC, (H + λE) ~ 0.8-0.9 (R_n – G). With up to a 20% closure deficit found at EC stations at most FLUXNET sites in North America (Wilson et al., 2002), the closure issue with EC can have significant implications on final ecosystem emissions of species such as CO_2, H_2O and CH_4. This issue has been studied extensively in attempts to resolve it (Aubinet et al., 2000; Barr et al., 2006; Eder et al., 2014; Foken and Wichura, 1996; Foken et al., 2006; Foken, 2008; Franssen et al., 2010; Gao et al., 2017; Goulden et al., 1996; Guo et al., 2009; Ham and Heilman, 2003; Hammerle et al., 2007; Heusinkveld et al., 2004; Hunt et al., 2002; Kanda et al., 2004; Kohsiek et al., 2007; Laubach and Teichmann, 1999; Massman and Lee, 2002; Masseroni et al., 2014; Mauder et al., 2007a, 2007b; McGloin et al., 2018; Moderow et al., 2009; Oncley et al., 2007; Soltani et al., 2017; Stoy et al., 2013; Wilson et al., 2002; Wohlfahrt et al., 2009). There are three general reasons why closure is not achieved by EC (Foken et al., 2006): (1) measurement and/or errors from post-processing, (2) errors from turbulent fluxes (i.e., H and λE) sampling different scales or regions than R_n and G measurements, and (3) errors as a result of low-frequency, larger-scale fluxes or advection from surface heterogeneity. Recent findings regarding errors in measurement of the vertical velocity component may change discussion of the closure problem to sensor performance (Frank et al., 2013; Kochendorfer et al., 2012). Careful analysis of the closure problem in ideal terrain can help lend further credence to EC-based field applications for all agriculture systems (i.e., crops and livestock like CAFOs), possibly helping to elucidate more information about the nature of the problem.

1.3 Objectives

The research presented in this dissertation includes three studies (described in three independent, manuscript-style chapters), all of which involve measurement of emissions using micrometeorological methods in the surface layer. The studies include: ammonia emissions from a beef feedlot in Colorado, methane emissions from an anaerobic dairy lagoon in Colorado, and energy balance closure when using eddy covariance over a pristine grassland in Kansas. Specific objectives for each chapter are:

Chapter 2) Measure NH_3 emissions from a commercial beef feedlot in Colorado:

1. compare fenceline emissions results from two inverse models (backward Lagrangian stochastic (bLs) model and analytical inverse model);
2. compare fenceline concentration data and emissions estimates from a line-integrated versus point NH_3 sensors; and
3. quantify NH_3 emission factors from a representative Colorado feedlot and compare to literature.

Chapter 3) Measure CH_4 emissions from an anaerobic manure lagoon on a dairy operation in Colorado:

1. make long-term measurements of CH_4 emissions from a large, anaerobic dairy lagoon using eddy covariance (~20 months);
2. compare estimates of emissions from a common bLs model to emissions from eddy covariance; and
3. determine CH_4 emission factors for a large dairy lagoon in Colorado and compare to literature.

Chapter 4) Evaluate energy balance closure for two eddy covariance towers deployed on upland and lowland locations in a native tallgrass prairie in Kansas.

1.4 Hypotheses

Emissions of feedlot NH_3 from the analytic inverse model will likely be smaller than those from the bLs model due to an existing agricultural study (Carozzi et al., 2013) demonstrating similar deviation between the same two models during instability (atmospheric conditions that comprised much of the time during which peak feedlot emissions occurred). From their results, mean model emissions estimates should differ up to 32%; attributable to each model's uncertainty and, moreso, to each model's different scalar diffusivity. Though models likely differ, concentrations between sensors should be similar, especially for sufficient turbulent mixing (i.e., daytime or windy conditions) and wind directions corresponding to the mean feedlot (or pasture) area. It is also anticipated that data from the more area-representative line-integrated sensor should have less variability (i.e., lower peaks) than the point sensor which has faster data retention and samples a smaller overall portion of the feedlot pens. The author also expects, from her own experiences with each, that line-integrated data will have lower retention than the point sensor due to particle obstruction present from frequent blowing dust caused by continuous feed truck traffic on perimeter feedlot roads and the point sensor's faster and more consistent sampling frequency. Summertime NH_3 EFs from this feedlot will be lower than Texas EFs due to lower regional winds and temperatures.

Methane emissions from the anaerobic manure dairy lagoon will be strongly seasonal. Specifically, most CH_4 emissions (>>50%) will occur when the lagoon sludge layer is >10-15°C (DeSutter and Ham, 2005). Additionally, lagoon emissions should have a diurnal pattern with a midafternoon peak due to surface heating and/or higher daytime winds. Seasonal emissions will have high variability (from other manure lagoon studies). When comparing EC and WT, few comparison studies exist from which to base a hypothesis, but logically, EC has been shown to have a closer sampling footprint (i.e., closer to the measurement) than the projected footprint of

WT. For times when the wind direction is favorable from the lagoon, this would likely result in the EC station sampling the lagoon closer to the south edge than the lagoon's center, which may be more appropriate to the slightly longer WT footprint. The intensive long-term study by DeSutter and Ham (2005) at a rectangular swine lagoon in nearby Kansas showed on a yearly basis that emissions from the lagoon center were 182% higher than emissions from the edges (i.e., the area where the lagoon is sloping downward to its maximum depth).

The outgoing (and continually underestimated) components of the surface energy balance are H and λE, and other EC studies show that areas with higher λE tend to have higher closure. In this scenario, the lowland site should have higher λE, and thus, higher closure than the upland site. Additionally, it is predicted that despite the intensive deployment methodology and subsequent data analysis employed in this study, that there will still exist a lack of closure. This is because: 1) there is overwhelming global evidence showing a lack of closure of 10-20% regardless of ecosystem, continent, season, or individual year; and 2) recent research has shown the majority of studies reporting lack of closure utilized an instrument which has been shown to induce a -10% bias in the vertical wind speed (which would, mathematically, propagate to a similar-sized error in the fluxes of H, λE, and any other scalar).

CHAPTER 2 – AMMONIA EMISSIONS FROM A BEEF FEEDLOT: COMPARISON OF INVERSE MODELING TECHNIQUES USING LONG-PATH AND POINT MEASUREMENTS OF FENCELINE NH_3[1]

2.1 Introduction

Animal agriculture is the largest global source of atmospheric ammonia (NH_3), comprising 50-64% of all anthropogenic emissions (FAO, 2006; NRC, 2003). Concentrated animal feeding operations (CAFOs) such as beef feedlots are considered NH_3 “hot spots” due to continual excretion of urea nitrogen (N) in waste within confined areas (e.g., cattle pens). Once airborne, volatilized NH_3 can travel downwind and have environmental impacts through N deposition at tens to hundreds of kilometers from the feedlot. Ecological consequences of NH_3 include eutrophication, biodiversity changes, and influences on water chemistry and the soil microbiome (Galloway et al., 2004; Vitousek et al., 1997), while also contributing to increased regional haze (Bauer et al., 2016; Behara et al., 2013).

Ammonia also enhances formation of particulate matter (Arogo et al., 2006), whereby NH_3 gas converts to ammonium (NH_4^+) aerosols that scatter light and have longer atmospheric lifetimes, making long-distance transport/deposition possible (Aneja et al., 2008). Additionally, NH_3 has an indirect effect on climate change after deposition, being a precursor to formation of strong greenhouse gases such as nitrous oxide and odd oxides of N (NO_x) (Erisman et al., 2011).

The implications of such issues are important for the northern part of Colorado’s *Front Range*; a heavily urbanized region coinciding with intensive crop, livestock, and industrial activities directly adjacent to sensitive mountain ecosystems. Year-round, regional upslope wind

[1] Shonkwiler KB, Ham JM. 2017. Ammonia emissions from a beef feedlot: Comparison of inverse modeling techniques using long-path and point measurements of fenceline NH_3. Agric. Forest Meteor. (in press), doi: 10.1016/j.agrformet.2017.10.031.

events can transport pollutants from this mixed-use corridor westward to sensitive alpine biomes along the eastern flank of the scenic Rocky Mountains where deposition of NO_x- and NH_3-containing compounds have been shown to have measurable effects on the ecosystem (Baron et al, 2000; Bowman et al., 2012; Burns, 2004; Lieb et al., 2011; Wolfe et al., 2001; Wolfe et al., 2003). A land use map of the Northern Front Range is shown in Fig. 2.1 which identifies Rocky Mountain National Park (RMNP) in addition to nearby CAFOs. There are over 500,000 head of cattle within 8 counties east of RMNP in 2014 (~150 km radius), with cattle in beef feedlots accounting for about 75% of the total (CDPHE, 2014). July wind roses in Fig. 2.1 for Greeley and Fort Morgan show that easterly (i.e., upslope) summertime winds are common. It follows that NH_3 emissions from CAFOs have been implicated as a significant source of N impacting the park (Malm et al., 2013).

While livestock emissions on the eastern plains are significant, determining source apportionments (i.e., finding the origin of deposited N) for RMNP is very complex and fraught with uncertainty (Gebhart et al., 2011; Malm et al., 2013; Rodriguez et al., 2011; Thompson et al., 2015). Apportionments are determined via atmospheric modeling, of which a major input parameter are CAFO NH_3 emissions (to constrain simulations). Unfortunately, most in-situ NH_3 emissions studies to date are from CAFO-heavy areas other than Colorado (such as Canada, Australia, and especially the Texas Panhandle, USA). Considering regional differences (climate, population, and proximity to RMNP) between the Texas Panhandle and Northern Front Range, more measurements of NH_3 fluxes from representative Colorado feedlots would improve the NH_3 inventory for the state and reduce uncertainty when modeling nitrogen transport to and deposition in RMNP.

Emissions factors (EFs) for NH_3 are usually determined from field studies and used to summarize how different management and operations influence overall NH_3 emissions on a per head (i.e., per animal) basis. These numbers are needed for model input, for comparison between operation types and management practices, and to assess the cumulative effect of thousands of animals at each hotspot. Many studies calculated beef EFs for summertime data, but seasonal data show NH_3 EFs are significantly lower during winter, with much interannual and regional variability (Faulkner and Shaw, 2008; Hristov et al., 2011; Todd et al., 2008).

Some of the first EFs used for livestock were developed in The Netherlands (Battye et al., 1994), with recent estimates for European beef cattle of 36 g hd^{-1} d^{-1} (Paulot et al., 2014). Currently, the literature contains many EFs for beef feedlots on several continents. Australian EFs range from 24-69 g hd^{-1} d^{-1} in the winter to >250 g hd^{-1} d^{-1} in the summer (Denmead et al., 2008 and Loh et al., 2008, respectively) while seasonal EFs for two feedlots in China ranged from 35 (winter) to 66 g hd^{-1} d^{-1} (summer) (Yang et al., 2016). North American studies include Canadian work where EFs neared 140 g hd^{-1} d^{-1} in the summer at a typical feedlot (McGinn et al., 2007) to as high as 318 g hd^{-1} d^{-1} for an operation where cattle were fed diets with unusually high crude protein (CP; related to N content in feed) (van Haarlem et al., 2008). Data from the USA are mostly from the Southern Great Plains region (i.e., Texas Panhandle) where studies of large feedlots show EFs from 94 ± 56 g hd^{-1} d^{-1} in the winter to 127 ± 45 g hd^{-1} d^{-1} in the summer (Baek et al., 2006; Cole et al., 2006; Flesch et al., 2007; Rhoades et al., 2010; Todd et al., 2005; Todd et al., 2008; Todd et al., 2011). Beef feedlots in Colorado are similar in operation to those studied in the Texas Panhandle. However, differences in climate, namely lower temperatures and wind speeds in Colorado, would likely result in lower NH_3 EFs compared to Texas.

Colorado's Front Range is a region where winds demonstrate high temporal and spatial variability due to mountain influences (e.g., Bossert and Cotton, 1994); a fact that makes understanding how NH_3 is transported to RMNP more challenging. Fully understanding how feedlot NH_3 emissions are impacting RMNP will likely require long-term monitoring programs at multiple CAFOs along the Front Range Corridor to provide some estimate of temporal and feedlot-to-feedlot variability. Historically, the most common measurement technique at large beef feedlots in the US and Canada has been collecting NH_3 concentrations with long-path (LP) tunable diode lasers. The line-integrated measurements of LP sensors can cover a large spatial area and work well with inverse models (i.e., provide emissions representative of a larger area; Flesch and Wilson, 2005), but are often high-maintenance due to shifts in misalignment of the sensor with its reflector array and from interference by precipitation or dust. Newer LP models have fewer issues but are still susceptible to dust and precipitation (Berkhout et al., 2017; Sintermann et al., 2016). Another option is using point concentration NH_3 sensors (e.g., Cavity Ring Down Spectroscopy (CRDS) analyzers), but these can be complicated to deploy and there is some concern over lack of spatial resolution causing further uncertainty in inverse dispersion model results. Furthermore, these closed-path instruments require pumps, heated tubes and filtration; problems that are avoided when using LP sensors. No studies have compared output from these two different analyzers when co-deployed at the same CAFO to determine if point sampling is sufficient to replace line-integrated measurements.

Regardless of the method to measure NH_3 concentrations at feedlots, inverse dispersion models must be utilized to find final emissions. Dispersion modeling combines fluid mechanics with Monin-Obukhov Stability Theory (MOST) to determine plume diffusion based on environmental conditions. Inverse-dispersion analyses use time series of downwind wind and concentration data to infer the magnitude of upwind emissions. That is, given the location and area of the NH_3 source and the distance to receptor (i.e., the measurement), what flux rates would be required at the source to match observed downwind concentrations (Harper, 2005).

In the literature, most NH_3 emissions are estimated from a backward Lagrangian stochastic (bLs) software package called WindTrax (WT) which has been used with much success (Carozzi et al., 2013; Denmead et al., 2014; Flesch and Wilson, 2005; Flesch et al., 2007; Loh et al., 2008; McGinn et al., 2007; McGinn et al., 2016; Todd et al., 2008; Todd et al., 2011; van Haarlem et al., 2008; Wilson et al., 2013; Yang et al., 2016). Unfortunately, high-quality results from this software require intensive computing power and time to run. With the same reasoning behind comparing sensor approaches (i.e., line-integrated versus point), it would be useful to compare the WT standard to another model with simpler algorithms (e.g., FIDES[2], an inverse model using similar input as WT; Loubet et al., 2001, 2009, 2010). Simpler models such as FIDES could be run on data-logging devices in the field (i.e., edge computing) for real-time fenceline monitoring of emissions.

The research presented in this paper had three goals related to NH_3 emissions from beef feedlots within the scope of real-time monitoring: (1) compare fenceline concentration data and emissions estimates from a line-integrated versus point sensor (LP and CRDS), (2) compare emissions results from two inverse models (WT and FIDES), and (3) quantify EFs from a representative feedlot in Colorado and compare to other EFs in the literature.

2.2 Materials and Methods

2.2.1 Site characteristics

Research was conducted at a beef cattle feedlot in Morgan County, Colorado with a capacity of 25,000-head; 100 to 150 km east of RMNP. Data were collected from 10 Jul to 26 Sep 2014 (day of year (DOY) 191 to 269). The pen-stocked area was mostly rectangular (~710 m x ~590 m), total pen area covering 43 ha. The feedlot had no empty pens during the study with a typical Front Range feedlot stocking density of 17.0 m^2 $head^{-1}$ (hd^{-1}) and placement weights of 286 ± 58 kg. Runoff was captured in two small retention ponds, and excess manure from pens was stored in a composting area southeast of the feedlot. Runoff ponds are relatively small at this feedlot due to low annual rainfall (361 cm; WRCC, 2011). Closest CAFOs were >5 km to the north. Terrain was flat with few obstructions within 1 km (such as tree lines).

2.2.2 Instrumentation

Ammonia concentrations in the feedlot plume were measured by two instruments for comparison purposes, placed west of the main concentration of pens. The western fenceline was chosen to quantify emissions for easterly transport in the direction of the mountains and

---

[2] Flux Interpretation by Dispersion and Exchange over Short Range (Loubet et al., 2001)

RMNP. Because access to the feedlot interior was unavailable, a fenceline monitoring approach was used (similar to methods used by the US EPA; DeWees, 2015).

The first NH_3 sensor used was a long-path (LP) open-air, infrared tunable diode laser (Table 2.1) with a path length of 226.5 m from the LP source housing to the retro-reflector, both at heights of 2.1 m. Second, a cavity ring-down spectroscopy (CRDS; G1103 NH_3 Analyzer, Picarro, Inc.) analyzer provided point NH_3 concentrations (Table 2.1). Teflon tubing (heated to 45°C to minimize water condensation and NH_3 adsorption) ran from a filtered inlet at 2.66 m to the CRDS in a temperature-controlled enclosure (model TCR202443-K1H-03-110701, EIC Solutions, Inc., Warminster, PA; to maintain a near constant cabinet temperature of 25°C). Air was sampled at 8-9 liters per minute using a diaphragm pump (model B162-BP-AA1, Air Dimensions Inc., Deerfield Beach, FL) downstream of the CRDS. Coarse particulate matter (i.e., dust) makes air sampling with a closed path instrument difficult at beef feedlots. Thus, the air inlet for the CRDS was equipped with a Chemcomb 3500 cartridge (Thermo Fischer Scientific, Inc., Waltham, MA) that included a Teflon-coated nozzle and PM_{10} impactor plate followed by two Teflon 1-μm PTFE filters. Normally, this cartridge is used as a denuder (e.g., Baum and Ham, 2009), but in this case the acid-coated honeycomb inserts were not installed so the device functioned solely as an impactor/filter. An additional 1-μm hydrophobic in-line PTFE filter was inside the CRDS enclosure immediately before the air stream enters the analyzer unit. All filters and the impactor plate at the inlet were replaced weekly to ensure accurate CRDS measurements. An internal filter was replaced with a new factory version prior to deployment.

These concentration sensors were chosen for comparison because the highest quality scientific emissions results come from a combination of WindTrax (the bLs model, better at near field solutions; see next section) and line-integrated concentration data (i.e., the LP sensor). This is because line-integrated data have greater spatial representation, especially for areal emissions sources such as feedlots (Flesch and Wilson, 2005). Additionally, LP sensors measure this reactive species without the need for tubing, pumps, or filters. The bLs method also better characterizes dispersion physics in the turbulent boundary layer at the feedlot scale, especially in the near field (Wilson et al., 2013). While both WindTrax and FIDES provide emissions estimates, comparing the more common approach of WindTrax + LP with a point sensor and simpler model (e.g., CRDS + FIDES) explores additional options for real-time fenceline monitoring of emissions at these sites.

Finally, wind data was needed for model input (Table 2.1). Sonic anemometer (sonic) wind speed data ($U_{u,v,w}$, m s^{-1}) allowed calculation of wind direction (θ, °), friction velocity (u*, m s^{-1}), roughness length[3] (z_0, cm), and Obukhov length (L, m) (Loubet et al., 2001; Crenna, 2006). A temperature/relative humidity (T/RH) probe was used to adjust concentrations for STP.

2.2.3 Data processing and inverse modeling

Instantaneous data from the LP and CRDS were processed simultaneously to match samples to within the nearest second. The LP output includes necessary quality control/quality assurance (QA/QC) parameters which were used to filter LP data for good samples[4]. Afterward, 15-minute means were created from available samples. Due to deployment on the western fenceline, emissions were only available for easterly winds (i.e., 45° < θ < 135°). Additionally, one-third of instantaneous LP data were rejected due to QA/QC, with further data loss from feed truck traffic causing dust to attenuate the laser's beam. Data from the CRDS did not suffer these issues. Sensor data retention is discussed in section 2.3.3.1.

Sonic data were post-processed according to standard methods using the software package EdiRe (v1.5.0.32., R. Clement, University of Edinburgh). Corrections included despiking, lag removal, frequency response corrections (Massman, 2000; Moore, 1986), sonic-

---

[3] Calculated to be 3.6 cm for this feedlot from filtered sonic data.
[4] Parameters for QA/QC were R^2 (goodness of fit) and the light value level (LVL) of the LP. Instantaneous LP data were not used for averaging if R^2 < 0.9 and LVL < 1,800 (out of 16,000).

temperature sensible heat flux corrections for humidity (Schotanus et al.,1983), and density corrections to RH measurements (Webb et al., 1980). Final sonic data files were compiled at 15-min for use with inverse dispersion models to estimate NH_3 emissions.

Due to their applicability to livestock emissions research and the favorable terrain (i.e., expansive, flat topography) at the feedlot for model testing, two methods will be utilized to compare model-based NH_3 emissions from the feedlot in this study.

The first inverse dispersion model used in this study is a backward-Lagrangian stochastic model (WindTrax (WT), Thunder Beach Scientific, Halifax, Nova Scotia, Canada). Emissions are estimated from WT via site mapping of sources (i.e., feedlot pens), and properties/location of any sensors (Crenna, 2006; Flesch et al., 2007). Simulations (i.e., runs) compute emissions from randomized particle trajectories (with particle count user-specified). For every run (i.e., each record in the input data), the model uses turbulence data to statistically trace (backwards) the path a random particle would have made from the sensors to the ground, determining if it originated from the feedlot pens. The no-alley approach of Flesch et al. (2007) was used. Flesch and Wilson (2005) argue LP concentration data are better suited to bLs models like WT because emissions estimates are usually based on higher touchdown ratios (TDR[5]) than for point concentration data such as that from a CRDS. To increase TDRs and reduce uncertainty in estimated emissions, CRDS runs were assigned three times the particle count as LP runs (300,000 particles versus 100,000). Background concentration (C_{bgd}; upwind of feedlot) was given as 30 μg m^{-3} (50 ppb$_v$) for all runs (based off prior two years of passive sampler background measurements at the same feedlot, not shown). It is possible that NH_3 background in this region is higher than other less-intensive livestock regions. Upwind C_{bgd} values used in other studies are typically less than half this value, however it is argued that final emissions estimates are relatively insensitive to this parameter because the difference between

[5] The ratio of area covered by particle touchdowns (A_{TD}) to source area (A_{Pens}).

C_{bgd} and plume from a large, active feedlot is orders of magnitude (ppm_v instead of ppb_v) (Flesch et al., 2007). Main WT inputs were u*, z_0, L, θ, source perimeter, sensor locations and heights, downwind NH_3 concentration (C_{NH3}), C_{bgd}, and component wind statistics (σ_u/u^*, σ_v/u^*, σ_w/u^*).

A second inverse dispersion model called FIDES (Flux Interpretation by Dispersion and Exchange over Short Range) was utilized to estimate emissions (for comparison with WT) due to its compatibility with NH_3 surface exchange processes and applicability to simple areal sources such as open-air feedlots (Loubet et al., 2001; Loubet et al., 2009; Loubet et al., 2010). The FIDES inverse model is a 2-D (in x and z; thus a 1-D horizontal model), steady-state analytical solution to the advection-diffusion equation (Philip, 1959), combined with a submodel for dispersion (Huang, 1979) and resistance analogue to account for possible influence of downwind bi-directional exchange (i.e., deposition or re-emission). In this study, sensors were close enough to the feedlot to consider deposition negligible. Chemical transformations are not considered. FIDES operates on the principle of advection that concentration at one location (x, z) can be related to source strength elsewhere (x_s, z_s) (Thomson, 1987; Raupach, 1989). Using an analytical dispersion function based on power laws for wind and vertical diffusivity, the transfer coefficient can be characterized for an areal source of constant flux to infer emissions from downwind concentration (assuming MOST applies) (Carozzi et al., 2013; Loubet et al., 2001). Main inputs are u*, z_0, L, source geometry[6], sampling height, C_{bdg}, and C_{NH3}.

WindTrax and FIDES, like all inverse field techniques, use a mixture of theory and measurements to make flux estimates. However, there are inherent differences between the two approaches that could affect accuracy. For example, WT can easily represent horizontal variation/patchiness in source geometry and can be adapted, with some trepidation, to deal with

[6] Horizontal source extent (i.e., feedlot pens), and downwind distance of sensors from source.

wind flow distortions (Wilson et al., 2013). However, spatial variation or multiple source areas are very difficult to implement in FIDES, and flow distortions cannot be handled realistically with the power law profiles used in the analytical solution. Carozzi et al. (2013) estimated NH_3 fluxes from a slurry injection experiment with both WT and FIDES. Results showed good agreement under neutral boundary layer conditions, but solutions disagreed by as much as 32% under stable and unstable conditions. This reflects inherent differences between the models on how scalar diffusivity is estimated under non-neutral conditions. Conceptually, WT is better at depicting near field transport and dispersion very close to the source, while FIDES with its power-law vertical profiles is a far-field solution.

Figure 2.2 depicts the framework used to determine emissions. After processing, all model input data were filtered using the criteria in Table 2.2. As will be shown in the results, a large fraction of data were excluded from the analysis because winds were not from the direction of the feedlot (first criterion in Table 2.2). The u* and L criteria in Table 2.2 are for occasions when environmental parameters deviated from MOST, and the last criterion is similar to other studies as a quality control constraint to ensure sufficient particle coverage of the source area (i.e., touchdown ratio; Flesch et al., 2007). Because z_0 was calculated for the site from feedlot turbulence data, this criterion was excluded from Table 2.2, but it is worth noting that a filtering criterion for z_0 is used in many studies where z_0 was not found experimentally. For completeness, whenever concentrations or emissions are referred to as “filtered” (unless specifically stated otherwise), they have gone through all the filters in Table 2.2.

2.2.4 Gap-filling procedure

Because measurements were located on the fenceline (not within the feedlot), major gaps occurred simply due to wind direction. Additional complications arose when longer gaps occurred due to dust or precipitation, instrument failure and removal for repairs. In this study, immediately east of the sensors and LP path was a feedlot road, heavily traveled by feed trucks.

This caused much LP data to be low quality and thus rejected. Despite the reason, gaps must be filled to calculate cumulative emissions (i.e., overall NH_3 loss to the atmosphere from a site).

The most common gap-filling method utilized in micrometeorology is called mean diurnal variation (MDV). With MDV, values for gaps are assumed to be the mean of corresponding data around when the gap occurred. For example, if a gap occurred at noon, MDV would select a moving window of several days and fill in the gap as the mean of all noon-time data for the moving window around the gap. There are many benefits to using MDV for NH_3 emissions and other ecological and pollutant data. Amongst a heavily-reviewed area of research such as gap-filling eddy covariance and other micrometeorological emissions data, MDV performs moderate-to-well when compared to other approaches, especially considering its algebraic simplicity (Falge et al, 2001). Using MDV for feedlot NH_3 emissions is reasonable because surface fluxes are strongly temperature dependent and thus exhibit diurnal patterns (Baum and Ham, 2009).

Often MDV is applied with two moving windows. The first is the hard window (measured in days), referring to the range of days (±) around the missing gap that the MDV average will encompass. The second is the soft window (measured in hours), describing how many records around the time of the missing gap to average on each day within the hard window. The moving windows used with the MDV method in this study is discussed in section 3.3.2. After filtering and gap-filling all model output, emissions were put into four groups for comparison (Fig. 2.2).

2.3 Results and Discussion

2.3.1 Weather conditions

In summer 2014, temperatures were typical of historical averages (WRCC, 2011). Daily feedlot weather during the study was mostly sunny in the mornings becoming partly to mostly cloudy after solar noon. Daytime maximum temperatures often exceeded 30°C, making for rapid volatilization of NH_4^+ on pen surfaces to NH_3. Precipitation was slightly above average, a possible influence of a stronger Pacific monsoon in 2014 (Doesken, 2014). Two rainfall events affected some data in mid-Aug. The first on DOY 231 caused the LP's removal for repairs (DOY 232 to 240). The second storm was on DOY 239. The CRDS dataset persisted through both events with care taken to change the inlet filters during this period, although changing wind directions did not allow for an accurate analysis of the effects of drydown on NH_3 emissions.

Daytime winds varied greatly in direction and intensity, while nighttime winds showed a strong southwesterly component. Unfortunately, during this study winds were highly unusual with less easterly winds than expected for this season (only 19.9% easterly winds: $45° < \theta < 135°$). In contrast, wind data from Fort Morgan for Jul and Aug showed 37% more easterly winds (IEM, 2017). This affected the results, with less useable data than most studies report. Although winds caused less filtered data to be retained, there were still more available data after processing than many short-term studies (representing much of the existing research), and the data retained also went through rigorous QA/QC protocol. Recall, the main rationale for placing equipment along the western fenceline was to quantify emissions towards RMNP.

2.3.2 Concentrations

Wind direction greatly affected LP and CRDS data due to obvious differences in source strength between the feedlot and short, sparse pasture to the west. High concentrations were associated with easterly winds, while near background concentrations prevailed from the west for both sensors (Fig. 2.3). To show the range of values, 5th and 95th percentiles of concentration are indicated. For consistency, all data in these plots are only from matching output (i.e., both LP and CRDS had corresponding data), filtered for u* and L to show favorable conditions. Values between sensors were similar for all wind directions. A closer look at these data show the SW wind sectors are influenced by frequent high values which occur between sunrise and sunset (but that there was no statistical reason to remove the data point). This could indicate an influence of stable conditions (i.e., nighttime data) on local concentrations. A major difference between datasets is sample size (6,293 15-min records for the CRDS dataset versus 2,568 for the LP due to road dust, misalignment, and short removal for repairs) (data not shown).

Despite slight differences in Fig. 2.3 for some northerly and southerly sectors (where the LP had lower source area due to its N-S orientation), there is good agreement in terms of response and magnitude of concentration between the CRDS and LP for all other winds. Mean 15-minute filtered concentrations (± standard deviation, σ) of easterly transport from the feedlot (i.e., 45° < θ < 135°) for all the LP and CRDS data were 623.2 ± 245.3 $\mu g\ m^{-3}$ (1049 ± 420 ppb_v) and 622.2 ± 286.9 $\mu g\ m^{-3}$ (1045 ± 490 ppb_v), respectively ($p = 0.467$). When only corresponding output between both sensors were compared (i.e., from times when both sensors had data for a given 15-minute record), the differences were statistically significant: 623.2 ± 245.3 $\mu g\ m^{-3}$ (1049 ± 420 ppb_v) for the LP, and 579.8 ± 244.2 $\mu g\ m^{-3}$ (976 ± 419 ppb_v) for the CRDS ($p < 0.001$). These differences are likely by different concentration footprints (line-integrated vs. point) rather than analytical differences between instruments. Both these findings are slightly higher than from other work at a beef CAFO in Colorado which ranged from 377 $\mu g\ m^{-3}$ in the winter to 563 $\mu g\ m^{-3}$ in the summer (Hutchinson et al., 1982). When STP is accounted for, Flesch et al. (2007) saw higher concentrations from a very large feedlot (>40,000 head) in Texas of 725 $\mu g\ m^{-3}$ in the spring to 1027 $\mu g\ m^{-3}$ in the summer, while Rhoades et al. (2010) found summertime values of 466 $\mu g\ m^{-3}$ at a Texas feedlot more similar in cattle populations to those in this study.

Instantaneous data (upon which all model input data are based) also agree well between sensors. Figure 2.4 displays a time series of instantaneous concentration from both sensors during a 12-day period of high data coverage and fidelity, with wind direction included to demonstrate sensor response to changing winds. While there is visually more spread in the LP (owing to contribution from a larger area), both sensors reacted simultaneously to changes in plume strength as wind direction fluctuations caused dramatic increases and decreases in the signal. Additionally, concentrations seemed to fluctuate around the same values for both sensors when winds were stable from the source. Data were more consistent between sensors when winds were easterly (DOY 195.4 to 196.7, 197.4 to 199.0, and 203.4 to 204.7; Fig. 2.4). With westerly winds (i.e., $225° < \theta < 315°$), values fell to near background like in Fig. 2.3 (DOY 199, 201, and 202; Fig. 2.4). Weather systems causing prolonged periods of similar wind directions lasted 2 to 4 days, while most other days saw simple convective diurnal changes.

As evident at the end of DOY 202, instantaneous peaks often exceeded thousands of ppb_v, the default unit of both analyzers (Fig. 2.4). This occurred for a situation when wind speed was extremely light from the direction of the feedlot for a prolonged period. This event occurred at night, when stable conditions often form. On this particular evening, wind speeds were at or below 2 m s^{-1} for most of the night, corresponding to very low friction velocities (indicative of lack of turbulent mixing). Such a scenario could cause possibly dangerous increases in surface concentrations from emissions sources, like that seen during atmospheric inversions. For the case of this rural feedlot, settling of highly stable air masses is typically short-lived as this area of Colorado tends to have higher wind speeds throughout much of the day.

Again, a major difference between the instantaneous datasets is that the LP had less overall data than the CRDS (see sample sizes, Fig. 2.4). With more records, the CRDS seems to have an advantage during dust and precipitation events (which would cause gaps in LP data), and it does not rely on maintaining alignment or a clean lens as long as the incoming air is well-filtered. From comparisons between the LP and CRDS, the major contributor to data gaps in the final 15-min data was wind direction due to sensor location, with a secondary loss of data for the LP due to dust, precipitation, or misalignment. If these measurements had been placed in the feedlot interior, significant gaps could have been avoided. This indicates that fenceline monitoring can miss a large portion of data if only one system is utilized per site. For a more complete dataset, it may be beneficial to attempt more centralized measurements (Flesch et al., 2007) or deploy an additional fenceline monitoring system on the opposite edge. For this study, transport towards RMNP was of interest, thus the west-side fenceline approach. However, strictly comparing viable concentration data between sensors in this study, point measurement with the CRDS created a dataset with higher data coverage than the LP, and the CRDS also matched concentrations measured by the LP well.

2.3.3 Emissions

2.3.3.1 By sensor and inverse model

Diurnal composites of emissions are shown in Fig. 2.5. Both sensors trended each other throughout the day, with CRDS data having slightly larger peaks than LP data for FIDES output (74.8 to 71.8 $\mu g\ m^{-2}\ s^{-1}$, respectively) and the reverse occurring for WT output (peak of LP composite data greater than CRDS by 97.6 to 91.9 $\mu g\ m^{-2}\ s^{-1}$, respectively). The larger magnitude of CRDS emissions could be due to more data in the CRDS dataset, with an extra 3.3 to 4.4 days of output (WT and FIDES, respectively) used for composites over the LP (Fig. 2.6). It is unlikely the difference in amount of data for composites is only a result of the LP being removed for repairs from DOY 232 to 240. Omitting these days from the CRDS dataset, there were still 2.0 to 3.1 more days of data for composites from the CRDS than LP for both models (WT and FIDES, respectively). Data availability for the composites has a pronounced diel pattern which one would expect from conditions that satisfy MOST (Fig. 2.6), with less data during the night/early morning and five to six times more data during the midday and afternoon when winds and air temperature tended to be greater. FIDES had a higher instance of emissions output after being filtered than with WT for both sensor datasets (left half of Table 2.3). WindTrax has more filtering criteria applied to the final datasets (see Table 2.2), thus resulting in removal of more data than for the final FIDES dataset. The composite graphs show signs of increased cattle activity in early evenings, a feature noted by Flesch et al. (2007) and McGinn et al. (2007).

Filtered 15-minute emissions ranged from 3.1 (LP_{FIDES}) to 144.9 $\mu g\ m^{-2}\ s^{-1}$ (LP_{WT}). Mean emissions from Fig. 2.5 (weighted by number of records ± 1σ) were 52.4 ± 27.2 and 55.4 ± 26.4

$\mu g\ m^{-2}\ s^{-1}$ for the LP and CRDS when averaged across both models, respectively (p=0.051). The largest difference appeared to be between models, with 24-hr WT emissions 25.2% higher on average than FIDES (60.4 ± 29.7 versus 48.2 ± 23.9 $\mu g\ m^{-2}\ s^{-1}$, respectively; p<<0.0001) (across both sensors) (Table 2.3). Overall mean 24-hour emissions of both sensors and models were 54.1 ± 26.7 $\mu g\ m^{-2}\ s^{-1}$. The effect of gap-filling is discussed in the next section. Correlations between NH_3 emissions and temperature or other climatic variables were attempted, but no statistically significant relationships were found.

Similar to this study, Carozzi et al. (2013) compared WT and FIDES for NH_3 emissions from fertilizer application in the Po Valley of Italy. They found FIDES overestimated WT in neutral stability but can be 20 to 30% smaller for stable and unstable cases, respectively. As discussed in section 2.3, this is because WT and FIDES have different scalar turbulent diffusivities, relating to the amount of dispersion in each model's physics based on stability.

Table 2.3 shows average emissions and other statistics for this study, while Table 2.4 shows this study contrasted to others. Our values fell in the range of other emissions found at beef feedlots in North America. McGinn et al. (2007) observed higher diurnal mean emissions (84 ± 43 $\mu g\ m^{-2}\ s^{-1}$) from a similar-sized feedlot in Western Canada. The first micrometeorological study at a feedlot by Hutchinson et al. (1982) in Colorado measured emissions of 38 ± 19 $\mu g\ m^{-2}\ s^{-1}$ for late spring/early summer using the flux-gradient (FG) method with acid-gas washing samplers (AGWS) during daytime hours. Similar Texas studies saw summer emissions (in $\mu g\ m^{-2}\ s^{-1}$) of 70 (Todd et al., 2005; used AGWS with FG), 61 (Baek et al., 2006; chemiluminescence analyzer with FG), ~96 (Flesch et al., 2007; used LP and WT)[6], ~112 (Todd et al., 2008; used AGWS with WT)[7], and 109 $\mu g\ m^{-2}\ s^{-1}$ (Rhoades et al., 2010; chemiluminescence with WT).

---

[7] Estimated from their results in kg d^{-1} and feedlot area.

When integrated beneath the curves (Fig. 2.5), LP and CRDS-based emissions totaled 1,884 and 1,983 kg d^{-1} of NH_3 for the entire feedlot area for WT, while FIDES totaled 1,423 and 1,633 kg d^{-1} (LP and CRDS, respectively) (Table 2.3). After gap-filling (shown in the next section), emission estimates decreased because they incorporated data from times of the day when LP and CRDS data were lacking (Fig. 2.6), such as night and morning.

2.3.3.2 Effect of gap-filling

Most emissions and ecological monitoring datasets contain missing data (i.e., gaps), where gap-filling can account for 24 – 56% of the final data in livestock emissions studies (Flesch et al., 2007; Yang et al., 2016). Due to unseasonable wind directions during this study, up to 90.3% of final, filtered emissions data had to be gap-filled (center column, Table 2.3). Gaps in 15-minute emissions occurred for two reasons: (1) data filtering from Table 2.2 criteria, and (2) sensor misalignment, removal, or failure. Loss of data within datasets due to Table 2.2 filtering consisted of 69–76% from θ alone, 2.1–3.8% from u* or L criteria, 1.4% of WT data due to low TDR (CRDS only; LP had no issues with TDR after θ-filtering), with 1.8–12% more filtering due to overlapping criteria (one or more of the first three in this list). Instrument malfunction or station issues only accounted for up to 0.6% of the CRDS dataset, while the LP's removal for repairs accounted for around 2-3% of the LP dataset (estimate based on mean number of filtered 15-minute emissions data points per day for the times when the LP was in collecting data the field, multiplied by the 9 days the LP was out for repairs).

Because the amount of missing data was extreme, a modified MDV (mMDV) was utilized with an iterative approach. The hard and soft windows for the mMDV were shortened to 1 day and 1 hour, respectively, for more responsiveness (see section 2.4 for more information on MDV and windows). One iteration was not sufficient to fill all gaps so the mMDV would iterate until no gaps remained. The gap-filling program was executed in Matlab™ vR2015a (The Mathworks, Inc.®, Natick, MA). The mMDV was tested for accuracy by randomly removing data points in each emissions dataset, then using mMDV on the randomly-inserted gaps to predict removed data. Regressions between mMDV-predicted and filtered emissions (i.e., WT or FIDES) differed by time of day. During the day (9 am to 5 pm local standard time, LST), values predicted by mMDV approximated filtered emissions with a mean (± 1σ) slope of 0.49 ± 0.08, intercept of 33.1 ± 6.6 $\mu g\ m^{-2}\ s^{-1}$, and R^2 of 0.28 ± 0.07 (all datasets). The mMDV predicted emissions data better during night (i.e., 9 pm to 5 am LST) where predicted emissions approximated filtered emissions with a mean slope, intercept, and R^2 (± 1σ) of 0.71 ± 0.07, 13.8 ± 4.6 $\mu g\ m^{-2}\ s^{-1}$, and 0.39 ± 0.08, respectively. These relationships are expected, as daytime NH_3 fluxes vary more in magnitude (>100 $\mu g\ m^{-2}\ s^{-1}$) than at night (usually <20 $\mu g\ m^{-2}\ s^{-1}$). This shows the mMDV approach performs fair for low data availability (i.e., night), and is sufficient to fill in gaps during the daytime, but with less certainty than for nighttime data.

Figure 2.7 and Table 2.3 (right half) show mean gap-filled emissions. Despite smoothing of the data from Fig. 2.5, gap-filled emissions still show a diurnal trend (Fig. 2.7). Considering the number of gaps, mean composite diurnal emissions after running mMDV were only 11.7% less than before gap-filling (Table 2.3). Again, this is expected as filtered data (i.e., non-gap-filled) were based on more daytime data (i.e., data with higher values) than other times of day (times usually consisting of lower emissions values) (see Fig. 2.6). However, considering the amount of gap-filling that was done, one might expect gap-filled emissions to deviate from filtered emissions by much more than 12%. It is possible for much of this difference to be made up by the addition of more nighttime (i.e., lower-value) data, rather than an artifact of the mMDV alone. Similarity in results before and after gap-filling shows that even extreme datasets such as this can be mostly resolved with a more responsive (i.e., smaller soft window) mMDV approach.

2.3.4 Emission factors, % fed-N

The feedlot in this study was at full capacity during measurements. When filtered emissions were adjusted for mean stocking density of the pens (17.0 $m^2\ hd^{-1}$), mean emission factors (EFs) for the four datasets ranged 66.7 to 89.9 g hd^{-1} d^{-1} (Table 2.4, shaded and bolded lines). The largest deviations again occurred between models rather than between sensors, with filtered 24-hr composite WT emissions 25.2% higher than FIDES when averaged across both sensors for each model (88.9 versus 71.0 g hd^{-1} d^{-1}, respectively). Overall mean of all available 24-hr composite filtered emissions (FIDES and WT) was 79.6 g hd^{-1} d^{-1}.

The means of all four datasets fall in the range of values shown from other studies. Similar approaches using LP line-integrated data with WT have a range of summertime EFs from 62.5 g hd^{-1} d^{-1} for small feedlots in China (<1,200 cattle; Yang et al., 2016) to 318 g hd^{-1} d^{-1} in Alberta, Canada at a farm with an unusually high CP diet (>20% CP; van Haarlem et al., 2008). Summertime studies from North America have a mean EF of 136 ± 65 g hd^{-1} d^{-1} (Baek et al., 2006; Flesch et al., 2007; Hutchinson et al., 1982; McGinn et al., 2007; Rhoades et al., 2010; Staebler et al., 2009; Todd et al., 2005; Todd et al., 2008; Todd et al., 2011)—53 and 92% higher than EFs reported from sensor-averaged WT and FIDES output in this study, respectively. Studies specifically from Texas or Southern Great Plains have higher EFs than those found here (mean of 146.4 g hd^{-1} d^{-1}; 65 and 106% higher than WT and FIDES, respectively, for summertime emissions), a result similar to those from concentration data in section 3.2 (to be expected, owing to the higher wind speeds and temperatures in Texas over Northern Colorado). This again highlights the importance of measuring local CAFOs to better calibrate regional emissions and transport models based on climatology.

If total emissions to the atmosphere are calculated from gap-filled emissions, the whole feedlot (i.e., all the pens) would contribute 100.5 – 158.5 tonnes (Mg) of NH_3 across 76 days of finalized gap-filled data. The average rate of decrease between summertime and wintertime emissions from Table 2.4 is 44.7 ± 23.4% (Baek et al., 2006; Denmead et al., 2008; Loh et al., 2008; Rhoades et al., 2010; Todd et al., 2005; Todd et al., 2011; Yang et al., 2016). Assuming the data from this study represents the high point (i.e., 79.6 g hd^{-1} d^{-1}) in yearly emissions, and that emissions decrease to 44.7% of their summertime peak (i.e., wintertime mean would be

35.6 g hd^{-1} d^{-1}), yearly emissions from this feedlot based on a constant cattle population of 25,000 would total 526.7 metric tons (i.e., Mg or Tonne) per year.

One way to determine the effectiveness of cattle diet is to express emissions in terms of the percent of cattle N intake that was emitted to the atmosphere from excreta as NH_3 gas. This is referred to as % fed-N, which other studies have reported to range from 18 to 48% of fed-N for the winter to 27 to 68% in the summer (Table 2.4). Mean filtered 24-hr composite values for FIDES and WT were 35.6 and 44.6% of fed-N being emitted as NH_3, with an average of 40.0% of fed-N for all four datasets. Feed records show dietary N during the study was 163.9 g hd^{-1} d^{-1}, corresponding to 13.25% CP. Studies from Texas had CPs of 12.9 to 18.8% (Flesch et al., 2007; Rhoades et al., 2010; Todd et al., 2005, 2008, 2011).

2.3.5 Towards real-time fenceline monitoring

2.3.5.1 Point or line-integrated measurements

From this study's results, a point sensor (such as the CRDS) can provide similar emissions results to line-integrated emissions, as long as care is taken to ensure accurate measurements and they are located in a relatively centralized location or downwind in the direction of transport concern (such as for RMNP transport in this study). The advantages and disadvantages of using a LP (e.g., Boreal Laser, Inc.) vs. a closed-path CRDS (e.g., Picarro, Inc.) instrument will likely depend on the deployment location, experience of the user, and goals of the experiment. Clearly both instruments can be viable options.

While using WT + LP is a proven technique that is well-tested in the literature (italicized citations from Table 2.4), the CRDS with FIDES has several benefits. First, stationary and mobile fenceline methods are already in use by the EPA (DeWees, 2015; USEPA, 2014) and other groups (Eilerman et al., 2016; Miller et al., 2015; Sun et al., 2015), and are more suited to point measurements. Second, (to expound upon why researchers choose the fenceline approach) is that point sensors are better suited for mobile measurement (vehicle-based snapshot studies) or mobile vehicle mapping. Third, results from this study showed point sensors had superior data retention while maintaining acceptable approximation of concentration (Fig. 2.4 and 6, Table 2.3). Overall, CRDS emissions tended to be slightly lower, attributable to a larger data span throughout the day compared to the LP which retained more data for daytime hours (i.e., higher-value data points) and thus fluctuate more, even during consistent wind periods (see Fig. 2.7).

If possible for the desired site, measurements should be placed near the center of the source if there is adequate fetch to allow for more data capture from all wind directions. However, if fenceline monitoring is the only available option, utilizing point sensors (either mobile or stationary; e.g., Miller et al., 2015 and Sun et al., 2015) provides similar results to line-integrated sensors, with the option of increased mobility.

2.3.5.2 Data analysis and dispersion model

Given the prevalence of WT in livestock emissions literature (Table 2.4), it was helpful to compare the simpler FIDES model to WT results. When both models are utilized with the same core input data (i.e., u^*, L, C_{NH3}, C_{bgd}, and z_0), WT results were 25% higher than FIDES when filtered 24-hour composite results are compared (not gap-filled emissions). There is no way to evaluate which system was more accurate without comparison to a more direct measurement like eddy covariance (Sun et al., 2015) or relaxed eddy accumulation (Baum and Ham, 2009).

It should be noted again, FIDES does not use θ like WT (i.e., FIDES is 2-D in x-z), which aligns with the greater uncertainty of 30-40% associated with FIDES (Loubet et al., 2010) (although emissions from FIDES and WT were still filtered in the end for optimal θ). Despite the difference in emissions (FIDES is 25.2% < WT), the authors suggest using FIDES (with point emissions) has potential for real-time monitoring applications and warrants further research.

2.3.5.3 Gap-filling

Regardless of model or sensor approach, if an emissions dataset contains significant gaps, it is recommended to perform gap-filling to obtain cumulative emissions over time. For datasets whose emissions are dependent on surface processes (and thus temperature; such as volatilization of NH_3 from urine and dung), MDV tends to perform well—especially for nighttime data. Because NH_3 emissions from feedlot pens are shown to exhibit a strong relationship to temperature (Todd et al., 2013), MDV was selected for gap-filling in this study. Gap instances in filtered emissions datasets were extremely high (up to 90%). This caused a shift in approach to a modified MDV with a 1-day hard window and 1-hour soft window. Over 54% of missing data occurred in an 8-hour period between 9 pm and 5 am LST (when MOST conditions were typically not satisfied and wind directions often shifted), causing an overestimation of the mean daily emissions (if only filtered data were used to summarize feedlot emissions). After gap-filling, mean emissions were only reduced by 11.7%, an expected value considering significant gaps occurred for low-value emissions. Despite the extreme missing data, gap-filling provided a reasonable result using an algebraically-simple, widely-used method.

2.3.5.4 Averaging Interval

Another set of model runs was completed using hourly data to examine the effect of changing this averaging interval. Hourly data caused a closer approximation between FIDES and WT than for shorter time-intervals, especially in regard to LP data (Fig. 2.8). This is because hourly means were more similar to each other than 15-minute data, and hourly data may also moderate the impact of short term dust events that affected the LP measurements. From these results, a time interval is suggested that is best suited for the research application, with the comfort in knowing that 15-minute emissions data are similar to 60-minute results. For real-time monitoring, 15-minute data would result in greater scatter but provide higher output frequency, while hourly data would provide less scatter but output less often. Either approach is satisfactory based on the above comparison.

Overall, as with most averaging, hourly emissions lost a degree of responsiveness to diurnal fluctuations and thus were slightly lower than those for 15-minute data. However, for the LP in specific, using hourly data resulted in drastically higher correlations between models.

2.4 Conclusions

Comparisons of concentration data between CRDS and LP showed similar results, despite the difference in sampling volume (i.e., point CRDS versus the line-integrated LP). Filtered 15-min concentrations (Table 2.2) for transport from the feedlot to nearby mountainous areas (i.e., easterly surface winds, $45° < \theta < 135°$) showed means ($\pm 1\sigma$) of 623.2 ± 245.3 and 579.8 ± 244.2 $\mu g\ m^{-3}$ for LP and CRDS, respectively ($p<0.001$ for simultaneous records). These numbers fall in the range of other studies and are less than Texas studies. This indicates that for concentrations from a uniform source (such as an active feedlot like that here), point sensors can measure concentrations with similar response and magnitude to that of a collocated line-integrated sensor. There were about 2.5 times more 15-min data points in the CRDS datasets than the LP dataset.

Emissions were run in FIDES and WT for both CRDS and LP datasets and then filtered (Table 2.2). Differences in output were greater between models than between sensors (Fig. 2.5). Mean 15-min filtered emissions from 24-hr composites ($\pm 1\sigma$) were 52.3 ± 27.2 and 55.4 ± 26.4 $\mu g\ m^{-2}\ s^{-1}$ for the LP and CRDS datasets (across both models), respectively (Table 2.3). Mean WT output was 25.2% higher than FIDES (60.4 ± 29.7 versus 48.2 ± 23.9 $\mu g\ m^{-2}\ s^{-1}$, respectively; $p<<0.0001$) (across both sensors) (Table 2.3). WindTrax is better at describing the near field solution and is likely more accurate for a feedlot environment than FIDES (though this cannot be quantified until both are compared to actual emissions). All emissions datasets showed an evening peak in NH_3 emissions after 9 pm LST (Fig. 2.5), related to increased cattle activity during this time. Higher data availability occurred for composites with CRDS datasets than for LP (Fig. 2.6), as well as more data with CRDS-based emissions after filtering than for the LP (Table 2.3).

Because the amount of data gaps was extreme (due to unseasonable θ), gap-filling was performed using a modified mean diurnal variation (mMDV) method with shorter windows to elicit more responsiveness in the gap-filling (1 day and 1 hour hard and soft windows, respectively). When filtered emissions were gap-filled, the new mean only varied from the filtered mean by 11.7% less, which is to be expected from the incorporation of more nighttime and early morning low-value emissions data. The gap-filling method here provided a reasonable result given the prevalence of gaps (e.g., 90.3% gaps for the LP_{WT} dataset).

The mean EFs for LP_{FIDES} and $CRDS_{FIDES}$ were 66.7 ± 34.7 and 73.8 ± 35.4 g hd^{-1} d^{-1}, respectively; while WT output had higher means (87.5 ± 45.2 and 89.9 ± 42.7 g hd^{-1} d^{-1} for the LP and CRDS, respectively). The mean of all datasets gives an overall feedlot EF of 79.6 ± 39.3 g hd^{-1} d^{-1}, which is less than most EFs reported in Texas research, as expected from the lower regional wind speeds and temperatures typically experienced on Colorado's Front Range. The percentage of fed-N lost as NH_3 from the surface was 40.0%. All data scale to other sites, keeping regional differences in mind (Table 2.4).

This dataset represents an extreme situation where conditions precluded high data retention after filtering, yet results presented are in good agreement with existing literature; validating the research efforts of this study despite the less than ideal wind conditions. We feel the inclusion of these results in current literature is important, as fenceline monitoring datasets will occasionally experience these extremes. Having a viable data processing and interpretation scheme (as outlined in section 2.3.5) for these rare situations will improve fenceline monitoring and interpretation of emissions from such systems in the future. Next steps would be to compare output of WT and FIDES to actual emissions from eddy covariance to determine each inverse model's accuracy.

If the US adapts to regulate NH_3 like Europe (Directive 2001/81/EC, 2001), there will be a major need for direct monitoring at hot spots like CAFOs. Additionally, because inverse dispersion models show good agreement between NH_3 emissions estimates using point-data and line-integrated data, development and use of point NH_3 sensors in the future would allow for easier monitoring of NH_3 from CAFOs. This could be applied to mobile drive-bys for addressing citizen concerns as well. By expounding upon this research, real-time emissions monitoring at NH_3 hotspots such as CAFOs may soon be a possibility.

2.5 Tables

Table 2.1. Instrumentation utilized in the study.

Dataset	Sensor Name	Variables Measured	Height (m)	Logging Speed	Sensor Model	Manufacturer	Manufacturer Location
Concentrations	LP†	C_{NH3}, R^2, LVL‡	2.10	Med[a]	GasFinder2.0	Boreal Laser, Inc.	Edmunton, Alberta, Canada
	CRDS	C_{NH3}	2.66	Med[b]	G1103	Picarro, Inc.	Sunnyvale, CA, USA
Turbulence	Sonic anemometer	U, θ, u*, L, z_0	3.00	High[c]	CSAT3	Campbell Scientific, Inc.	Logan, UT, USA
	Temp/RH probe	T_{air}, RH	3.00	High[c]	HMP45C	Campbell Sci.	Logan, UT, USA
	Turbulence datalogger	—	—	High[c]	CR1000	Campbell Sci.	Logan, UT, USA

[a] 0.09 Hz, 5.6 records min^{-1}
[b] 0.35 Hz, 21.2 records min^{-1}
[c] 20 Hz, $1.2x10^3$ records min^{-1}
† LP concentration data is line-integrated, all others are point-measurements. One-way path length was 226.5 m.
‡ LVL = light value level, see footnote 4 in section 2.2.3.

Table 2.2. Filtering criteria for emissions from both models. Shaded criteria apply to WindTrax emissions only.

Parameter	Symbol	Units	Filter if:	Reason
Wind Direction	θ	deg	θ<45°, θ>135°	Signal not from pens
Friction velocity	u*	$m\ s^{-1}$	< 0.15	Wind speeds too low
Obukhov length	|L|	m	< 10	Extreme stabilities
LP Touchdown Ratio (TDR_{LP})	$\frac{A_{TD,LP}}{A_{Pens}}$	$m^2\ m^{-2}$	< 0.15 (15%)	Sufficient particle coverage in pens
CRDS Touchdown Ratio (TDR_{CRDS})	$\frac{A_{TD,CRDS}}{A_{Pens}}$	$m^2\ m^{-2}$	< 0.10 (10%)	Sufficient particle coverage in pens

Table 2.3. Mean 24-hour emissions from composite graphs (*italicized*). Before (left; see Fig. 2.5) and after gap-filling (right; see Fig. 2.7). Also included are number of data points for calculated means and amount of gap-filled data. Emissions reported in kg d^{-1} are feedlot-scale (i.e., representative of all cattle on the feedlot; 43 ha in area).

		Filtered, Composite Emissions				Gap-Filled Composite Emissions				
Sensor	Model	Mean ($\mu g\ m^{-2}\ s^{-1}$)	Mean (kg d^{-1})	n	% gap-filled	Mean ($\mu g\ m^{-2}\ s^{-1}$)	Mean (kg d^{-1})	Total NH_3 (Tonne)	n_{MDV}	% Change in mean
LP	FIDES	*45.3 ± 23.6*	*1889*	733	90.2	*41.4 ± 16.3*	*1542*	*117.2*	7300	-8.7
CRDS	FIDES	*50.2 ± 24.1*	*2004*	1160	84.5	*42.0 ± 18.2*	*1565*	*119.0*	7300	-16.3
LP	WT	*59.5 ± 30.7*	*2483*	731	90.3	*56.0 ± 21.8*	*2085*	*158.5*	7300	-5.9
CRDS	WT	*61.1 ± 29.0*	*2462*	1044	86.1	*52.0 ± 21.9*	*1937*	*147.3*	7300	-14.9

Table 2.4. Comparison of mean NH_3 emissions, EFs, and % of fed-N lost as NH_3 for a range of beef feedlot studies. Italicized lines are WT + LP studies (10 studies, including current). Shaded lines show current results for comparison.

Reference	Season	NH_3 Emissions ($\mu g\ m^{-2}\ s^{-1}$)	NH_3 EF ($g\ hd^{-1}\ d^{-1}$)	% Fed-N	Dispersion model	Location
This study - LP_{FIDES}	**Jul - Sep**	**45.3 ± 23.6**	**66.7 ± 34.7**	**33.4**	**FIDES**	**Colorado, USA**
This study - $CRDS_{FIDES}$	**Jul - Sep**	**50.2 ± 24.1**	**73.8 ± 35.4**	**37.0**	**FIDES**	**Colorado, USA**
This study - LP_{WT}	***Jul - Sep***	***59.5 ± 30.7***	***87.5 ± 45.2***	***43.9***	***WT***	***Colorado, USA***
This study - $CRDS_{WT}$	**Jul - Sep**	**61.1 ± 29.0**	**89.9 ± 42.7**	**45.1**	**WT**	**Colorado, USA**
This study - FIDES mean	**Jul - Sep**	**48.2 ± 23.9**	**71.0 ± 35.1**	**35.6**	**FIDES**	**Colorado, USA**
This study - WT mean	**Jul - Sep**	**60.4 ± 29.7**	**88.9 ± 43.7**	**44.6**	**WT**	**Colorado, USA**
This study - Overall mean	**Jul - Sep**	**54.1 ± 26.7**	**79.6 ± 39.3**	**40.0**	**BOTH**	**Colorado, USA**
Hutchinson et al. (1982)[a]	Apr - Jul	38.3 ± 19.4	48.4	—	N/A	Colorado, USA
Erickson et al. (2000)	Summer	—	—	66	N/A	Nebraska, USA
Erickson et al. (2000)	Wnt, Spr	—	—	41	N/A	Nebraska, USA
USEPA (2004)	—	—	31.3	—	N/A	N/A
Todd et al. (2005)	Summer	70	99.4[b]	55	—	Texas, USA
Todd et al. (2005)	Winter	34	50.3[b]	27	—	Texas, USA
Todd et al. (2005)[c]	Summer	—	—	45	—	Texas, USA
Todd et al. (2005)[c]	Winter	—	—	43	—	Texas, USA
Cole et al. (2006)	Summer	—	—	58	N/A	New Mexico, USA
Baek et al. (2006)	Summer	61.2	89.3	—	—	Texas, USA
Baek et al. (2006)	Winter	5.3	7.1	—	—	Texas, USA
Flesch et al. (2007)	*Summer*	*96.0[d]*	*146.8*	*63*	*WT*	*Texas, USA*
Flesch et al. (2007)	*Spring*	*80.2[d]*	*151.4*	*65*	*WT*	*Texas, USA*
Harper et al. (2007)	*Summer*	—	—	*53*	*WT*	*SGP, USA[e]*
Harper et al. (2007)	*Winter*	—	—	*28*	*WT*	*SGP, USA[e]*
McGinn et al. (2007)	*Summer*	*84 ± 43*	*140*	*63*	*WT*	*Alberta, Canada*
Denmead et al. (2008)	Winter: 1[f]	—	24 ± 3	—	N/A	Queensland, AUS
Denmead et al. (2008)	Winter: 2[f]	—	69 ± 22	—	N/A	Victoria, AUS
Loh et al. (2008)	*Summer: 1[f]*	*45.9[g]*	*253*	—	*WT*	*Queensland, AUS*
Loh et al. (2008)	*Summer: 2[f]*	*27.1[g]*	*125*	—	*WT*	*Victoria, AUS*
Todd et al. (2008)	Summer	111.5 ± 23.7	128 ± 25	68	N/A	Texas, USA

Todd et al. (2008)	Winter	50.0 ± 15.3	64 ± 21	36	N/A	Texas, USA
van Haarlem et al. (2008)	*Fall*	*—*	*318*	*72*	*WT*	*Alberta, Canada*
Baum & Ham (2009)[a]	Jul - Sep	92.1 ± 20.6	—	38	N/A	Kansas, USA
Staebler et al. (2009)	*Sep*	*64 ± 4[h] to 88 ± 5[h]*	*204.0[h] to 278.4[h]*	*—*	*WT*	*Alberta, Canada*
Staebler et al. (2009)	Sep	84 ± 115[i]	—	—	—	Alberta, Canada
Todd et al. (2009)	Annual	—	82 to 149	51 to 69	—	Texas, USA
Rhoades et al. (2010)	Summer	77.2 ± 7.2	95.3 ± 9.0	49.5	WT	Texas, USA
Rhoades et al. (2010)	Winter	40.2 ± 11.0	66.5 ± 15.7	40.5	WT	Texas, USA
Rhoades et al. (2010)	Annual	70.7 ± 19.8	85.3 ± 26.5	48.8	WT	Texas, USA
Todd et al. (2011)	*Annual - 1[f]*	*—*	*115.3*	*59*	*WT*	*Texas, USA*
Todd et al. (2011)	*Annual - 2[f]*	*—*	*79.8*	*52*	*WT*	*Texas, USA*
Todd et al. (2011)	*Summer (1&2)[f]*	*—*	*130.5*	*62*	*WT*	*Texas, USA*
Todd et al. (2011)	*Winter (1&2)[f]*	*—*	*65.5*	*48*	*WT*	*Texas, USA*
Denmead et al. (2014)	*Sum, Wnt (1&2)[f]*	*110.0 ± 41.7[j]*	*139 to 192[k]*	*—*	*WT*	*Qns & Vctr, AUS*
McGinn et al. (2016)	*Sum, Fall*	*50*	*85*	*39*	*WT*	*Alberta, Canada*
Yang et al. (2016)	*Annual - 1[f]*	*—*	*57.6*	*25*	*WT*	*Jing-Jin-Ji, China*
Yang et al. (2016)	*Annual - 2[f]*	*—*	*50.8*	*26*	*WT*	*Jing-Jin-Ji, China*
Yang et al. (2016)	*Summer (1&2)[f]*	*—*	*62.5*	*27*	*WT*	*Jing-Jin-Ji, China*
Yang et al. (2016)	*Winter (1&2)[f]*	*—*	*40.4*	*18*	*WT*	*Jing-Jin-Ji, China*
Overall means	Summer	69.7 ± 26.0	128.5 ± 52.3	54.1 ± 12.1		
	Winter	32.4 ± 19.2	47.0 ± 27.5	34.4 ± 10.5		
	Annual[†]	64.1 ± 35.9	92.9 ± 57.5	46.1 ± 14.7		

[a] Daytime sampling only
[b] Calculated from mean concentration (kg d^{-1}) and cattle population
[c] Calculated from N:P ratios
[d] Estimated from kg d^{-1} and pen area
[e] Southern Great Plains region (Oklahoma and Texas)
[f] Studies that researched two different feedlots
[g] Estimated from EF and cattle population
[h] From hourly EFs
[i] From aircraft measurements
[j] Calculated from kg ha^{-1} d^{-1}
[k] Calculated from tonne d^{-1} and mean cattle populations
[†] Annual is mean of summer and winter for same study except where explicitly reported

2.6 Figures

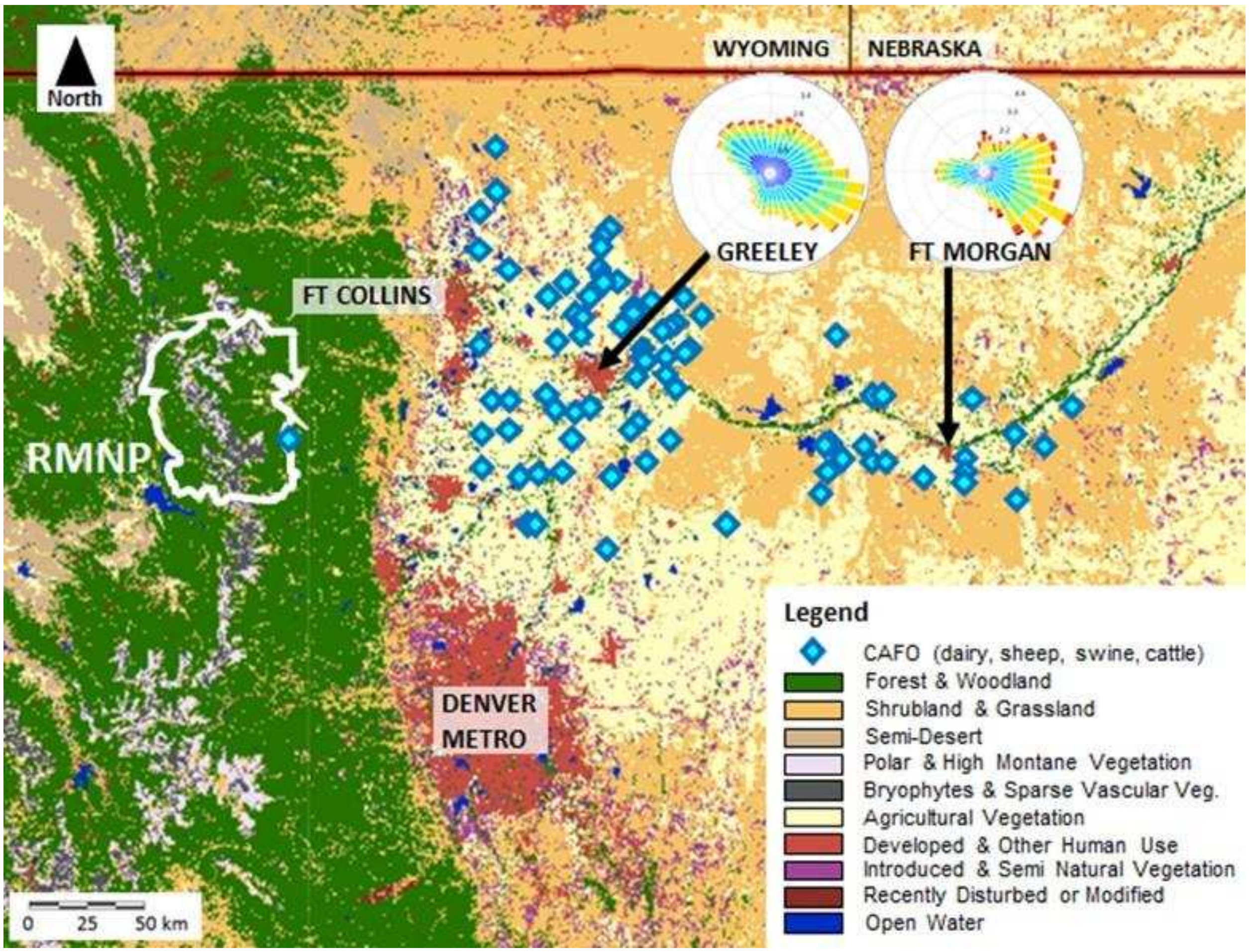

Figure 2.1. Land use map for Colorado Front Range (USGS, 2017), with major cities and known large CAFOs (beef and some sheep feedlots with 1,000+ head or dairies with 700+ head). July 5-year wind roses (for cities Greeley and Fort Morgan, locations designated by black arrows) show summertime winds near areas of high CAFO concentration tend to have a significant upslope component. Note proximity of urban (reds/purple) to forest/woodland (green) and high instances of agricultural vegetation (light yellow) amidst grassland (orange), where most CAFOs reside.

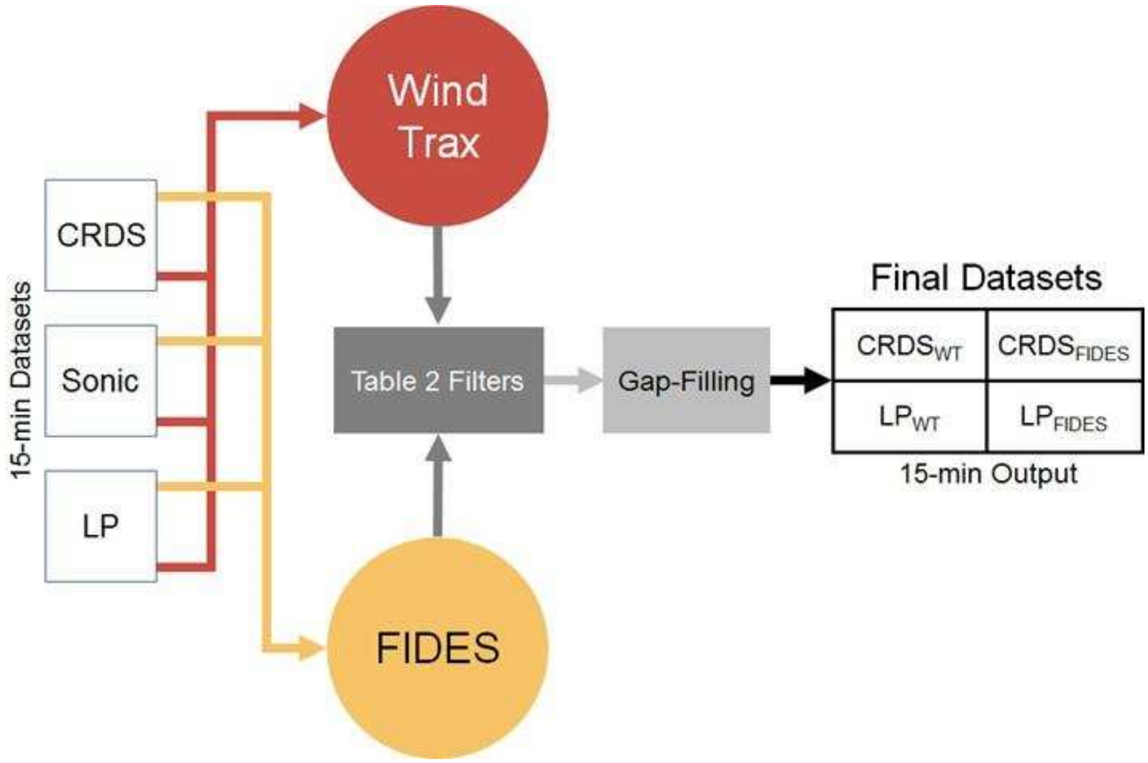

Figure 2.2. Process for producing final emissions. Squares represent datasets (CRDS = cavity ring-down spectroscopy analyzer, Sonic = sonic anemometer, LP = long-path laser). Circles represent inverse models (WT = WindTrax, FIDES = Flux Interpretation by Dispersion and Exchange over Short Range). Filled rectangles are processing procedures. Open rectangles are final datasets of each sensor and model.

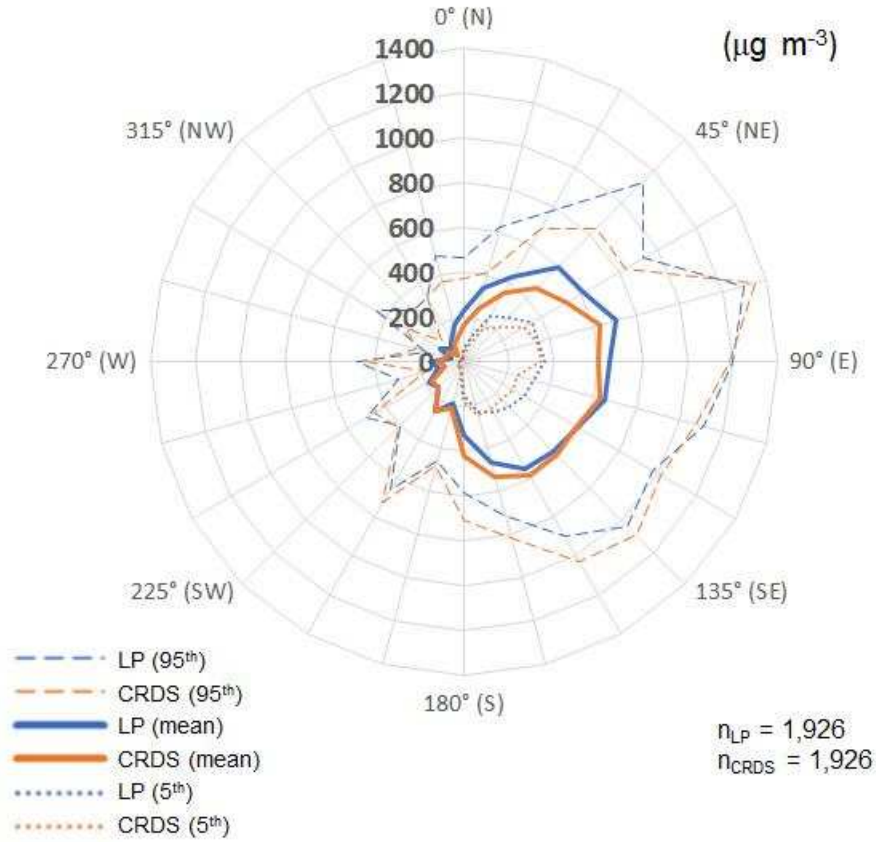

Figure 2.3. Sector plot of 15-minute mean concentration (μg m^{-3}) for LP (blue) and CRDS (orange); corrected for height difference and STP. Bold lines are mean concentrations for each wind direction sector. Dotted and long-dashed lines are 5th and 95th percentiles, respectively, for each sector. Wind direction sectors are in 15° increments. Sample sizes inset in lower right. Concentration data were filtered for u* and L only (to remove unfavorable environmental conditions such as low turbulence and extreme stabilities).

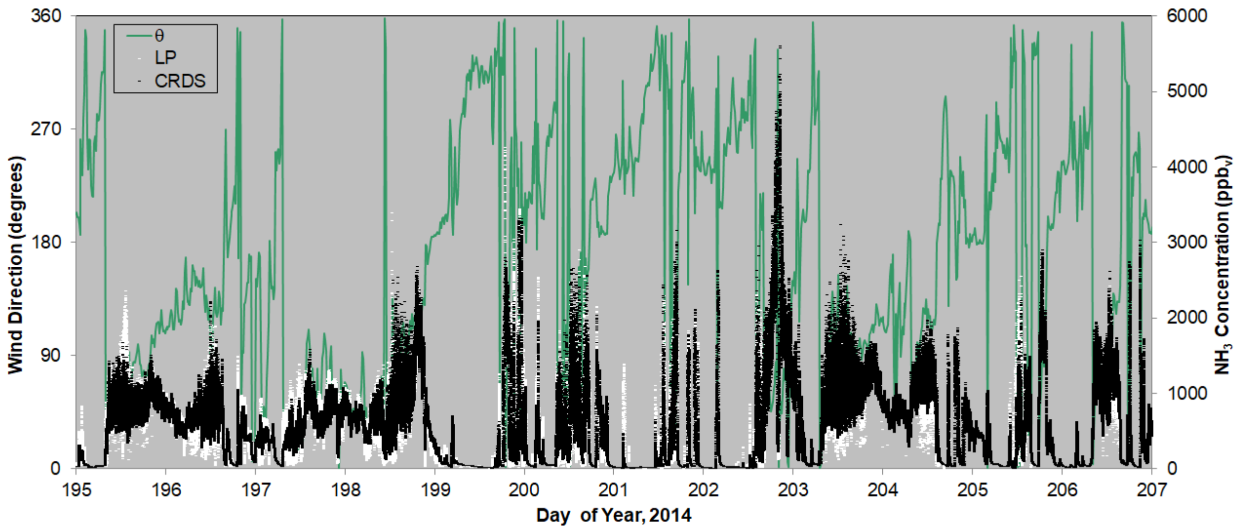

Figure 2.4. Time series of wind direction (green, left axis) with respect to LP (white) and CRDS (black) instantaneous concentration samples (right axis) for a 12-d period with relatively high data retention. Filters for LP include $R^2 > 0.9$ and LVL > 1,800. Number of samples (n_{LP}, n_{CRDS}) inset, upper left. Concentrations corrected for difference in sampling height and STP. No additional filtering applied regarding θ, u*, or L.

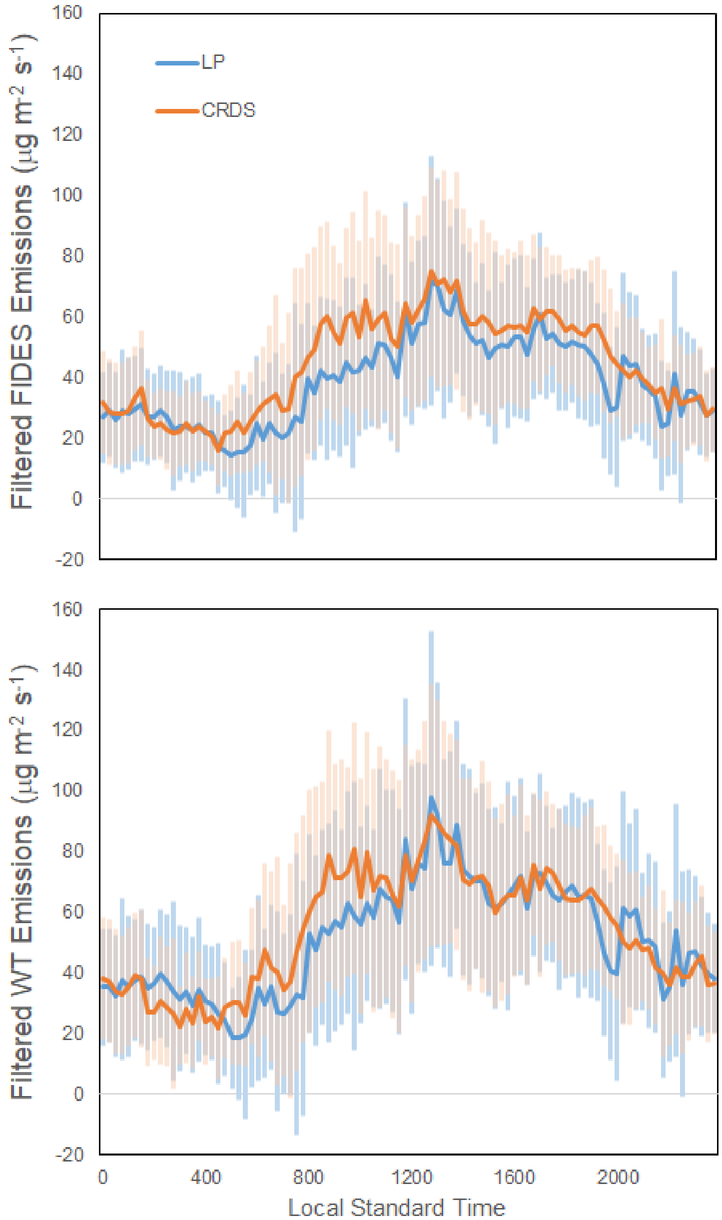

Figure 2.5. Mean diurnal composites and standard deviations (DOY 191 to 269) of filtered emissions by sensor (blue is LP, orange is CRDS) and inverse model (top: FIDES, bottom: WT).

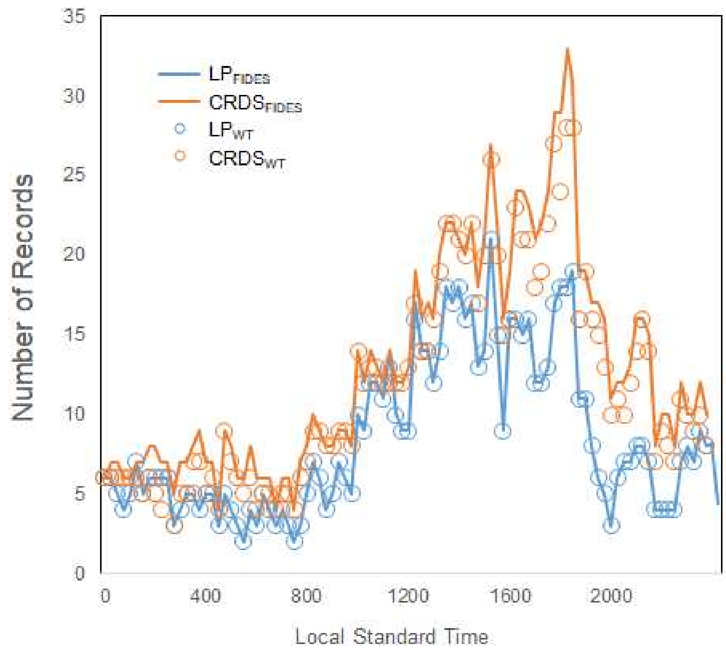

Figure 2.6. Diurnal composites of total observations per 15-minute record for filtered data throughout the study (DOY 191 to 269). The data in Fig. 2.5 is based off these record counts.

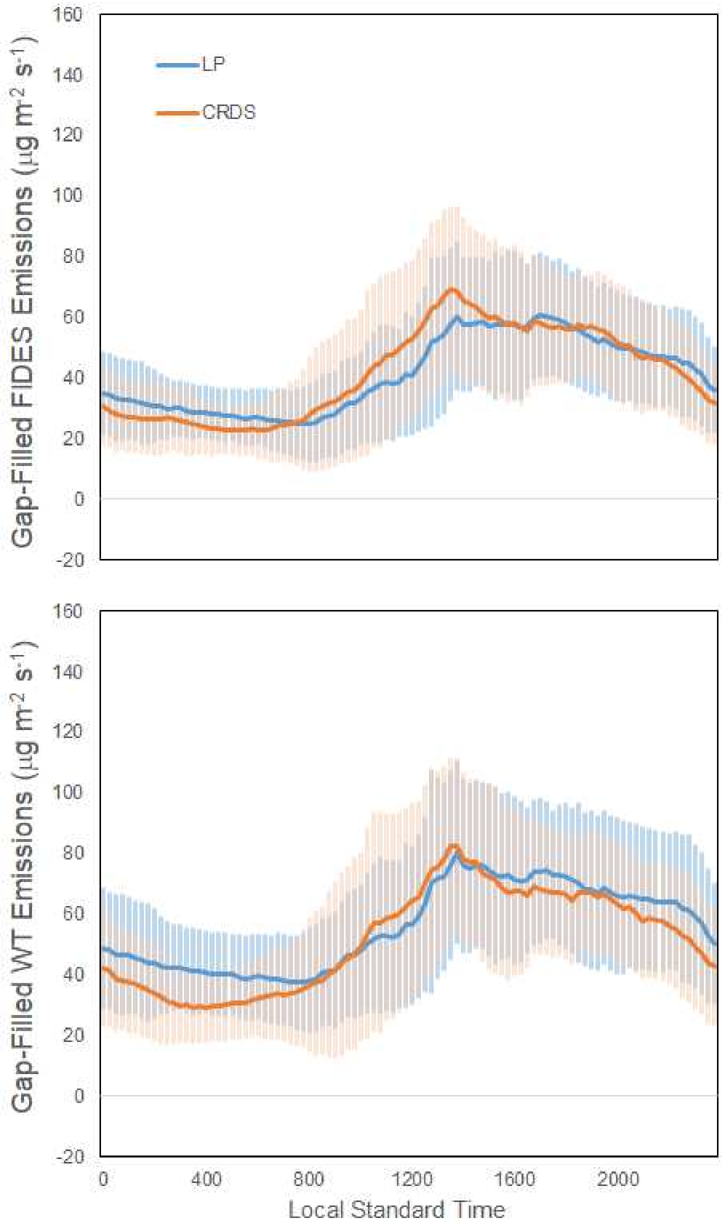

Figure 2.7. Mean diurnal composites and standard deviations (DOY 192 to 268) of gap-filled emissions by sensor (blue is LP, orange is CRDS) and inverse model (top: FIDES, bottom: WT). Presented with same y-limits as Fig. 2.5 for comparison. Due to the gap-filling procedure, first and last days of the study were omitted from these composites.

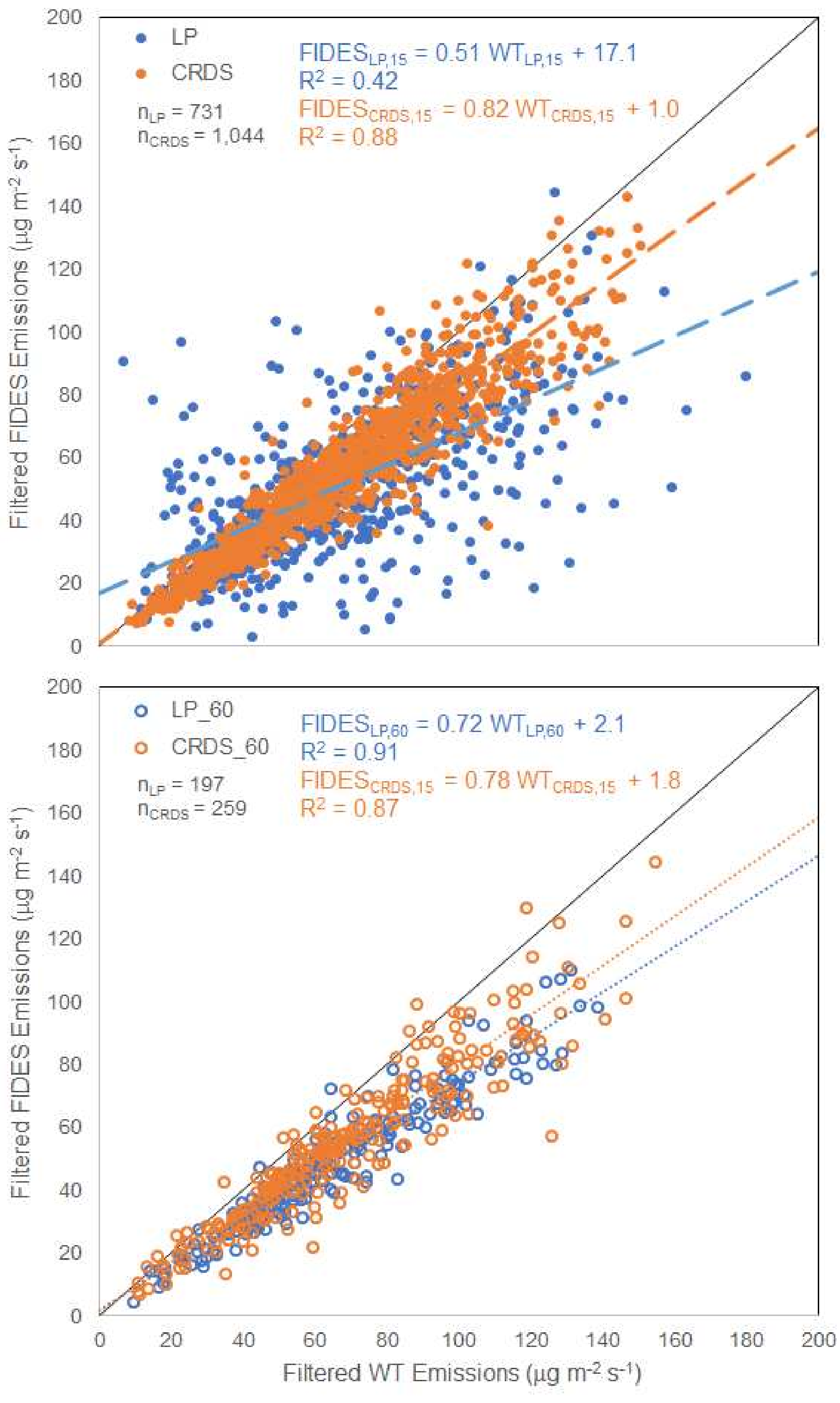

Figure 2.8. Scatterplot showing effect of averaging interval on correlations between FIDES and WT results for each sensor (LP = blue, CRDS = orange). Top: filtered 15-minute emissions output (i.e., LP_{15}, $CRDS_{15}$). Bottom: filtered hourly emissions output (i.e., LP_{60}, $CRDS_{60}$). Inset in color are regression equations with R^2 value for each sensor and each averaging interval. Annotations below legend show sample sizes.

CHAPTER 3 – METHANE EMISSIONS FROM AN ANAEROBIC MANURE LAGOON AT A COLORADO DAIRY: FLUX ESTIMATES BY EDDY COVARIANCE AND INVERSE MODELING

3.1 Introduction

Methane (CH_4) is a powerful greenhouse gas (GHG), comprising 17% of the total radiative forcing from all globally-mixed GHGs (Allen, 2016). Atmospheric CH_4 molecules can lead to formation of tropospheric ozone, a powerful oxidizer (Seinfeld and Pandis, 2016). Agriculture is a large contributor to the methane budget, with the greatest portion coming from livestock enteric fermentation (i.e., CH_4 from digestive processes in ruminants like cattle, sheep and goats) and manure management at confined feeding operations (e.g., dairies, beef feedlots). Enteric fermentation from cattle depends mostly on the amount and type of feed consumed and is the major component of GHG emissions from confined feeding (beef feedlots, dairies) and grazing livestock. However, enteric CH_4 from modern dairy cattle is typically not the major source of GHGs at dairies. Despite higher protein content in their feed (equating to more enteric emissions per lactating cow), there is a higher impact per head from manure management at dairies than for feedlots, for example. Though outnumbered in the US by beef cattle on feed (17.5% higher feedlot population; USDA, 2017a, 2017b), dairy cattle account for over half of the contribution of manure management to the US annual methane inventory from all livestock types (ruminant and non-ruminant), with 32.2 out of the total 61.2 million metric tons of carbon dioxide equivalent emissions in 2016 (USEPA, 2016).

To accommodate demand, the US dairy industry has experienced rapid growth in recent decades, causing a 119% increase in CH_4 emissions from manure management from 1990 to 2014 (USEPA, 2016). Especially at larger dairies (1,000+ lactating cows), cows are often housed in free-stall barns between milkings where waste is commonly flushed from barn floors with water. At many operations, the resulting liquid manure slurry is eventually pumped into open-air, anaerobic lagoons (as opposed to dry manure storage). Based on organic loading, these liquid storage systems can be strong local sources of CH_4 (Hart and Turner, 1965). Methane is produced when materials of high organic matter content are decomposed into volatile solids in low-oxygen (O_2) environments (due to rapid consumption of O_2 by microbial populations in the lagoon), with liquid storage of slurries typically showing the largest corresponding CH_4 emissions (USEPA, 2016).

The dairy industry is an excellent example of best management practices resulting in lower overall emissions, where North America leads the world in most efficient dairy systems (NDFP, 2017). The efficiency of US dairies has changed dramatically over time, where in 2007 dairies produced the same amount of milk as in 1944 with 21% fewer cows, 23% less feed, 35% of the water, on 90% less land (Capper et al., 2009). Unfortunately, much uncertainty belies current inventories for manure management, with much literature suggesting refinement of CH_4 inventories for dairy lagoons, specifically (Johnson and Ward, 1996; Kaharabata et al., 1998; Miller et al., 2013; Owen and Silver, 2015; Turner et al., 2016; VanderZaag et al., 2014), with a strong need to quantify seasonal variability from these sources (Todd et al., 2011).

Emissions from anaerobic lagoons should be investigated further because studies that include direct measurements of emissions are limited, with some research indicating that lack of data results in an underestimate of manure management contribution to the GHG budget (Bjorneberg et al., 2009; Leytem et al., 2017; Owen and Silver, 2015). An extensive summary of field-scale studies showed anaerobic lagoons had the highest global warming potential per head at most dairies, with CH_4 the primary component of GHG emissions (Owen and Silver, 2015). Additionally, current USEPA and IPCC models for CH_4 emissions from manure management at dairies, specifically, might underestimate actual emissions by up to 130% (Baldé et al., 2016; Lory et al., 2010). This is attributable to large ranges in reported emissions factors (EFs), determined from a small sample of field studies (Leytem et al., 2017; Owen and Silver, 2015). Such issues can make accurate modeling of emissions difficult as well (Gao et al., 2009; Grant and Boehm, 2015).

Emissions factors convert the number of dairy cattle (i.e., head [hd]) to mean farm-scale emissions on a per day or per annum basis. In North America, CH_4 EFs for liquid manure range several orders of magnitude—from 4.7 to 1,028 g hd^{-1} d^{-1} (Leytem et al., 2017). Many countries use the IPCC (1996) CH_4 EFs for manure management for dairy cattle, which are given from Tier 1 (simpler, more general climate-based approach) and Tier 2 methods (more complex approach with many user-defined parameters). Based on a temperate climate region, dairy cattle manure management from the Tier 1 approach (Table 4-4 in IPCC, 1996) has general annual EFs of 148 g hd^{-1} d^{-1}. Owen and Silver (2015) performed an IPCC Tier 2 analysis using parameters typical of dairies in Idaho, New Mexico, Texas and North Carolina (usually these states are similar in dairy operation to Colorado) and found annual EFs for anaerobic lagoons in these regions of 893 g hd^{-1} d^{-1}, while their summary of 9 field studies shows annual EFs averaging 1008 g hd^{-1} d^{-1}. High variability in EFs is likely due to variations in operation management, nutrient rationing, and climate; yet manure management likely has the largest effect on the range of EFs seen in literature (Owen and Silver, 2015). The lack of in-situ data causes difficulties in determining patterns between operational, animal, and climatic influences.

Advances in instrumentation have allowed for direct measurement of GHG from methane sources such as livestock via eddy covariance (EC) (Dengel et al., 2011; Felber et al., 2015; Prajapati and Santos, 2017; Taylor et al., 2017). These measurement systems are well-suited to such environments where techniques such as chamber methods (which typically had small spatial coverage) or emissions estimation approaches (e.g., inverse dispersion modeling) were previously required to approximate emissions. There is little literature on EC from an anaerobic lagoon (Sokol et al., 2016), and such data from a long-term study would be valuable to help further elucidate emissions characteristics of these multifaceted CH_4 sources.

Though EC has not been utilized much at anaerobic lagoons, much current research on lagoon emissions is a result of inverse dispersion modeling using the backward Lagrangian stochastic (bLs) method which uses wind and concentration data to infer downwind emissions from known source areas (Flesch and Wilson, 2005). Many groups have used this approach at livestock operations such as beef feedlots for ammonia emissions (Flesch et al., 2007; Shonkwiler and Ham, 2017; Todd et al., 2008), while others have had further success at dairies with CH_4 emissions from bLs (Baldé et al., 2016; Bjorneberg et al., 2009; Gao et al., 2011; Grant and Boehm, 2015; Grant et al., 2015; Leytem et al., 2011, 2013, 2017; McGinn and Beauchemin, 2012; Todd et al., 2011; VanderZaag et al., 2014). It is important to add quality datasets to the body of knowledge, especially a major emissions source such as anaerobic livestock lagoons.

The objectives of this research were to (1) make long-term measurements of CH_4 emissions from a large, anaerobic dairy lagoon using eddy covariance (~20 months); (2) compare estimates of emissions from a common bLs model to actual emissions from eddy covariance; and (3) determine emissions factors for a large dairy lagoon in Colorado, USA and compare to EFs for anaerobic lagoons from IPCC (1996) and others in the literature.

3.2 Materials and Methods

3.2.1 Site characteristics

Research was conducted at a dairy with 1,400-head of lactating cows (elevation 1,600 m) in Larimer County, Colorado with an annual milk production of 13,300 kg per lactating cow. Data were collected from 03 Mar 2012 to 17 Oct 2013. The dairy included four covered free-stall barns for lactating cows, a milking parlor, and several pens for non-lactating cows and calves (Fig. 3.1). Manure from barns and the milking parlor was removed three times daily using a fresh water flush system. The resultant slurry was routed by concrete-lined basins to a 3.94-ha anaerobic lagoon with a depth of 3 m (~170-200 m x ~250 m, see Fig. 3.1). Prior to entering the lagoon, the slurry was diverted through a settling basin which lowered the total solids entering the lagoon to 3-5%. Dry composting of solids from the settling basin and manure from non-lactating cow pens was operated in the area east of the lagoon (Fig. 3.1). The lagoon had a partial crust (floating organic layer) including several large mat segments throughout the study (Fig. 3.2). No methane hotspots such as other livestock facilities were nearby.

3.2.2 Instrumentation and data processing

The EC equipment was placed on a trailer-mounted tower with a motorized tram for achieving the final deployment height of 6.2 m above the lagoon surface (Fig. 3.2) on the south downwind edge. Wind rose plots showed the prevailing wind direction was from the north (Fig. 3.3) (WRCC, 2011). Fetch from the EC tower to the NW far lagoon edges was 168 to 250 m, while dairy areas NE of the EC tower had fetch beyond 400-500 m. Recent research regarding EC footprints suggests that these shorter fetches to the NW are adequate for exclusive sampling of the centroid of the lagoon surface (Arriga et al., 2017). Methane concentrations (i.e., [CH_4]) were sampled using an open-path CH_4 analyzer (LI-7700, Licor, Inc., Lincoln, NE, USA). A sonic anemometer (sonic) (CSAT3, Campbell Scientific, Inc., Logan, UT, USA) sampled turbulent velocities in both horizontal (u, v) and vertical (w) dimensions and sonic temperature, allowing calculation of horizonal wind speed (U), wind direction (θ), friction velocity (u*, m s^{-1}), Obukhov length (L, m), and roughness length (z_0, m). Additionally, a temperature/relative humidity (RH) probe (CS500, Vaisala Corp., Helsinki, Finland) provided ambient T and RH, and lagoon temperature (T_{lagoon}) was sampled with a weighted temperature probe (109 temperature sensor, Campbell Sci.) at the bottom of the lagoon in the sludge layer ~5 m from the edge of the lagoon in the tower's sampling footprint.

All parameters were sampled at 20 Hz and post-processed to determine 30-minute fluxes of CH_4. Corrected fluxes were found with the software package EdiRe (v1.5.0.32., R. Clement, University of Edinburgh) using standard EC methods (Baum et al., 2008). Raw time series data corrections including despiking, lag removal, frequency response corrections (Massman, 2000; Moore, 1986), sonic-temperature sensible heat flux corrections for humidity (Schotanus et al.,1983), and density corrections (Webb et al., 1980). Corrected [CH_4] from this process were used for concentration analyses (section 3.3.2). Final, 30-min fluxes of CH_4 (F_{CH_4}, mg m^{-2} s^{-1}) were used for emissions analyses (section 3.3.3). Fluxes were split into two source areas based on θ : lagoon source (275° < θ < 5°) and NE footprint contributions (10° < θ < 90°; includes far-right edge and inlet of lagoon, compost area, some enteric emissions from free-stall barns, and settling basins) (Fig. 3.1). Additionally, data were partitioned for the field to the south (100° < θ < 260°) that was growing corn during the summer and fallow during the winter. There was exclusion of data with θ from 5° to 10°, 90° to 100°, and 260° to 275° because these directions occurred at transitions between sources and including data from these directions would have introduced additional uncertainty. All final EC data were filtered according to Table 3.1. Additionally, 30-min sonic and [CH_4] data were used for input into an inverse dispersion model to estimate CH_4 emissions for comparison to EC (see next section).

3.2.3 Inverse-dispersion analysis for lagoon

When an in-situ method like EC is not in use, concentration and wind measurements can be used with an inverse dispersion model to obtain estimates of emissions. A popular approach is the backward Lagrangian stochastic (bLs) method which takes wind, concentration, and site/sensor properties to determine where the particles originated that impacted a given set of scalar readings from various sensors (Flesch and Wilson, 2005; Shonkwiler and Ham, 2017). For this study, a commonly-used bLs software package called WindTrax (WT, Thunder Beach Scientific, Halifax, Nova Scotia, Canada), was implemented to find estimates of CH_4 flux ($F_{CH_4,WT}$) based on inputs of u*, z_0, L, θ, source (i.e., lagoon) perimeter, sensor locations and heights, [CH_4], C_{bgd} (in ppm_v), and component wind statistics (σ_u/u*, σ_v/u*, σ_w/u*). Other major user-defined variables in this study were total particle count (1×10^6), constant z_0 of 2.85 cm (calculated from sonic data), and mean C_{bgd} (as the 5th percentile of monthly [CH_4]) varying from 2.27 to 2.50 ppm_v). Emissions estimates from WT were filtered according to the criteria in Table

3.1, with the additional criterion of touchdown ratio (TDR; i.e., percent of particles covering the lagoon source in WT).

3.2.4 Gap-filling

Because measurements were located on the lagoon edge and the dairy's locale experiences extremely bimodal diurnal wind patterns, major gaps occurred due to wind direction (θ not from source). Additional gap-filling occurred from lack of stationarity, low wind speeds, or lack of turbulent conditions (low u*); which disallowed EC measurements of the source areas. Often these conditions would occur for the same times of day for several consecutive days (especially θ shifts and low u*). Further complications arose when longer gaps occurred due to instrument failure or power loss. Results pertaining to data loss due to varying issues is discussed in section 3.3.3.2.2. Regardless of reason, gap-filling must be done to calculate cumulative emissions (i.e., overall CH_4 loss to the atmosphere from a site).

The most common gap-filling method utilized in micrometeorology is called mean diurnal variation (MDV). With MDV, values for gaps are calculated as the mean of available data corresponding to when the gap occurred. For example, if a gap occurred at noon, MDV would select a moving window of several days and fill in the gap as the mean of all noon-time data for the moving window around the gap. There are many benefits to using MDV for CH_4 emissions and other ecological and pollutant data. Amongst a heavily-reviewed area of research such as gap-filling eddy covariance and other micrometeorological emissions data, MDV performs moderate-to-well when compared to other approaches, especially considering its algebraic simplicity (Falge et al, 2001). Using MDV for lagoon CH_4 emissions is reasonable because fluxes are strongly temperature dependent and thus exhibit diurnal patterns (Husted, 1994; Montes et al., 2013).

Often MDV is applied with two moving windows. The first is the hard window (measured in days), referring to the range of days (±) around the missing gap that the MDV average will encompass. The second is the soft window (measured in hours), describing how many records around the time of the missing gap to average on each day within the hard window. In this study, the hard window for all gap-filling for CH_4 fluxes was 7 days and the soft window used was 6 hours. All single 30-min gaps were filled by linear interpolation. Additional gap-filling results (such as reasons attributable to gaps) are discussed in section 3.3.3.2.2.

3.3 Results and Discussion

Because most of the anaerobic emissions occur when the microbial substrate in the lagoon's sludge layer are above 15°C (DeSutter and Ham, 2005), the majority of analyses were done on a seasonal basis. Seasons were split based on month (MAM = spring, JJA = summer, SON = autumn, DJF = winter) starting in the spring of 2012 and ending in the autumn of 2013 for a total of 7 seasons representing 19.5 months.

3.3.1 Environmental conditions

Daily mean temperatures mostly exceeded 30-year normals, though deviation from normal depended on season (WRCC, 2011). Spring 2013 was the only season below normal (1.8°C less than normal). Warmest periods were 3.5-4.9 °C above normal: autumn 2013, spring 2012, and summer 2012. Autumn 2012 and summer 2013 were only slightly above normal. Winter was closest to climate normals (+0.3°C). Precipitation amounts were less than normal for every season except the final one (SO 2013), with 92 mm more than normal. The largest deficits (i.e., driest seasons; in mm from normal) were MAM 2012 (-102), JJA 2013 (-70), and JJA 2012 (-55); with smaller deficits for SON 2012 (-31), DJF 2012-13 (-31), and MAM 2013 (-18). In general, less precipitation and higher mean temperatures than normal would equate to higher than normal evaporative demand especially during the summer and autumn months when microbial decomposition of slurry, and thus emissions (also called fluxes) of CH_4, peaks. The annual wind rose (Fig. 3.5) shows a high frequency of northerly winds, putting the EC tower downwind of the lagoon 55.7% of the time and allowed for 168 to 250 m of fetch. The NE contribution was much less (>10% of the time) with a fetch beyond 400 m.

3.3.2 Methane concentrations

Final 30-min [CH_4] from the EC data showed a strong dependence on θ and thus, source region (Fig. 3.4). After applying filters for each CH_4 source area (see Table 3.1), overall study mean [CH_4] was 2.9 ppm_v above background for the lagoon source and 2.5 ppm_v above background for the NE sectors of the EC footprint. There were occasional large concentrations (>20 ppm_v) for the field source which were associated with high standard deviations of θ (σ_θ; data not shown). These data points represent outliers from the field source but may be realistic due to wide sweeping of the wind (usually large σ_θ are also associated with slower-moving winds, which can also churn up large, less well-mixed eddies). During these conditions, the EC sensors could be detecting scalar ramps, a result of coherent turbulent structures which can develop from strong stability and/or large sweeps or changes in the wind (Paw U et al., 1992).

Summer and autumn (i.e., JJA and SON) had the highest concentrations of all seasons (Fig. 3.5), with the highest values again typically associated with NW and easterly θ-sectors (Fig. 3.6). For the entire study, the mean [CH_4] tended to increase in the summer and autumn (from about DOY 170 to 340; Fig. 3.9) and remained low for winter and spring, with occasional outliers (possibly owing to the scalar ramping issue discussed previously). The lagoon typically had the highest associated concentrations, with NE sectors second and the field mostly showing background levels (though this dataset also trends higher in the warm season due to higher ambient temperatures). The second summer and autumn experienced some data loss due to site operations, which is why there are noticeable gaps in 2013's warm season. Values for all seasons fell to near-background for southerly wind sectors whose contribution is mostly from the field (Fig. 3.6). The 95^{th} percentile of [CH_4] was affected by spurious high concentrations that would occasionally occur for southerly wind directions as methane from the lagoon likely circulated back over the tower during light variable winds.

Figure 3.7 compares a given [CH_4] data point with its corresponding mean wind speed (U) organized by time of year and likely source (i.e., lagoon (275° < θ < 5°) or NE sectors (10° < θ < 90°) to the north, or field (100° < θ < 260°) to the south). The scatterplots have similar patterns with some notable features. During colder months (spring and winter), 30-minute concentrations were usually lower for a given range of wind speeds. The summer and autumn showed a greater amount of higher concentration values for the lagoon and NE sources at lower wind speeds, while the field source tended to accumulate values near background, regardless of wind speed. The relationship between [CH_4] and U were best described by exponential or power functions with better regression fits (i.e., R^2, the goodness of fit) for the lagoon (R^2 = 0.20 to 0.24) than NE sectors or the field (R^2 = 0.10 to 0.28 and R^2 = 0.02 to 0.04, respectively) (data not shown). This power relationship is what one would expect from Monin– Obukhov similarity relationships (Monson and Baldocchi, 2014; Philip, 1959). To further test this, WT was run solving for concentration at the EC tower using the lagoon with incremented fluxes and wind speeds specified (rather than the reverse to determine flux estimates from concentration, the results of which are discussed in section 3.3.3.1). Results show a power relationship between [CH_4] and U varying with magnitude of emissions (Fig. 3.7).

As expected, higher concentrations were observed during low wind speeds, a feature also noted by Kaharabata et al. (1998) at both swine and dairy slurry tanks in Canada. Note, [CH_4] at 6.2 m as measured by this system may vary significantly from those closer to the surface. Todd et al. (2011) observed concentrations less than 2m above the surface from 3 to 12 ppm_v with a mean of 5.6 ppm_v over a dairy lagoon with similar operations in New Mexico in summertime using tunable diode lasers (TDLs). Bjorneberg et al. (2009) used an open-path FTIR spectrometer at about 3 m height and found highest concentrations associated with dairy cattle in pens, then the wastewater storage pond. Mean concentrations from the storage pond were larger in the summer; however mean concentrations were elevated over measured upwind C_{bgd} by only 0.11 to 0.49 ppm_v (around 1.9 to 2.2 ppm_v mean storage pond [CH_4] over a several-day sampling period each season). Grant and Boehm (2015) used two different systems to sample a Midwestern dairy lagoon in November and found a range of 2.2 to 6 ppm_v for a FID/SOPS system (combined flame-ionization detector and synthetic open-path system) and 1.9 to 9 ppm_v from a TDL. Miller et al. (2015) observed peaks of 80 ppm_v downwind of an anaerobic lagoon on a dairy in the San Joaquin Valley using mobile eddy covariance.

3.3.3 Methane emissions

Regardless of the technique used to estimate flux, methane emissions were very seasonal and strongly correlated with the temperature of the sludge layer on the bottom of the lagoon (Fig. 3.8). Note, the mass of organic matter entering the lagoon each day was essentially constant over the entire study period and water levels were also very stable. Thus, the pattern of emissions was clearly driven by the effect of temperature on microbial dynamics (populations of acetogens and methanogens and their respective activities), a mechanism noted in other studies of anaerobic manure lagoons (DeSutter and Ham, 2005). Emissions[8] (F_{CH_4}) remained low (<10 g m^{-2} d^{-1}) in late autumn (Nov) through late spring (May) and then increased rapidly in early summer when lagoon temperature reached about 10°C. Peak emissions (>~70 to ~110 g m^{-2} d^{-1}, depending on the technique employed, see next section) occurred between DOY 200 and 260 after the temperature of the lagoon's sludge/biomat[9] reached about 18-20°C (Fig. 3.8). Similar features were noted at a swine lagoon in nearby Kansas by DeSutter and Ham (2005). Each warm season seemed to have a highly productive period where daily emissions peaked to tenfold over 2 months (from mid/late Jun to early-Aug) and then remained high but tapered off

[8] After gap-filling; refer to sections 3.2.4 and 3.3.3.2.2.

[9] Biological material (i.e., the community of acetogens and methanogens living at the base of the anaerobic system; DeSutter and Ham, 2005).

for about 2 months (mid-Aug to mid/late-Oct) until a sharper decline (measured the first fall, see "measured" data) and return to quiescent cool season conditions. The springtime increase is due to the lagoon's sludge layer heating up to temperatures favorable for microbial activity and thus increased methanogenesis, causing more ebullition to the surface (DeSutter and Ham, 2005). There is also ample substrate for the microbes in the spring because organic matter accumulates in the lagoon during the winter months. In many ways, a dairy lagoon is analogous to a continuous feed batch reactor as employed in chemical engineering where, in this case, the process is governed by seasonal changes in temperature.

3.3.3.1 Comparison of eddy covariance and inverse modeling estimates of methane flux

Daily estimates of emissions by WindTrax (WT) were higher than those measured by EC (Fig. 3.8). Based on diurnal composites (see next section; not shown for WT), the ratio of emissions estimates from WT to F_{CH_4} measured by EC was 1.56 (Table 3.2). The difference in fluxes could be explained by several things. First, advection or heterogeneous surface emissions could have had an impact on how WT predicted emissions versus what the EC system directly measured (Grant and Boehm, 2015). Second, parameterization in WT could be partially responsible. For example, lagoon size was slightly altered for several WT runs to determine other reasons why the difference would be so large, but there was little effect on emissions using the smallest and largest possible lagoon sizes (based on minimum and maximum depths from the edge) (less than 1% difference in WT output, not shown). Third, footprint mismatch could be responsible, where EC has a smaller sampling footprint than WT (thus, the EC system is biased toward emissions relatively close to the tower; Arriga et al., 2017) and was likely measuring fluxes with high influence from the edges of the lagoon, while WT estimates were more strongly influenced by areas farther upwind near the center of the lagoon. DeSutter and Ham (2005) showed an effect of reduced emissions near edges of anaerobic lagoons. This spatial mismatch may also explain the differences between WT (larger due to center of lagoon) and EC (smaller due to more edge effects).

Especially when inhomogeneities exist, emissions estimates (i.e., WT) can deviate drastically from measured emissions (i.e., EC). Grant and Boehm (2015) studied the effect of partitioning source areas of a rectangular lagoon smaller than the one in the current study and found that emissions were reduced by 57% when WT estimated emissions for a two-source lagoon versus specifying a one-source lagoon in the software. This indicates that even small lagoons experience inhomogeneities that can affect overall emissions interpretation. Considering the changes in estimates seen by Grant and Boehm, the difference between WT and EC in the current study could be the result of heterogeneity. Deploying multiple towers around the periphery of the lagoon or using a mobile sampling platform would be one way to investigate this question.

Gao et al. (2009) used a controlled release system for CH_4 to look at the effect of stability on WT F_{CH_4} estimates and found that WT tends to overestimate actual emissions during stable conditions, be most accurate near neutral stability, and to underestimati during unstable conditions. Ro et al. (2013) also noted these overestimation (underestimation) tendencies of WT during stable (unstable) environments in a similar controlled-release study of CH_4 over an area with lagoon-like properties. To test these findings in the current datasets, filtered 30-minute data were pooled by season between the EC and WT datasets for times when both had matching output. The seasonal mean percent difference of filtered 30-minute output for the lagoon (not the composites) were then compared based on the stability classification (Fig. 3.9). Similar to Gao et al., WT tended to overestimate EC for all measurements during stable environments, while unstable conditions mostly tended to underestimation. There was much scatter in the comparisons (see error bars in Fig. 3.9), with neutral conditions having some overestimations similar to stable conditions, with the unstable-near neutral atmosphere being the most accurate environment for WT when compared to EC. There were also more data for stable conditions than unstable for the study (see sample sizes in Fig. 3.9 caption). These differences lend further credence to the presence of spatial heterogeneity in CH_4 emissions from the surface for these systems and possible sampling footprint mismatch, whereby a more homogenous surface should result in closer values between WT and EC. Also, this verifies current research that WT accuracy is also tied to atmospheric stability, which should be considered when interpreting emissions estimates. Given stable conditions prevailed more so than neutral or unstable conditions at the lagoon site in this study, this would explain the overall overestimation of F_{CH_4} from WT when compared to the EC measurements and would also confirm the findings of Gao et al. (2009) and Ro et al. (2013).

3.3.3.2 EC-based emissions

3.3.3.2.1. By source

When filtered according to the criteria in Table 3.1 and plotted based on θ sector, EC-based CH_4 emissions (Fig. 3.10) had similar seasonal patterns to concentration radar plots. In the winter and spring, emissions were extremely low (>0.1 to 0.2 mg CH_4 m^{-2} s^{-1}), over one order of magnitude less than in summer. Particularly during summer and autumn, larger F_{CH_4} was associated with NW winds whose contribution was from the lagoon (275° < θ < 5°), or the NE sectors (10° < θ < 90°). Lower or near-zero emissions occurred for wind directions from the field south of the lagoon (100° < θ < 260°), except for sectors on the edges of the field's θ-range, again most noticeable in the summer and autumn (Fig. 3.9). There was some concern that fetch for EC might not be adequate when winds were more westerly. If this was the case, lower CH_4 fluxes would have been observed from the west when the sampling footprint extended beyond the lagoon. However, emissions along the NW arc from 270° to 360° showed no discernable decrease with more westerly θs suggesting fetch was adequate within the full arc. These data support recent experimental evidence that EC footprints are often quite small (Arriga et al., 2017; Baum et al., 2009)

Figure 3.11 shows the composite diurnal mean emissions of filtered 30-min F_{CH_4} final data from the eddy covariance system for the lagoon source and NE sectors: eastern edge of the lagoon, settling basin, compost pile, and some enteric emissions. The enteric component, though, is likely a very small component, noticeable from the difference between cool and warm months (Fig. 3.11d-f) (if the enteric portion was apparent, there would be more consistency between cool and warm months because enteric emissions don't change from season-to-season). Based on these composites, summary data were compiled in Table 3.2 (italic columns). Both springs and the one winter season showed similarly low values, while the first summer (i.e., 2012) was higher than the subsequent autumn and the second summer and autumn were almost identical (in 2013). This is likely because the first autumn included the end of Oct and all of Nov, which also reflected a return to quiescent flux conditions associated with lower total radiation and thus, temperatures (Park et al, 2006; VanderZaag et al., 2010; Wood et al., 2013); while the second year's autumn only included Sep through mid-Oct, the time of autumn with highest associated F_{CH_4}. Though there is a difference in both years (in terms of temperature and precipitation; see section 3.3.1), the relative mean diurnal difference from winter/spring to summer is the similar (about one order of magnitude; Table 3.2).

Table 3.4 shows CH_4 emissions and emissions factors for the lagoon in this study. Maximum daily (i.e., summertime) fluxes measured by EC (62.5 ± 10.7 g CH_4 m^{-2} d^{-1}) were higher than those seen by Todd et al. (2011) at a dairy in nearby NM (40 g CH_4 m^{-2} d^{-1}). Yearly emissions from the lagoon reported here were also slightly higher than annual emissions for a dairy lagoon in Southern Idaho (24.3 ± 12.0; Bjorneberg et al., 2009) versus our results of 29.3 ± 25.5 g CH_4 m^{-2} d^{-1}. Our seasonal values were similar to values for similar times of year for reported midwestern dairies (5.5 and 12.5 g CH_4 m^{-2} d^{-1} for two dairies in Nov by Grant and Boehm, 2015; and 4.3 to 23.2 g CH_4 m^{-2} d^{-1} for Oct-Jan and 3.1-34 g CH_4 m^{-2} d^{-1} for early spring and late summer to winter by Grant et al. 2015) while our yearly value from EC was slightly over half the mean determined by Owen and Silver (2015) for 9 dairy lagoon studies (29.3 ± 25.5 for the lagoon in this study versus their 56.6 ± 15.7 g CH_4 m^{-2} d^{-1}, respectively). Our EC results for spring and winter (7.0 and 6.1 g CH_4 m^{-2} d^{-1}, respectively) were similar to those in late winter by

Khan et al. (1997) (7.1 g CH_4 m^{-2} d^{-1}) who used micrometeorological mass balance at a dairy in New Zealand. Safely and Westermann (1992) used a floating chamber at a dairy tank in N. Carolina and found annual emissions (96 g CH_4 m^{-2} d^{-1}) nearly identical to our mean WT estimates for the summer (86.9 g CH_4 m^{-2} d^{-1}).

When mean annual WT emissions estimates (41.3 ± 37.3 g CH_4 m^{-2} d^{-1}; seasonal values in Table 3.4) are compared to literature, they are more similar to results on the higher end like those from Owen and Silver as well as from a tank in Japan (44.5 g CH_4 m^{-2} d^{-1} annual mean; Minato et al., 2013). Despite the discrepancy between WT and EC (see section 3.3.3.1 for more on this comparison), both values fall in the ranges given within the literature. This difference could be due to more than stability (Gao et al., 2009), but also could be attributable to theoretical issues such as heterogeneity of emissions from sources such as lagoon surfaces.

3.3.3.2.2. Gap-filling: Approximation of cumulative annual fluxes and emission factors

Many emissions datasets contain missing data (i.e., gaps), where gap-filling can account for 24 – 56% of the final data in livestock emissions studies (Flesch et al., 2007; Yang et al., 2016). During this study, up to 89.5% of final, filtered emissions data had to be gap-filled (Table 3.3). Gaps in 30-minute emissions occurred for three reasons: (1) data filtering from Table 3.2 criteria, (2) sensor or power failure, and (3) post-processing errors like spikes, drop-outs, or other issues. Loss of data within datasets due to Table 3.2 filtering consisted of ~37% from θ alone, 1.0–5.6% from u* or L criteria, 7.6% of WT data due to low TDR, 0.1 to 1% for outliers (outliers were considered $>3\sigma$ from a moving average of 12 hours), with 3.2–6.3% more filtering due to overlapping criteria (one or more of the first three in this list). Various sensor malfunctions, station issues, or post-processing errors accounted for up to 10.3%.

Because the amount of missing data was extreme, shorter windows were used with an iterative approach. The hard and soft windows for the MDV were shortened to 7 days and 6 hours, respectively, for more responsiveness (see section 3.2.4 for more information on MDV and windows). One iteration was not sufficient to fill all gaps so the MDV would iterate until no gaps remained. The gap-filling program was executed in Matlab™ vR2015a (The Mathworks, Inc.®, Natick, MA).

Figure 3.12 shows mean gap-filled emissions from EC and Table 3.3 shows gap-filled data for the lagoon for EC versus WT (see section 3.3.3.1). Smoothing of data occurred from Fig. 3.11, with gap-filled emissions still showing a diurnal trend (Fig. 3.12). These data were totaled on a daily basis for sums shown in Fig. 3.8 and means and totals presented in Table 3.3. To achieve final annual statistics, modeled wintertime values were assumed from missing winter months (i.e., Jan and Feb 2012 and Dec 2013, see values in parenthesis in Table 3.3), with the missing portion of the last autumn (end of Oct and all Nov 2013) modeled based on the first autumn. This approach is similar to that used by Leytem et al. (2011) to predict yearly emissions and is a safe assumption because wintertime values make up less than 20% of total annual emissions.

Overall, gap-filling slightly reduced emissions, with the highest reduction from 30-minute filtered values (up to 13.8%) for summer and fall (Figs. 3.11b-c,e-f and 3.12b-c,e-f). This is because due to filtering, 30-minute EC data tended to contain higher numbers of values from times when fluxes were higher (like daytime when turbulent conditions tended to occur more frequently). Such a dataset results in gap-filling of more low-value data (i.e., from times when filtered would have created a gap), incorporating more low values into the final, gap-filled diurnal composites.

3.3.4 Methane emission factors

On average, mean EFs in the summer and autumn were highest (Fig. 3.8); seasonal means peaked over 1700 g CH_4 hd^{-1} d^{-1} for the entire lagoon in summer for the EC system (i.e., measured fluxes), with seasonal means peaking over 2400 g CH_4 hd^{-1} d^{-1} (from WT). These EFs are much higher than most of the literature on summer emissions. Borhan et al. (2011a) reported up to 666 g CH_4 hd^{-1} d^{-1} using chambers for a dairy primary lagoon in Texas in summer and VanderZaag et al. (2014) saw summertime EFs of 673 g CH_4 hd^{-1} d^{-1}.

On average, annual EFs from EC-measured and WT-estimated CH_4 flux were 819 ± 774 and 1163 ± 1049 g CH_4 hd^{-1} d^{-1}, respectively. Our CH_4 EFs are much higher than the annual values of 147.8 g hd^{-1} d^{-1} from the IPCC (1996) Tier 1 values for dairy cattle in a temperate region (see Table 3.4). However, the IPCC Tier 2 annual estimate for this lagoon is 1012 g hd^{-1} d^{-1} (using similar values for anaerobic lagoons in IPCC's equation from Owen and Silver (2015) of 2770 kg VS hd^{-1} yr_{-1}, field-based methane conversion factor of 84%, and maximum CH_4 production rate based on VS (B_0) of 0.24). This Tier 2 value is slightly higher than EC-based measurements (819 ± 774 g hd^{-1} d^{-1}) and slightly less than WT-based estimates (1163 ± 1049 g hd^{-1} d^{-1}) from this study's lagoon. If the Tier 2 methodology is properly parameterized, it can be very close to actual emissions, however the Tier 1 approach from IPCC (1996) is much less than CH_4 EFs found in this study, indicating using the Tier 1 approach causes underestimation. However, this is likely a widespread issue with Tier 1 methodologies due to their simple nature.

Measured F_{CH_4} (from EC) is similar to EFs of 893 g CH_4 hd^{-1} d^{-1} calculated by Owen and Silver (2015) for some similar regions of the US (ID, NM, TX, SC) using the IPCC (1996) Tier 2 methodology. This study's mean annual EFs (Table 3.4) fall in the ranges shown from extensive reviews by Owen and Silver (2015) (range: 11 – 7704 g CH_4 hd^{-1} d^{-1}) and Leytem et al. (2017) (range: 4.7-1028 g CH_4 hd^{-1} d^{-1}).

3.4 Conclusions

Eddy covariance (EC) was used to characterize methane (CH_4) concentrations, CH_4 emissions, and estimate emission factors (EFs) for CH_4 from a large anaerobic dairy manure lagoon in Colorado. Methane concentrations varied by source (lagoon to the NW, NE dairy sectors of the EC footprint) and season (Figs. 3.4-3.7). Methane emissions were highest in the summer and early autumn, with 80.7% of yearly emissions occurring between DOY 150-300 (late May – late Oct).

Eddy covariance measurements of GHG were analyzed in detail. CH_4 flux was highest from the lagoon, then the composting, settling basins, and barn areas (Figs. 3.10-3.11). Emissions from both major sources were highest in the summer and early autumn with a near tenfold decrease for winter and spring months when ambient temperatures and total daytime solar radiation were much lower than other times of the year (strong drivers of microbial processes affecting lagoon GHG emissions). Gap-filling smoothed emissions from those in Fig. 3.11, with slightly elevated daytime emissions still evident; presumably associated with higher wind speeds and increased turbulent conditions typically experienced during daytime hours (Fig. 3.12).

Methane EFs vary by time of year (Fig. 3.8, Table 3.4) with very small values based on EC data in the winter and spring (197 and 172 g CH_4 hd^{-1} d^{-1}, respectively) and values up to 10 times higher in summer and autumn (1757 and 1152 g CH_4 hd^{-1} d^{-1}, respectively for EC data). The mean EC-based CH_4 EF for the lagoon in this study was 819 ± 774 g CH_4 hd^{-1} d^{-1}. EC-based EFs from this study were similar to those from the IPCC (1996) Tier 2 approach for anaerobic lagoons and the mean of field studies by Owen and Silver (2015) (yet were much higher than those from the IPCC Tier 1 approach). Lagoon CH_4 EFs were also very close to those from a 10,000-hd dairy in S. Idaho (Leytem et al., 2013). The annual CH_4 lagoon EF for emissions estimates from WT data was 1163 ± 1049 g CH_4 hd^{-1} d^{-1}.

Anaerobic lagoons emit CH_4 based on microbial populations in the base, which are typically heterogeneous in distribution. Additionally, these liquid manure systems occur in many countries, over many differing climates, and can have widely varied management. More long-term studies of anaerobic lagoons helps create more in-depth knowledge of the dynamics controlling CH_4 emissions in the context of interannual and seasonal variability. Furthermore, multiple perimeter sampling points (attainable with newer low-cost instruments becoming available) of such strong sources will aid in spatial interpretation of emissions therein, regardless of micrometeorological technique used.

3.5 Tables

Table 3.1. Filtering criteria for emissions from eddy covariance and WindTrax. Italicized criteria apply to WindTrax emissions only.

Parameter	Symbol	Units	Filter if:	Reason
Wind direction, Lagoon	θ	degrees	$5 < \theta < 275$	Signal not from lagoon
Wind direction, NE	θ	degrees	$\theta < 10$, $\theta > 90$	Signal not from NE
Wind direction, Field	θ	degrees	$\theta < 100$, $\theta > 260$	Signal not from field
Friction velocity	u*	$m\ s^{-1}$	< 0.15	Wind speeds too low
Obukhov length	|L|	m	< 10	Extreme stabilities
Touchdown ratio (TDR)	$\frac{A_{TD}}{A_{lagoon}}$	*$m^2\ m^{-2}$*	*< 0.10 (10%)*	*Sufficient lagoon particle coverage*

Table 3.2. Daily mean measured emissions by season based on 24-hr composites from eddy covariance (EC; italicized columns; see Fig. 3.11) for the lagoon and NE sources, daily mean emissions estimates based on 24-hr composites from WindTrax (WT; composites not shown), and ratio of WT to EC.

			Composite Mean Emissions			
Year	Season	Months	*EC, Lagoon ($g\ m^{-2}\ d^{-1}$)*	*EC, NE ($g\ m^{-2}\ d^{-1}$)*	WT, Lagoon ($g\ m^{-2}\ d^{-1}$)	WT:EC
2012	Spring	MAM	*7.5 ± 2.3*	*6.5 ± 5.1*	12.4 ± 5.6	1.65
2012	Summer	JJA	*73.2 ± 33.5*	*33.2 ± 19.7*	110.9 ± 46.2	1.51
2012	Autumn	SON	*46.5 ± 20.8*	*19.9 ± 11.6*	62.8 ± 18.6	1.35
'12-'13	Winter	DJF	*6.4 ± 1.7*	*3.3 ± 1.8*	9.0 ± 1.7	1.41
2013	Spring	MAM	*5.9 ± 1.7*	*3.9 ± 2.0*	12.1 ± 6.6	2.04
2013	Summer	JJA	*60.8 ± 18.0*	*30.7 ± 15.2*	76.0 ± 33.8	1.25
2013	Autumn	SO	*54.5 ± 15.9*	*28.8 ± 17.7*	81.9 ± 16.3	1.50
					Weighted mean:	1.56

Table 3.3. Final, gap-filled methane flux (F_{CH4}) means (on an area basis and entire-lagoon basis), and cumulative totals for EC-based emissions measurements (left set; italicized) and for WT-based emissions (estimated fluxes based on inverse dispersion modeling, right set) along with ratio between WT and EC mean by area (far right column). Values in parenthesis are for months when data were not collected but are provided to allow for more accurate annual emissions based off 2 full years of data (mixture of 19.5 months of measurements and 5.5 months of assumed seasonal values). Values in square brackets indicate that the means are not necessarily representative of a typical season due to measurements ending before the remainder of the season was experienced (such as the end of Oct and Nov in autumn 2013). Portion of data gap-filled for EC was 70.4-88.6% by season with a weighted mean of 77.1%. Portion of data gap-filled for WT estimates was 78.6-89.5% by season with a weighted mean of 84.7%.

		Gap-filled, Measured F_{CH4} (EC, Lagoon)			Gap-filled, Estimated F_{CH4} (WT, Lagoon)			WT:EC
Year	Season/ Months	*Mean by area ($g\ m^{-2}\ d^{-1}$)*	*Lagoon Mean[a] ($kg\ d^{-1}$)*	*Total CH_4 (Tonne)*	Mean by area ($g\ m^{-2}\ d^{-1}$)	Lagoon Mean[a] ($kg\ d^{-1}$)	Total CH_4 (Tonne)	
2012	JF[b]	*(6.1)*	*(242)*	*(14.5)[b]*	(10.0 ± 0.8)	(400)	(24.0)[b]	
2012	MAM	*7.6 ± 1.4*	*300 ± 54*	*27.3[b]*	12.6 ± 2.3	502 ± 93	45.7[b]	1.66
2012	JJA	*64.3 ± 12.4*	*2533 ± 488*	*230.5*	90.8 ± 12.5	3616 ± 496	329.1	1.41
2012	SON	*41.9 ± 8.0*	*1649 ± 317*	*148.4*	56.0 ± 5.8	2232 ± 231	200.9	1.34
'12-'13	DJF	*6.1 ± 0.8*	*242 ± 32*	*21.5*	10.0 ± 0.8	400 ± 31	35.6	1.64
2013	MAM	*6.4 ± 1.2*	*251 ± 48*	*22.8*	10.9 ± 0.9	434 ± 37	39.5	1.71
2013	JJA	*60.6 ± 9.0*	*2386 ± 355*	*217.2*	83.0 ± 9.7	3307 ± 387	300.9	1.37
2013	[SO]	*[66.1 ± 12.5]*	*[2604 ± 317]*	*[234.3]*	[90.8 ± 12.5]	[4054 ± 236]	[364.9]	[1.54]
	SON	*(40.0)*	*(1577)*	*(143.6)[b]*	(57.4)	(2507)	(228.1)[b]	
2013	D[b]	*(6.1)*	*(242)*	*(7.5)[b]*	(10.0 ± 0.8)	(400)	(12.4)[b]	
	Annual[b]	*(29.3 ± 25.5)[c]*	*(1154 ± 1004)[c]*	*(833.3)[d]*	(41.6 ± 34.6)[c]	(1638 ± 1362)[c]	(1216.2)[d]	1.52[e]

[a] Based off lagoon surface area (~3.94 ha or 39,390 m^2)
[b] Modeled from measurements of matching months (see text, section 3.3.3.2.2)
[c] Mean excluding values in square brackets
[d] 2-year total excluding values in square brackets
[e] Weighted mean of values in column

Table 3.4. Mean lagoon emissions and mean lagoon emission factors (EFs) for CH_4 (italicized; EC measurements and WindTrax estimates). Annual EFs in bold.

Emissions timeframe	Gas	Mean Emissions (g m^{-2} d^{-1})	CH_4 EF (g hd^{-1} d^{-1})	Emissions Approach
Spring	CH_4	7.0 ± 1.3	197 ± 37	EC
Summer	CH_4	62.5 ± 10.7	1757 ± 301	EC
Autumn	CH_4	41.0 ± 10.3	1152 ± 288	EC
Winter	CH_4	6.1 ± 1.4	172 ± 39	EC
Annual	**CH_4**	**29.3 ± 25.5**	**819 ± 774**	**EC**
Spring	CH_4	11.8 ± 1.6	331 ± 45	WindTrax
Summer	CH_4	86.9 ± 11.1	2445 ± 311	WindTrax
Autumn	CH_4	56.7 ± 5.9	1545 ± 165	WindTrax
Winter	CH_4	10.0 ± 0.8	281 ± 23	WindTrax
Annual	**CH_4**	**41.6 ± 34.6**	**1163 ± 1049**	**WindTrax**

3.6 Figures

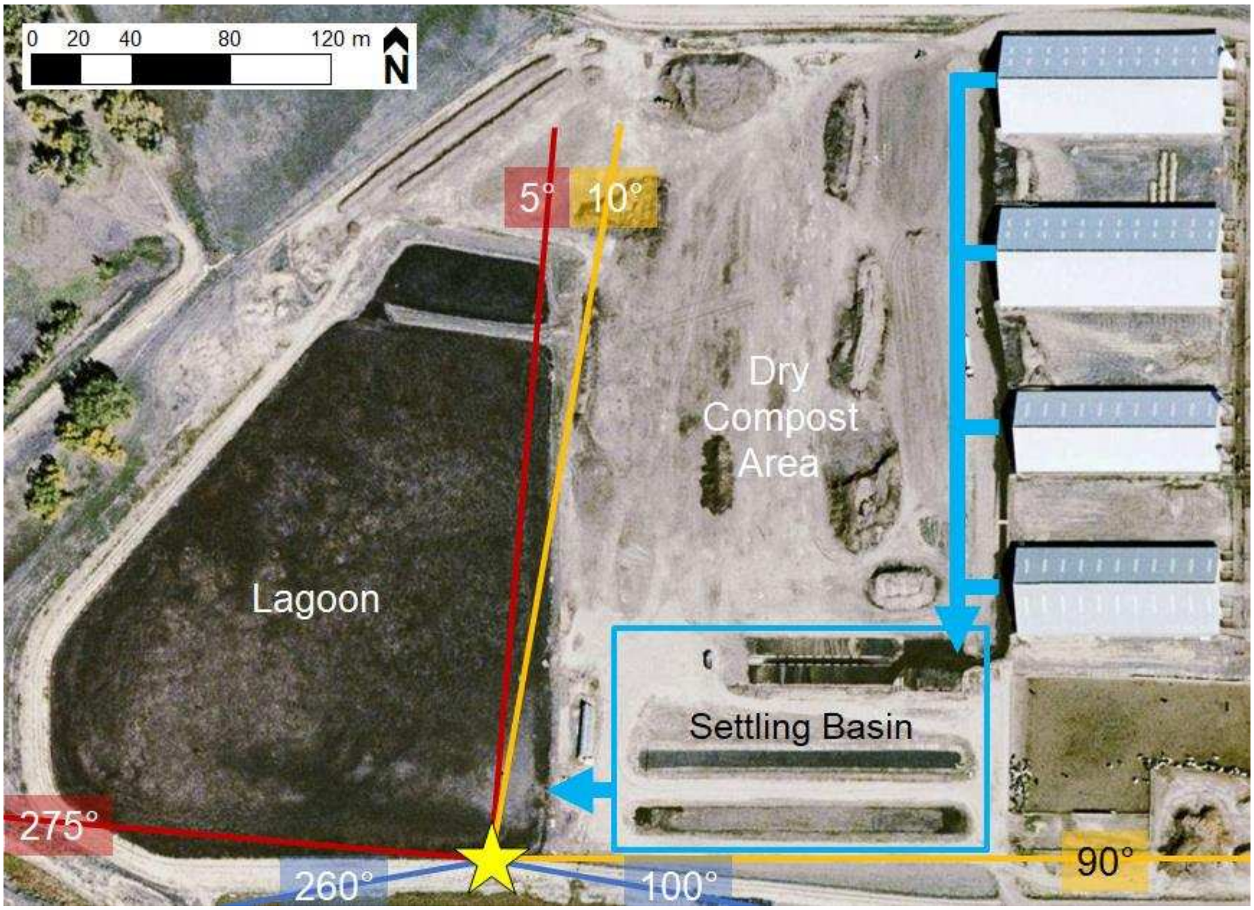

Figure 3.1. Satellite image of manure management and the free-stall barns on the dairy. The eddy covariance station is indicated by a yellow star, while light blue arrows show the flow of waste from the lactating cow barns. Before being pumped into the lagoon via an underground pipe, washed waste flows through a sedimentation basin (lower right) to reduce total solids. Lagoon (left), dry compost area (right), sedimentation basin (lower right), and lactating cow barns (far right) are methane sources. Colored lines and associated labeled wind direction (θ) angles are to indicate how θ filtering was done based on source area (red for lagoon source of 275° < θ < 5°, yellow for NE sectors of the EC footprint with 10° < θ < 90°, and blue for the field source designated for 100° < θ < 260°; excluded θ's are 5°-10°, 90°-100° and 260°-275°.

Figure 3.2. Panoramic photo of eddy covariance station and lagoon. Natural crusting can be seen on the lagoon surface including some floating mats, with typically little or no open water visible at this site.

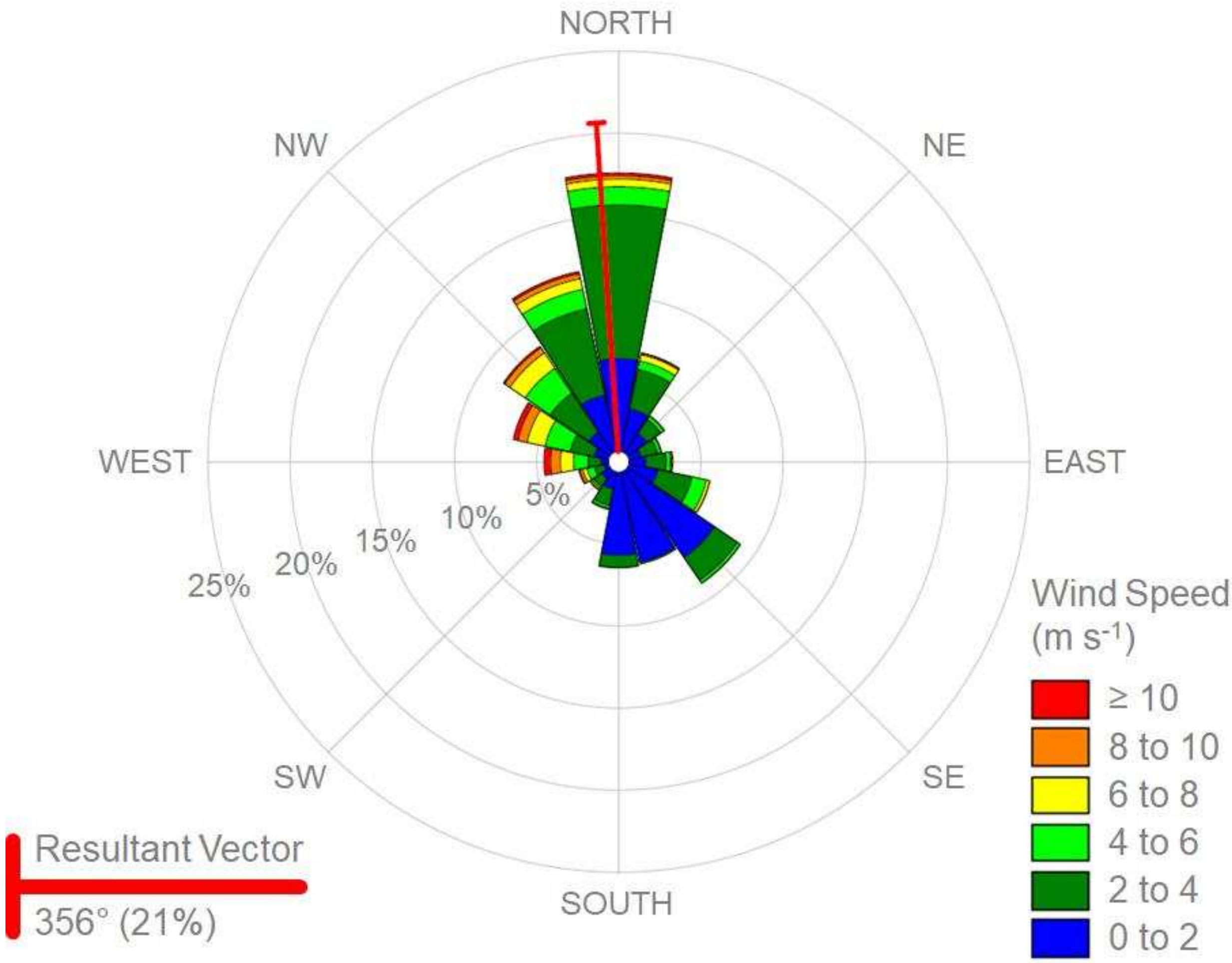

Figure 3.3. Wind rose at 6.2 m for the entire study (Mar 2012 to Oct 2013).

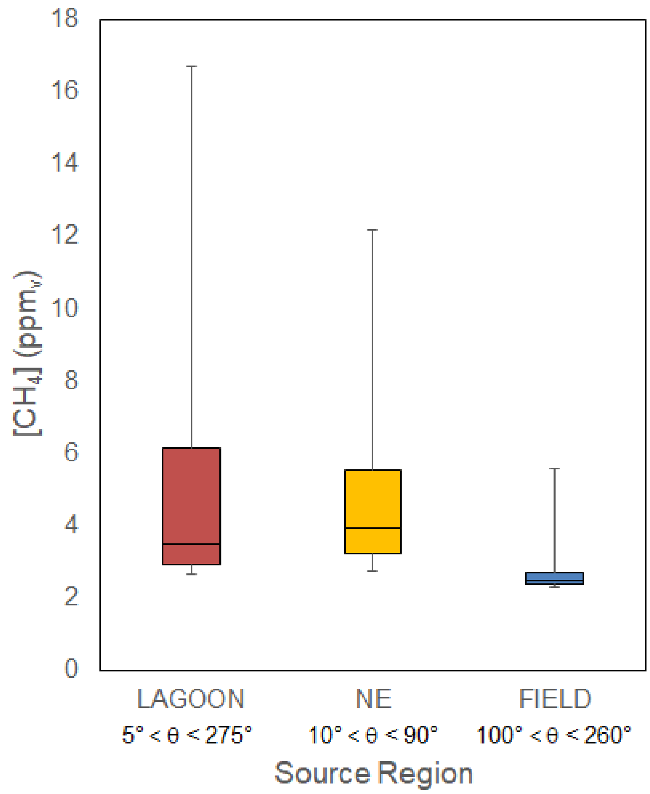

Figure 3.4. Box and whisker plot of 30-min methane concentrations at 6.2 meters (filtered for u* and L) for each source area with respect to the EC tower. Boxes are 25th, 50th (median), and 75th percentiles. Whiskers are 5th and 95th percentiles.

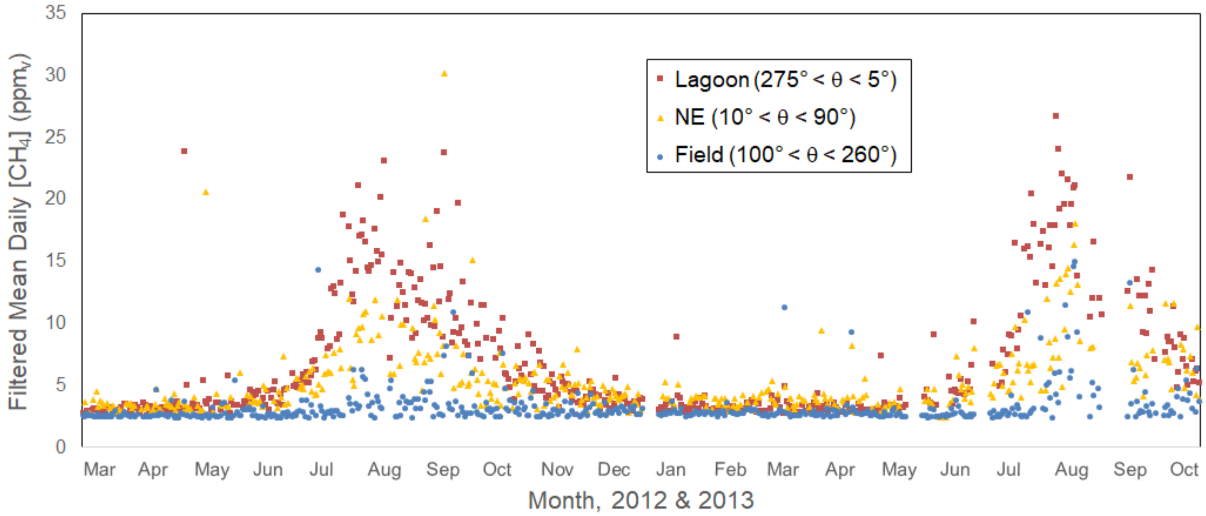

Figure 3.5. Mean methane concentration ([CH_4], ppm$_v$; at 6.2 m) per day of the study for different source areas: Lagoon (red squares), NE sectors (yellow triangles), and Field (blue dots).

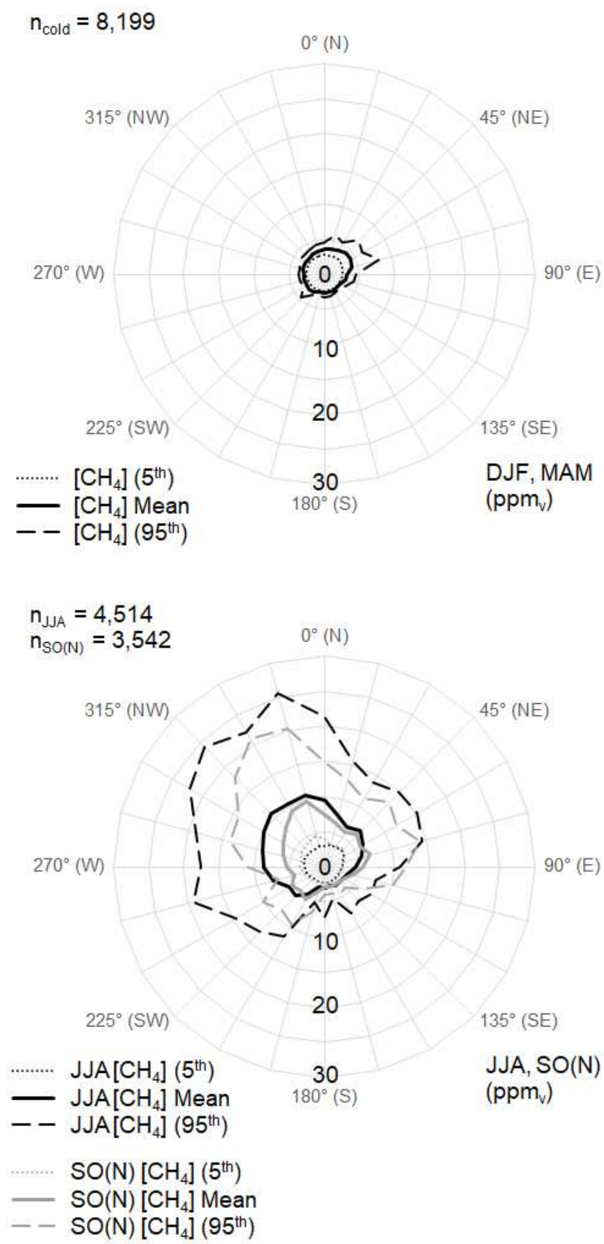

Figure 3.6. Seasonal methane concentration ($[CH_4]$, (ppm_v) at the EC tower for 15° sectors of θ. Bold line is mean $[CH_4]$, while dotted and dashed lines are 5^{th} and 95^{th} percentiles, respectively, of all records of $[CH_4]$ corresponding to each 15° θ-sector (sample size, n; upper left corners). Cold month presented as a mean of both springs and the one winter (top graph). Warm months presented as two seasons (i.e., summer and autumn, black and gray, respectively; bottom graph). Seasons designated by month: spring = MAM, summer = JJA, autumn = SON, and winter = DJF (lower right corners). Concentrations were filtered for u* and L to exclude unfavorable conditions.

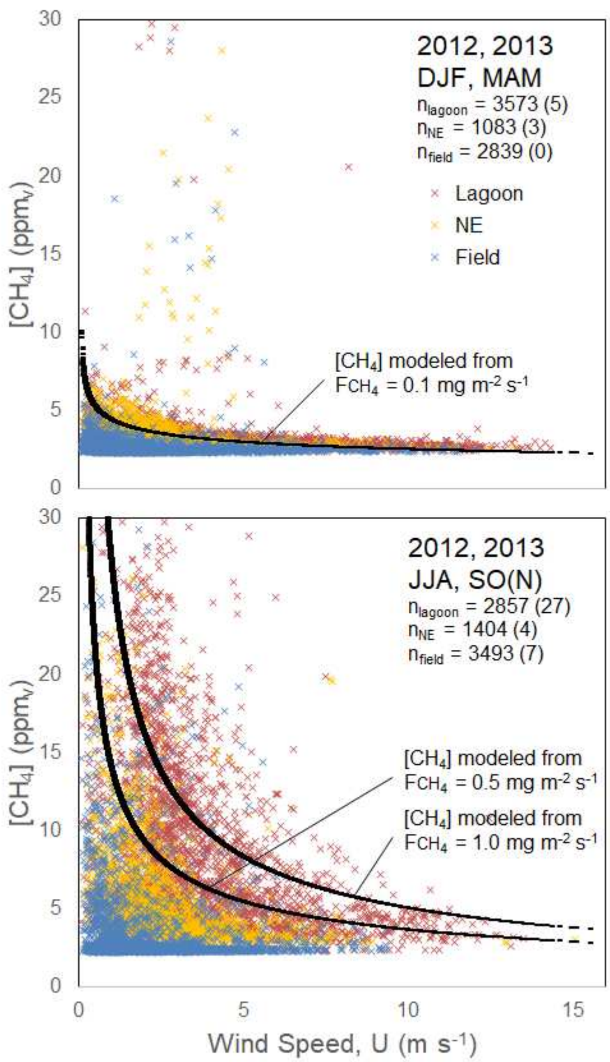

Figure 3.7. Mean 30-minute methane concentration ([CH_4], ppm_v) versus wind speed (U, m s^{-1}) for cool months (winter and spring; top graph) and warm months (summer and autumn; bottom graph). Ordinate limit was set to 30 ppm_v to show the distribution of [CH_4] closer to background (~2.3 to 2.55 ppm_v), but because concentrations exceeded this, the number of [CH_4] records > 30 ppm_v are shown in parenthesis next to the sample sizes (upper right of each plot). Sources are defined by wind direction: Lagoon = 275 < θ < 5°; NE = 10 < θ < 90°; and Field = 100 < θ < 260°. Concentrations were filtered for u* and L to exclude unfavorable conditions. Modeled [CH_4] power relationships (thick black lines) found from running WindTrax in same mode but using given values of fluxes near seasonal means from Table 3.2 (0.1, 0.5, and 1.0 mg m^{-2} s^{-1}) for the lagoon source area and telling the program to estimate resulting [CH_4] for given ranges of wind speeds (assuming neutral stability, |L| = ~115-200 m).

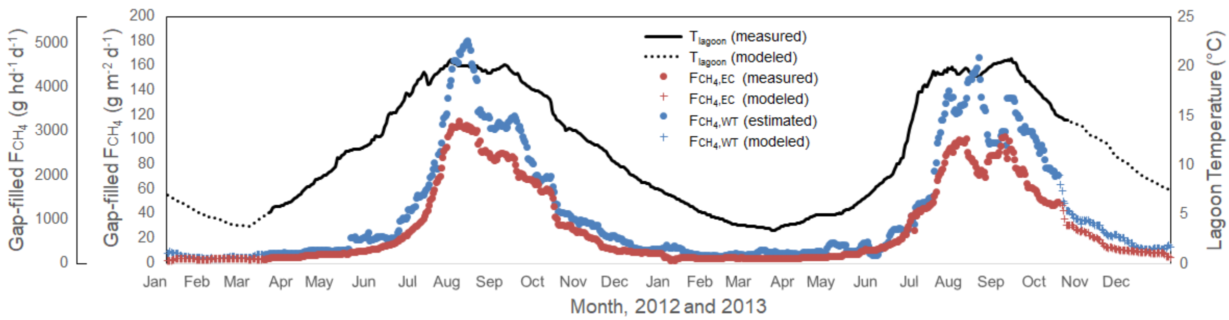

Figure 3.8. Two years of daily cumulative gap-filled CH_4 flux (F_{CH4}; left axis) in g m^{-2} d^{-1} (area basis) and as emissions factors (EFs) in g hd^{-1} d^{-1} (see section 3.3.4 for more EFs) for the lagoon using WT-estimated (blue) and EC-measured (red) emissions. Also shown are two years of lagoon sludge layer (i.e., biomat) temperature (T_{lagoon}; black lines; right axis). The gap-filled data (i.e., 11 Mar 2012 to 11 Oct 2013) are designated by filled markers (F_{CH4}) and solid line (T_{lagoon}). Modeled/interpolated data for times when measurements were not available are marked by pluses and dotted lines.

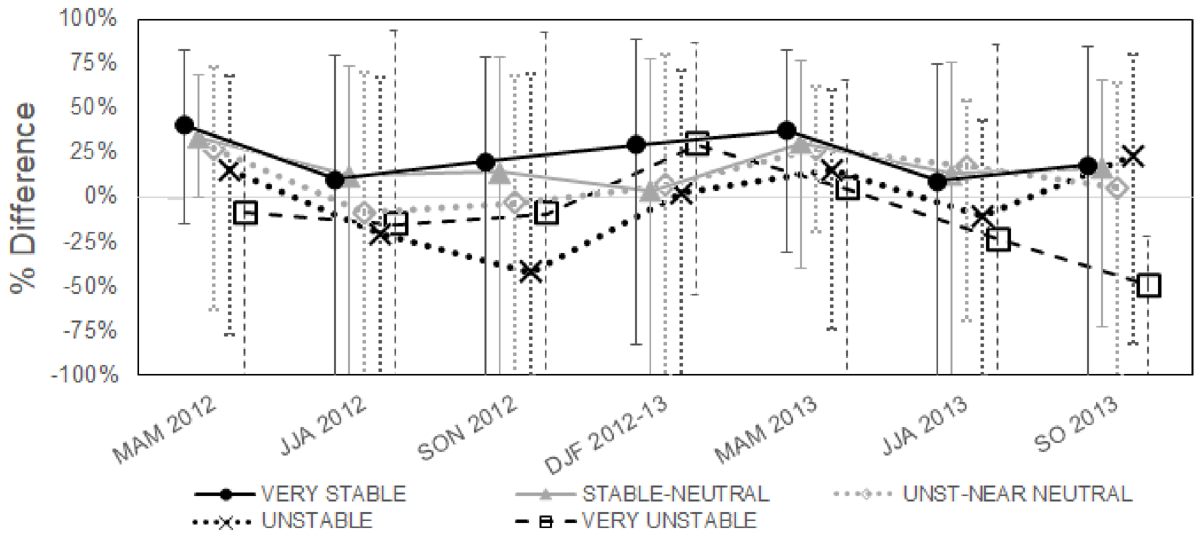

Figure 3.9. Percent difference between filtered 30-minute WT emissions estimates and EC measured emissions (for matching output) based on stability classification (following Gao et al. (2009) where VERY STABLE corresponds to 0.1 > 1/L > 0.017; STABLE-NEUTRAL corresponds 0.017 > 1/L > 0; UNST-NEAR NEUTRAL corresponds to 0 > 1/L > -0.01; UNSTABLE corresponds to -0.01 > 1/L > -0.033; and VERY UNSTABLE corresponds to -0.033 > 1/L > -0.1). Sample sizes for stability classes were n_{very_stable} = 1363, $n_{stable\text{-}neutral}$ = 1474, $n_{unst\text{-}near\_neutral}$ = 657, $n_{unstable}$ = 320, and $n_{very\_unstable}$ = 135. Percent difference calculated with respect to WT (i.e., % diff = 100*[(WT – EC) / WT]), where positive values represent WT overestimating EC emissions. To show the range of differences in the data error bars were inserted. Negative error bars represent the 5th percentile of all % differences based off 30-minute filtered emissions, while positive error bars are the 95th percentile of all % differences. The 5th percentile bars of several series are cut-off to keep the ordinate range reasonable.

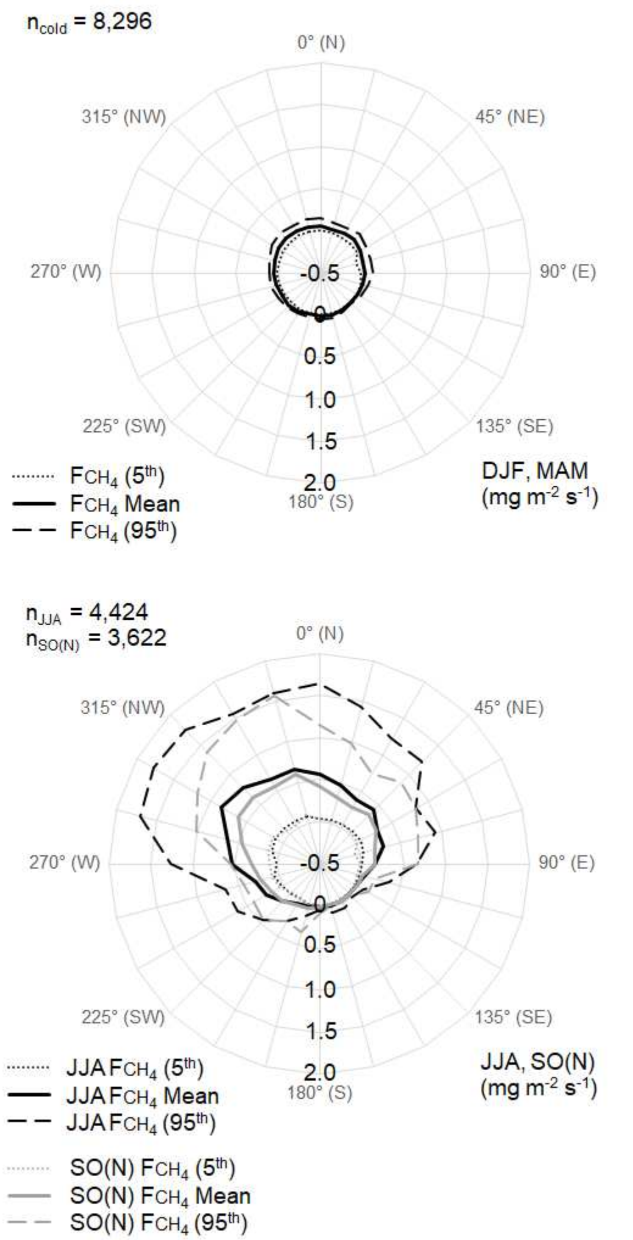

Figure 3.10. Seasonal lagoon EC-based methane flux (F_{CH4}, mg m^{-2} s^{-1}, not-gap-filled) for 15° sectors of θ. Bold line shows mean F_{CH4}, while dotted and dashed lines are 5th and 95th percentiles, respectively, of all plot records of F_{CH4} corresponding to each 15° θ-sector (sample size, n; upper left corners). Cold month presented as a mean of both springs and the one winter (top graph). Warm months presented as two seasons (i.e., summer and autumn, black and gray, respectively; bottom graph). Seasons designated by month: spring = MAM, summer = JJA, autumn = SON, and winter = DJF (lower right of each plot). Fluxes/emissions in these plots were filtered for u* and L to exclude unfavorable conditions.

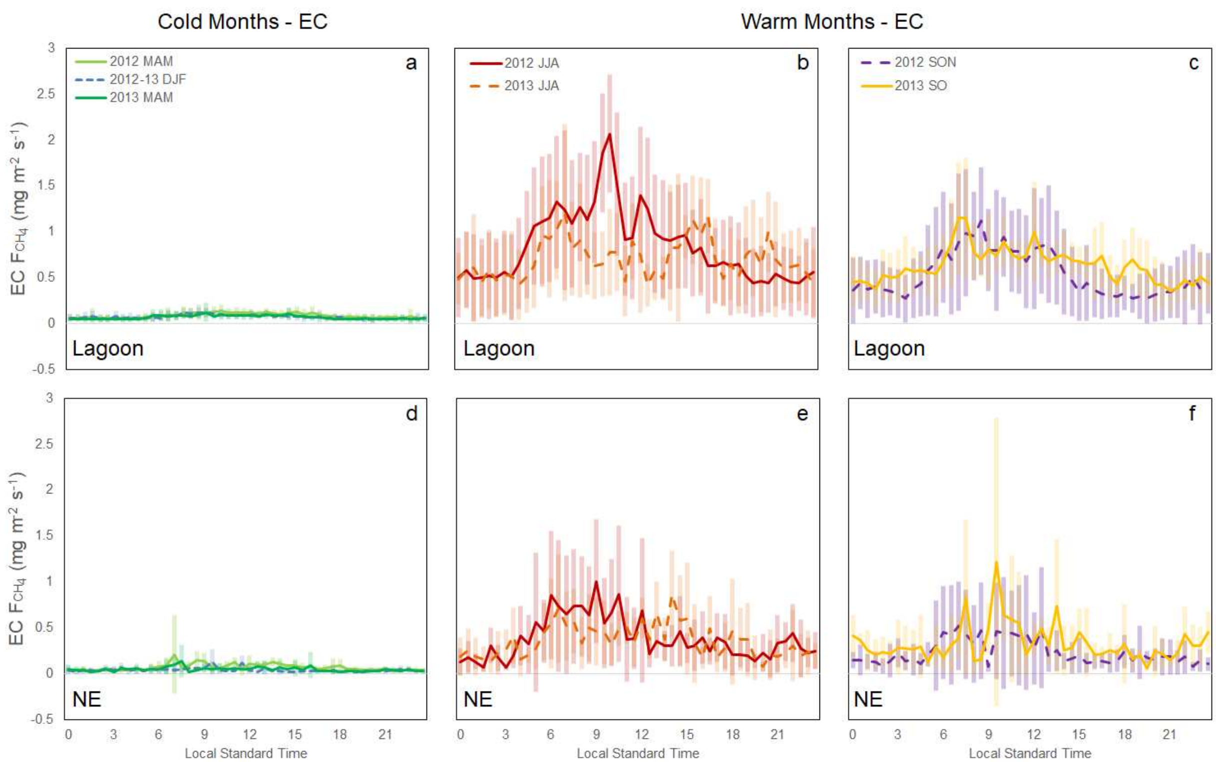

Figure 3.11. Diurnal composites of mean non-gap-filled EC-based methane fluxes (F_{CH4}) for the lagoon (top graphs) and NE sectors of the EC footprint (i.e., settling basins, lagoon far E edge, compost area, and edges of lactating cow barns; bottom graphs) for each season of the study (from left to right: cold months, summer, and autumn). Seasons designated by month (spring = MAM, summer = JJA, autumn = SON, and winter = DJF). Vertical error bars are full standard deviation about the mean for all records at each timestamp. Table 3.2 values for lagoon and NE are from these 24-hr composites.

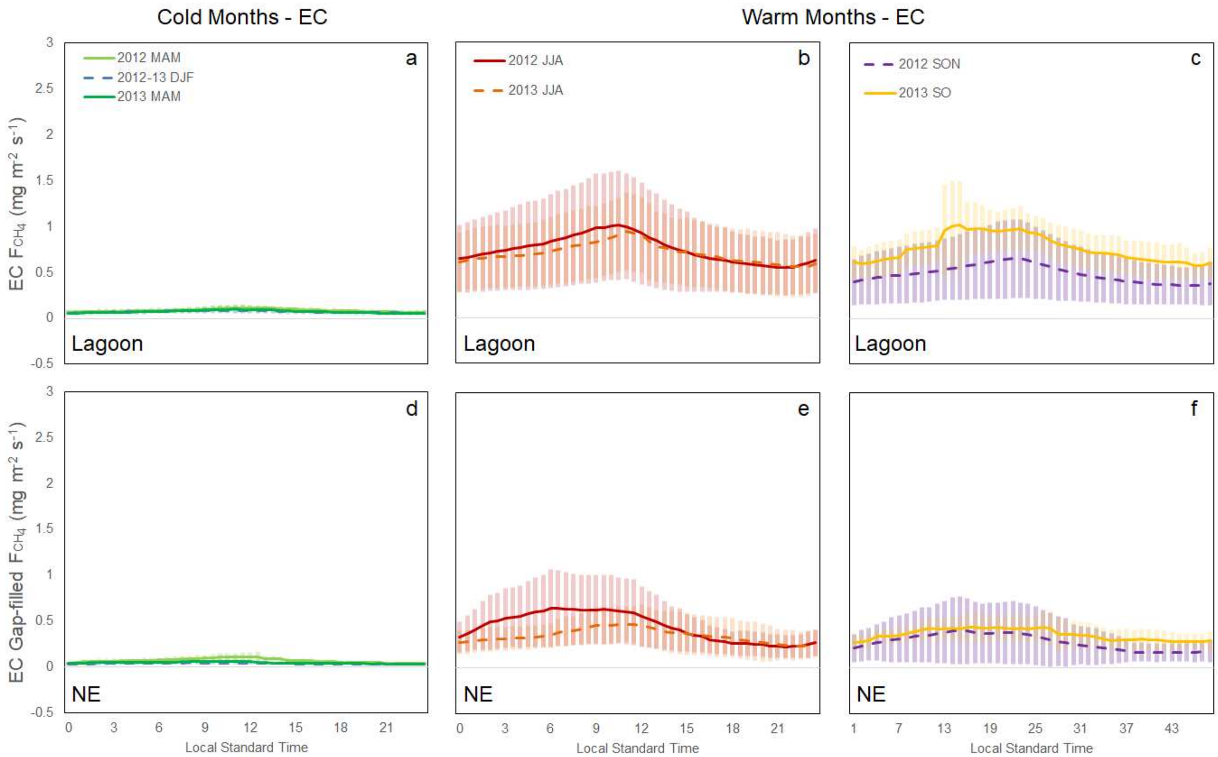

Figure 3.12. Diurnal composites of mean gap-filled EC-based methane fluxes (F_{CH4}) for the lagoon (top graphs) and NE sectors of the EC footprint (i.e., settling basins, lagoon far E edge, compost area, and edges of lactating cow barns; bottom graphs) for each season of the study (from left to right: cold months, summer, and autumn). Seasons designated by month (spring = MAM, summer = JJA, autumn = SON, and winter = DJF). Vertical error bars are full standard deviation about the mean for all records at each timestamp. Table 3.3 values for lagoon are from these 24-hr composites.

CHAPTER 4 - ENERGY BALANCE CLOSURE AT TWO LANDSCAPE POSITIONS IN TALLGRASS PRAIRIE USING EDDY COVARIANCE

4.1 Introduction

Eddy covariance (EC) is an important micrometeorological technique used for studying the exchange of water, carbon, and energy in the surface boundary layer (Baldocchi et al., 1988). Eddy covariance provides noninvasive, continuous flux observations of different climates, terrains, and ecosystems. This methodology is used by continental-scale flux networks such as AmeriFlux, Euroflux, OzFlux, AsiaFlux, ChinaFLUX, and Fluxnet Canada (e.g, Aubinet et al., 2000; Baldocchi et al., 2001). Data from flux networks have widespread use for identifying terrestrial carbon sinks and sources, verification and parameterization of ecological models (Kucharik et al., 2006), and remote sensing (Turner et al., 2006). Additionally, management decisions are often administered at the field or watershed scale, and EC can be used to compare the effects of land management (e.g., grazing, fire) on fluxes at comparable scales (Owensby et al., 2006). Given its wide-spread implementation, it is important that EC provides an accurate method for long-term flux measurements.

Eddy covariance is often employed to understand and quantify important biogeochemical processes that govern the water and carbon balances of different ecosystems. Grasslands, in particular, are a major player in the carbon cycle. Nearly 70% of the planet's agricultural land is classified as grassland (FAO, 2009). It follows that assessing the role of grasslands in the global carbon cycle will yield detailed, vital information regarding climate change, carbon storage and release, and land-use and sustainability practices within the scope of the world's grasslands (Owensby et al., 2006; Suttie et al., 2005; Suyker and Verma, 2001). The term "grassland" encompasses many sub-biomes such as savannah, steppe, mesic, montane, and xeric shrublands, perhaps the most productive of which are the temperate grasslands including the North American prairie (Suttie et al., 2005). Eddy covariance has often been used, particularly in grasslands, to study water, carbon, and energy balances (Bremer and Ham, 1999, 2010; Ham and Knapp, 1998; Jacobs et al., 2008; Meyers, 2001; Owensby et al., 2006; Verma et al., 1992; Wohlfahrt et al., 2009, 2010). It is imperative that measurements from the EC method be as reliable as possible to accurately quantify the scalar and energy budgets within this valuable ecosystem.

Much research has been done to ascertain the viability of EC measurements through verification of fundamental processes, specifically the law of conservation of energy. The energy balance (EB) at the Earth's surface must satisfy the following:

$$R_n - G - \Delta S = H + \lambda E \tag{4.1}$$

where R_n is net radiation, G is soil heat flux and heat storage in the soil, ΔS is the change in heat storage for the biomass and air below the EC measurement height in addition to the energy stored within chemical bonds associated with photosynthesis, H is sensible heat flux, and λE is the latent heat flux, all in W m^{-2}. The ratio of the system's available energy, $R_n - G - \Delta S$, to turbulent energy flux, $H + \lambda E$ (measured by EC), should approximate unity — this is called EB closure. Sometimes ΔS is neglected because data are not available or it is considered negligible in short vegetation; thus, $(H + \lambda E)/(R_n - G)=1$ is the most general expression for closure in the literature.

However, most applications of EC do not achieve closure. A majority of EB studies report the overall ratio of $(H + \lambda E)/(R_n - G)$ to be about 0.80 (Foken, 2008; Wilson et al., 2002), but values often range from 0.7 to 0.96. Nevertheless, there is a systematic underestimate of closure that implies that either meteorological measurements of $R_n - G - \Delta S$ are overestimated (i.e., R_n too large or G and ΔS are too small) or EC measurements of $H + \lambda E$ are underestimated. Because EC instruments measure CO_2 in the same way as λE, EC-derived carbon flux could also be in error (Barr et al., 2006; Goulden et al., 1996; Twine et al., 2000).

This so-called "energy balance closure problem" has been studied extensively (Aubinet et al., 2000; Barr et al., 2006; Eder et al., 2014; Foken and Wichura, 1996; Foken et al., 2006; Foken, 2008; Franssen et al., 2010; Gao et al., 2017; Goulden et al., 1996; Guo et al., 2009; Ham and Heilman, 2003; Hammerle et al., 2007; Heusinkveld et al., 2004; Hunt et al., 2002; Kanda et al., 2004; Kohsiek et al., 2007; Laubach and Teichmann, 1999; Masseroni et al., 2014; Massman and Lee, 2002; Mauder et al., 2007a, 2007b; McGloin et al., 2018; Moderow et al., 2009; Oncley et al., 2007; Soltani et al., 2017; Stoy et al., 2013; Twine et al., 2000; Wilson et al., 2002; Wohlfahrt et al., 2009, 2010, 2016; Wohlfahrt and Widmoser, 2013; Zhengquan et al., 2005). Foken et al. (2006) described three factors with EC that may contribute to the closure problem: (1) measurement and post-processing errors, (2) errors resulting from the turbulent fluxes (H and λE) sampling different scales and source areas than R_n and G (i.e., footprint mismatch), and (3) errors resulting from advection and low-frequency fluxes caused by heterogeneity of the land surface. A detailed discussion in an overview paper by Foken (2008) suggested the first factor is resolved for most applications because of widespread agreement in established post-processing procedures. Foken (2008) and Kohsiek et al. (2007) showed that the second factor (often associated with the accuracy of radiation and storage measurements) has a negligible effect on the lack of closure when great care is made to obtain accurate R_n and G measurements, and emphasizing spatial heterogeneity is the likely culprit.

Foken's overview article also suggests that the magnitude to which the low-frequency portion of the third aspect is a concern can be determined through Ogive (i.e., cumulative frequency) analyses (Foken and Wichura, 1996; Oncley et al., 1990); but for EC over short vegetation covering large regions (i.e., grasslands), sampling frequencies >10 Hz with 30-min integration allows for the capture of the majority of turbulent flux (see section 4.3.3). However, the effect of large-scale heterogeneity across the landscape remains a proposed rationale for lack of closure in many systems (Guo et al., 2009; Kanda et al., 2004; Laubach and Teichmann, 1999).

Classic applications of EC locate net radiation and soil measurements in an area representative of but exterior to the main tower footprint or source area. Foken (2008) stated that this spatial mismatch in the R_n – G and H + λE source areas has been a concern. He also cited the Energy Balance Experiment (EBEX-2000) by Mauder et al. (2007a) concerning R_n – G measurements, in which it was estimated that errors in these data are no more than 5% of the energy budget during daytime, not accounting for the 20% lack of closure.

Collecting EC data at multiple locations across major topographical positions within a watershed would help isolate whether closure can be achieved by considering spatial variations in EB across the landscape. Moreover, interannual variability can play a large role in the degree of closure reported for long-term data acquisition. Specifically, is closure affected by the ratio between H and λE (i.e., the Bowen ratio), a parameter influenced by precipitation, soil water content, and plant water relations?

The goal of this project was to evaluate the degree of EB closure across multiple years at two landscape positions in a native tallgrass prairie ecosystem. Two EC towers (one each at an upload and lowland landscape position) were deployed in combination with a large aperture *scintillometer* on the same watershed. Specific objectives were to (1) minimize measurement and post-processing errors (as in other studies such as EBEX-2000) and (2) examine the effect of spatial heterogeneity or sampling scale by collecting data at multiple locations across a homogenous landscape.

4.2 *Materials and methods*

4.2.1 Site description

Research was performed at the Konza Prairie Biological Station (KPBS) approximately 14 km south of Manhattan, KS, USA (39.08°N, 96.56 °W, 330 m). Data on turbulent fluxes were used from two EC stations that operated in the summers of 2007 and 2008. The EC stations were within the boundary of an ungrazed watershed with a controlled-burn each spring. One site was on upland terrain (441 m), and one was at a lowland position (427 m) located approximately 350 m south of the upland site. The source area for the upland tower included very level, uniform terrain. The lowland site was on a gently sloping footslope near the bottom of the catchment that drained the watershed. Both sites had highly uniform vegetation dominated by warm-season, perennial C_4 grasses including *Andropogon gerardii* (big bluestem), *A. scoparius* (little bluestem), *Sorghastrum nutans* (indiangrass), and *Panicum virgatum* (switchgrass) (Gibson and Hulbert, 1987). Annually burned watersheds showed, on average, 384 and 581 g m^{-2} aboveground biomass for uplands and lowlands, respectively, over a 16-year study (Heisler and Knapp, 2008). Historical surveys demonstrate that lowland sites possess deeper soils with greater water holding capacity than uplands (Briggs and Knapp, 1995). Soils at each EC station are silty clay loams (Benfield series: fine, mixed, mesic Udic Argiustolls; Bremer and Ham, 1999). The 30-year average annual precipitation for all sites is 859 mm. Additional background information on tower measurements in the watershed can be found in Ham and Knapp (1998) and Bremer and Ham (1999).

4.2.2 Instrumentation and sampling

Eddy covariance stations were composed of a main tower supporting the core EC measurements of sensible heat, latent heat, and CO_2 fluxes and an ancillary (meteorological) instrumentation site to sample available energy (R_n – G) in the footprint. Eddy covariance instruments were mounted at 3 m on each main tower and consisted of an open-path infrared gas analyzer (LI-7500, Licor, Inc., Lincoln, NE), a sonic anemometer (CSAT3, Campbell Scientific, Inc., Logan, UT), and a temperature/relative humidity probe (HMP45C, Campbell Sci.). Sensor separation between the CSAT3 and the LI-7500 was 0.14 m, CSAT3 orientation was 210° magnetic, and the LI-7500 was rotated 15 degrees vertically toward the footprint to obtain the least obstruction of flow by sensor body on the infrared beam and also to allow water to run off the lens. Eddy covariance data were logged at 20 Hz using a CR1000 data logger (Campbell Sci.) and collected via Compact Flash card at each site. All other meteorological data were sampled at 10-s intervals, and averages of these data were computed and logged every 30 min. In situ calibration was performed to zero and span the CO_2 and H_2O measurements from the LI-7500 every 2 weeks using tank gas and a LI-610 portable dewpoint generator (Licor, Inc.)

Net radiation and G were measured in the footprint of each tower. A CNR2 net radiometer (Kipp and Zonen, Delft, The Netherlands) was deployed at 2 m near the center of each tower's source area approximately 30 m south of the EC instruments (i.e., along the prevailing wind). Soil heat flux was determined via the combination method (Fuchs and Tanner, 1968; Kimball and Jackson, 1979), and these measurements were also placed 30 m south of the EC tower (near the CNR2 measurements) with a replication installed 3 m south of the tower. Soil instrumentation at each replication included two soil heat flux plates at a 7-cm depth (HFT3, REBS Inc., Seattle, WA), soil moisture sensors at a 3.5-cm depth (ML2x Theta Probe, Delta-T Devices, Cambridge, UK), and type-E soil thermocouples at 2- and 5-cm depths (TCAV, Campbell Sci.). Soil heat flux at the surface was approximated as the sum of heat flux at the depth of the plates (7 cm) and the rate change in heat storage in the 0-7 cm layer above the plates. Soil heat capacity needed for the heat storage term was computed from soil water content and soil bulk density (1.0 g cm^{-3}, from field samples) using the equation of deVries (1963). Meteorological data were logged with Campbell Scientific CR23X data loggers and AM16/32 multiplexers.

Longwave radiation as measured by the pyrgeometer on the CNR2 net radiometer was calibrated in the laboratory using a longwave source (personal communication, J.L. Heilman, Texas A&M University, College Station, TX). The calibration of the up- and down-facing pyranometers on the CNR2 radiometers was checked against an Eppley PSP Pyranometer (The Eppley Lab, Inc., Newport, RI). Factory calibration of the pyranometers proved accurate against the Eppley PSP; however, longwave measurements from the pyrgeometers needed adjustment by +40.9 and + 34.1% from factory calibration at the upland and lowland CNR2s, respectively. The calibrated CNR2s were also compared with a CNR1 (4-component Kipp and Zonen radiometer) and found to be in excellent agreement.

Soil moisture probes were site-calibrated against gravimetric soil samples taken near the location of each set of probes across various moisture contents throughout the summer and compared with lab output per recommended calibration procedures. Field data for biomass and leaf area index were collected manually at early, peak, and late growth stages at both sites (Table 4.1). Each biomass harvest consisted of clipping four 0.25-m^2 samples at 15-m intervals each from an east and west transect around the main tower footprint (eight samples total per site). Early and peak samples were analyzed for photosynthetic leaf area index using a LI-3100C Area Meter (Licor, Inc.) and weighed after drying to obtain biomass estimates representative of the footprint for each EC site.

The aboveground change in heat storage (ΔS) between the soil surface and the EC measurement height (3 m) was calculated from the rate change in air and canopy temperatures. The aerodynamic surface temperature (T_o) and air temperature profile were estimated using logarithmic wind profile theory; roughness length (z_0) and displacement height (d) were estimated from canopy height (Campbell and Norman, 1998). The sonic anemometer-derived estimates of friction velocity and the EC measurements of H were used to solve for T_o and the temperate profile every 30 min. The canopy temperature was assumed to be homogeneous and equal to T_o, whereas canopy-specific heat was approximated from biomass data following the approach of Meyers and Hollinger (2004). The air and canopy temperature time series data coupled with estimates of corresponding heat capacities were used to estimate the change in heat storage within the 0-3 m air layer and canopy biomass. Calculations of ΔS also included energy fluxes for photosynthesis. These fluxes were estimated by multiplying the CO_2 flux (measured with EC) by the energy required for glucose formation during photosynthesis (10.83 J mg CO_2^{-1}). As discussed in section 4.3.3, the magnitude of ΔS was small because of the low measurement height and short vegetation; however, given the focus of the study, it was important to include ΔS in the EB.

In 2007, a large-aperture scintillometer (LAS; Kipp and Zonen) was used to collect path-averaged turbulence data along a 500-m horizontal transect south of both EC stations. The transmitter and receiver were situated on upland terrain in the study watershed and adjacent watershed with similar management practices. The measurement transect spanned a large region of the watershed upwind of the tower sites (when wind direction was from the prevailing southerly direction). The LAS was accompanied by a weather station that measured R_n and G at an upland position using a CNR1 radiometer (Kipp and Zonen) and soil heat flux instrumentation. Details on the LAS system and methods of calculations are provided in Brunsell et al. (2008). The LAS measurements of H were compared with those from the upland and lowland EC towers.

4.2.3 Data processing

Post-processing of the EC data closely followed the procedures outlined in Baum et al. (2008). Post-processing included using the EdiRe software package (version 1.4.3.1167, J. Moncrieff, University of Edinburgh, UK) to correct EC data for despiking, lag removal, planar fit coordinate rotation (Lee et al., 2004; Wilczak et al., 2001), frequency response corrections (Massman, 2000; Moore, 1986), sonic-temperature sensible heat flux corrections for humidity

(Schotanus et al., 1983), and density corrections on CO_2 and H_2O measurements (Webb et al., 1980).

4.3 Results and Discussion

4.3.1 Interannual environmental conditions and biomass

Calculations of EB closure were based on data from 21 Jun to 30 Sep (day of year, DOY, 172 to 273) for both 2007 and 2008. This timeframe encompasses the most productive portion of the growing season in tallgrass prairie and, therefore, reflects maximized fluxes of λE and R_n. In 2007, growing-season precipitation between 1 May and 30 Sep was 496 mm; this is 21 mm below the historical average. However, 67% of this rainfall occurred in the first 2 months, and almost half of the total precipitation occurred in May alone (45%, Fig. 4.1). The study started on 21 Jun during a relatively wet part of the 2007 season when average volumetric soil moisture at the upland and lowland sites was at field capacity (~ 0.40 $cm^3 cm^{-3}$). Air temperatures for 2007 (as observed in Manhattan, KS, 14 km north of the study location) were only 0.2 °C below average from 1 Jun to 31 Jul, but daily air temperatures exceeded the historical mean by 2.1 °C, on average, for the remainder of the summer from 1 Aug to 30 Sep (Weather Data Library, Kansas State Univ.). During heat-stressed portions of the summer, two significant drydown periods occurred: DOY 180 to 203 and 216 to 232. The water demand was substantial during the latter part of the summer in 2007. Reference-crop evapotranspiration (ET_o; Allen et al., 1998) from DOY 172 to 273 was 459 mm, exceeding precipitation by 278 mm.

In contrast, 2008 was a much wetter year (total precipitation was 747 mm, 230 mm above average for 1 May to 30 Sep). Precipitation events occurred at nearly even intervals, and monthly rainfall totals and soil moisture remained consistent over the summer. This is atypical; precipitation events in this region tend to be intense and sporadic. In addition, air temperatures were 1.2 °C lower than average which lessened the effect of heat stress on the vegetation. On the initial date from which data were collected for comparison with 2007 observations, volumetric soil moisture paralleled 2007 data; it was about 0.40 cm^3 cm^{-3} at each site. In 2008, the environment experienced little water stress because precipitation exceeded reference-crop ET by 113 mm (for DOY 172-273: ET_o = 397 mm, precipitation = 510 mm). This resulted in exceptionally large biomass production compared with 2007 (Table 4.1). Heisler and Knapp (2008) used similar techniques for biomass collection and compiled peak biomass data for KPBS ungrazed, annually burned watersheds; the 16-year average for upland and lowland positions was 384 and 581 g m^{-2}, respectively. Aboveground biomass harvests in this study exceeded the 16-year average at the upland and lowland EC sites by 26 and 2%, respectively, in 2007 and by 40 and 33%, respectively, in 2008.

4.3.2 Landscape position effects

All fluxes were filtered with respect to wind direction (θ), friction velocity (u^*), and daytime R_n. Isolating the data most representative of the EC footprint during the diurnal efflux peak yields maximum fluxes used to determine closure. Data were included for closure computation if the corresponding filter parameters met the following criteria: prevailing southerly wind directions (165° < θ < 255°), sufficient turbulent mixing (u^* > 0.15 m s^{-1}; Barr et al., 2006; Goulden et al., 1996), and daytime radiation (R_n > 125 W m^{-2}). In this paper, reference to all data is defined by the latter statement unless stated otherwise, in which case the data would be shown with no filtering ("unfiltered"; e.g., for analysis of diurnal data).

4.3.2.1 Energy balance components

Composite diurnal trends were compiled from unfiltered data of H, λE, R_n, and $G - \Delta S$ for three periods of equal length throughout the summers of 2007 (Fig. 4.2) and 2008 (Fig. 4.3) at the upland and lowland sites. Each 34-d-long period corresponds to one third of the timeframe for collection commencing on the summer solstice and concluding at the end of Sep. During summer, EB of the tallgrass prairie ecosystem is largely driven by R_n and λE. Obtaining accurate measurements of λE is very important for determining the degree of closure within this system. Latent heat flux was the dominant form of energy loss in early 2007, but was even more dominant in 2008 when water was not limiting (Table 4.2a). On average, λE fluxes were about 8% greater at the lowland site for both years (Table 4.2b), which was expected as a result of the higher water availability and leaf area at the lowland site. Data from 2007 demonstrate this result well. As the environment became more arid in late 2007, the lowland experienced less stress than the upland. During this timeframe, the largest difference between upland and lowland λE for the entire study was seen (14.5%, Table 4.2a). For the most part, this trend was noted in both summers (despite the wetness of 2008). Sensible heat flux varied little between sites despite the differences across the landscape and, as expected, H increased after the canopy reached its peak and began senescence in the late summer. Fluxes of H and λE are discussed more in section 4.3.4.

Throughout both summers, the storage terms (i.e., $G + \Delta S$) deviated marginally in magnitude and between sites (Table 4.2a, b). Because these data span the most productive part of the growing season, during which the canopy largely controls the energy exchange to the surface, storage or release of heat in the soil and canopy remained small. Measurements of soil heat flux recorded during FIFE (the First International Satellite Land Surface Climatology Project [ISLSCP] Field Experiment), conducted on the KPBS in 1987 and 1989, show agreement with our observations (Figs. 4.2 and 4.3) in that G differed little between uplands and lowlands (daytime maximum of ~10 W m^{-2} higher at uplands during the growing season; Smith et al., 1992).

Net radiation was similar between the two sites (i.e., within 2.1% on average). Any discrepancies are likely due to differences in surface albedo and possibly patchy cumuliform cloud cover (Smith et al., 1992). The maximum deviation between sites for net radiation occurred in midsummer 2007; the upland site had 1.0 MJ m^{-2} d^{-1} more integrated R_n than the lowland site (Table 4.2a). The minimum difference occurred from 21 Jun to 24 Jul in 2008, during which the average daily accumulation of net radiation was equivalent at both sites. Averages for each year show that the upland site received more net radiation per day than the lowland site by 0.5 and 0.2 MJ m^{-2} d^{-1} in 2007 and 2008, respectively. This disagrees with the trend between hilltops and bottoms noted by Smith et al. (1992), but it is important to stress that these differences were very small (~2% for both years, Table 4.3b) in our study.

Despite the homogeneity of the study watershed, differences exist between prairie uplands and lowlands that are consistent throughout the Flint Hills: (1) upland locations typically experience higher wind speeds, (2) lowlands see increased drainage and have a deeper soil layer that allows for better retention of moisture, and, therefore, (3) higher biomass production is generally observed within watershed bottoms. Considering these differences, one might expect larger variations in the energy budget than were observed in the present study. Data suggest that topography-induced differences in soil water within a catchment create λE differences in the range of 5 to 13% between uplands and lowlands (Table 4.2b). Otherwise the deviation across the landscape was quite small, at least with the precipitation levels of 2007 and 2008. Of all variables discussed, the largest difference between the two sites was that λE accounted for more of the net radiation flux at the lowland position (Table 4.2a, b), which is consistent with the greater soil water holding capacity usually seen in these topographical regions.

4.3.2.2 Regression comparison of incoming and outgoing energy

The EB closure coefficient, α, represents the portion of available energy that is fulfilled by the sensible and latent heat fluxes:

$$(R_n - G - \Delta S) = \alpha (H + \lambda E) + b \tag{4.2}$$

where b is the intercept, or offset, of the regression analysis between incoming and outgoing energy and α is the slope. Coefficient and intercept estimates result from an ordinary least-squares (OLS) linear fit during the same three consecutive periods previously discussed (Figs. 4.4 and 4.5). In early summer 2007, values of α at the upland and lowland sites were 0.803 and 0.811, respectively. Midsummer to late-summer closure coefficients tended to increase as the prairie system became increasingly water and heat stressed in 2007 (Fig. 4.4). From late Jul through Aug, a slightly greater deviation in slope of 3.7% occurred between sites; α was 0.846 at the upland site and 0.883 at the lowland site. End-of-summer closure coefficients were nearly identical (α = 0.856 and 0.854 from 28 Aug to 30 Sep for upland and lowland sites, respectively). For the most part, α leveled off after increasing midsummer as the environment gradually became more desiccated from the heat and a strong precipitation deficit. Summer 2007 did not, however, demonstrate a marked overall difference in lack of closure between upland and lowland sites, which displayed closure coefficients of 0.828 (upland) and 0.844 (lowland) with intercepts of 19.4 and 19.3 W m^{-2} (upland and lowland) for OLS plots of the entire summer at each site (not shown).

The lowland site displayed greater α than the upland site in 2008 on average, and both sites had higher average offsets for most of the timeframes in 2008 than for those in 2007 (Fig. 4.5). Upland coefficients were 0.775, 0.887, and 0.854 for the first, second, and third periods in 2008, respectively. In 2008, the EB coefficient was much larger at the lowland for the first period (0.876), converged with upland α for the second time period (0.886), and exceeded the upland site for the third period (0.891). Offsets for the 2008 regression plots of the entire summer were 26.8 and 33.0 W m^{-2} at the upland and lowland sites, respectively. The larger intercept values in 2008 indicate a positive bias in the data, but again, differences in *b* between years were small.

On average, α_{up} = 0.828 and 0.809 and α_{low} = 0.844 and 0.885 in 2007 and 2008, respectively. The mean upland intercept in both years was 23.1 W m^{-2}, whereas the lowland intercepts averaged 26.2 W m^{-2}. Variation in α_{up} was –1.9 % from 2007 to 2008, and α_{low} was 4.1% higher in 2008 than in 2007. The average offsets for the entire summer increased 7.4 W

m^{-2} from 2007 to 2008 at the upland site and 13.7 W m^{-2} from 2007 to 2008 at the lowland site. When data from the two years were compared, regression analysis suggested that EC performed in a lowland position within tallgrass prairie has a marginally higher degree of closure than EC performed at an upland location in the same watershed. The average overall closure coefficient over both years was 0.819 at the upland site and 0.865 at the lowland site. Topographical deviation in α and b was not large based on the overall combined yearly average throughout the entire watershed (α = 84.2 ± 3.2%, b = 24.6 ± 6.6 W m^{-2}).

Hammerle et al. (2007) reported similar findings over meadows in Austria where EC data were tested for closure using measurements from two different elevations along a mountain slope. They saw that turbulent surface fluxes averaged 71 and 72% of the available energy for the two locations (high and low elevations, respectively). The variation in closure between the two sites was smaller than what was observed at the Konza Prairie, which is especially interesting considering that the Hammerle et al. study had a drastic elevation difference of 800 m between sites, whereas the upland and lowland sites in our study differed by only 14 m. Though Hammerle et al. (2007) partitioned EC data into growing season intervals (as we did in our study), their closure data were not presented on a periodic basis, thus seasonal drift in closure could not be compared with our results.

Hunt et al. (2002) studied a tussock grassland in New Zealand by using the EC method and found good closure over the summer (0.87 to 1.03). The tussock grassland system does not, however, depend on λE as a strong driver of the daytime energy budget. In tallgrass prairie, productive grasses resulted in maximum evapotranspiration values upward of 8 mm d^{-1} (seen in early Aug 2008 at the lowland site, data not shown), but the short tussock grassland had a maximum evapotranspiration rate of 3.8 mm d^{-1}. Of the 3 days analyzed for closure by Hunt et al., λE values decreased from 5.1 to 1.0 MJ m^{-2} d^{-1}, and H increased dramatically from 4 to 9.8 MJ m^{-2} d^{-1}.

In 2002, Ham and Heilman (2003) conducted EC in a cedar forest near Manhattan, KS, USA, and at the same KPBS upland location used in this study. Closure coefficients in June were 0.96 at the forest, whereas fluxes of H were much higher than those at the prairie. For the same period at the prairie, $\alpha = 0.79$ (regression data adjusted to a zero-intercept for both sites). Ham and Heilman's (2003) prairie data are very similar to our results in Figs. 4.4 and 4.5. Results from 2002 and 2007–2008 for the upland site show no obvious difference in closure despite the year-to-year variation (e.g., severe drought in early summer 2002 but little to no early growing season precipitation deficit in 2007 and 2008).

The linear fit for each plot in Figs. 4.4 and 4.5 had little scatter. Coefficients of determination (R^2) indicated good correlation, ranging from 0.84 to 0.95, between incoming and outgoing energy in both years. Verification of OLS estimates of EB closure was performed by implementing the reduced major axis (RMA) methodology of Meek et al. (1998), which was adapted to FLUXNET data by Wilson et al. (2002). The RMA technique provides good validation of OLS data because of inherent assumptions to which OLS regression is subject, particularly the assumption that there are no random errors in the independent variables, which in this case is the available energy term ($R_n - G - \Delta S$). Because these data are periodic with time (i.e., they display a pattern that is not innately random), the basic assumptions for OLS regression are essentially broken, and though that does not necessarily render the OLS statistics invalid, it is good practice in this case to have a check on these regression data. Table 4.3 shows the results of RMA analyses for corresponding OLS regression information, and there was good agreement between OLS and RMA numbers.

4.3.2.3 Residual surface energy

When the EB cannot be closed, eq. 4.1 can be modified to quantify any leftover energy, referred to as the EB residual. Calculations of residual energy were made by solving eq. 4.1 inferring lack of closure:

$$E_{res} = R_n - G - \Delta S - H - \lambda E \qquad (4.3)$$

where E_{res} is measured in W m^{-2}. As fluxes of the various terms from the EB increase, the energy residuum increases. This energy has a distinct diurnal trend that did not vary much throughout the study period (Fig. 4.6). Seasonal composites of average half-hourly residual energy showed a maximum during midday, demonstrating strong correlation with patterns of λE and R_n (Figs. 4.2 and 4.3). In 2007, both sites showed agreement, with maximum residuals of approximately 82 and 75 W m^{-2} at the upland and lowland sites, respectively. But in 2008, the sites differed more near solar noon; upland E_{res} peaked around 83 W m^{-2} and E_{res} at the lowland was 53 W m^{-2}. Residual values became negative during the night and tended to be similar between sites. The energy deficit approached zero only at dawn and dusk. The integrated daily residual (Fig. 4.6) was 1.2 and 1.1 MJ m^{-2} d^{-1} in 2007 and 2008, respectively, at the upland, whereas the lowland site accrued 0.8 and 0.3 MJ m^{-2} d^{-1} in 2007 and 2008, respectively. Accumulated daily residuals were positive (i.e., turbulent fluxes underestimated available energy in the system).

Researchers who evaluate EC for closure commonly find that energy imbalance manifests as a deficit of available energy. In east central Germany, Laubach and Teichmann (1999) paid special attention to inhomogeneities within the EC flux footprint and noted the propensity for underestimation of available energy in flux data over a mixed-grass site (α ranging from 0.76 to 1.07 with small negative intercepts). Each value for closure was determined from various sensor heights on the EC tower (to change the source area) over two consecutive summers. On average, the closure coefficients found by Laubach and Teichman were good the first year (0.89) and very good the second year (0.97), but the underestimation was still evident. Consideration of sensor uncertainty and addition of energy storage by photosynthesis did not explain the energy residuum, which approached nearly 100 W m^{-2} during daylight. Those researchers also mentioned that the components of available energy were not representative of the entire study area because much of the footprint varied in canopy height and species composition, but this effect on closure was deemed negligible. They posited that detailed source area analysis could resolve the variability in closure based on seasonality and wind direction, but studying heterogeneities does not reveal them as the reason for lack of closure or why turbulent fluxes typically underestimate available energy. Laubach and Teichmann (1999) concluded that based on Monin-Obukhov similarity theory applications (i.e., EC) are only apposite over impeccably homogeneous landscapes which, in actuality, are unrealistic. Such findings can give weight to EC performed in landscapes that are relatively homogeneous and flat, where basic theoretical assumptions regarding the application of EC are more likely to lend validity to corresponding measurements. Despite this assertion, which has been generally agreed upon in the scientific community, ideal locations for EC continually turn up energy imbalances as well (Oncley et al., 2007; Paw U et al., 2000; Wilson et al., 2002).

Note that our filter criteria vary from those of other studies. Our objectives were to isolate data from the upland and lowland EC towers that would be the most accurate for each EB component and to narrow down a dataset that corresponds to daytime hours when the residual is generally highest. Most studies filter for prevailing wind speed (after post-processing), and a few filter for friction velocity (see discussion of filtering techniques at the beginning of section 4.2).

4.3.3 Concomitant source areas and low-frequency fluctuations

To date, extensive work has been done to determine the accuracy with which available energy can be measured, particularly in regard to estimates of net radiation (Kohsiek et al., 2007; Laubach and Teichmann, 1999; Moderow et al., 2009; Schmid, 1997; Twine et al., 2000). This is important to establish as net radiation is usually the dominant energy input into terrestrial ecological systems. Radiation measurements generally exact the most precise data while sampling the EB (Kohsiek et al., 2007; Twine et al., 2000), but despite the dependability of the instrument, landscape heterogeneities that may exist between the field of view of the radiometer(s) and the EC footprint have often been considered a possible contributor to the overall energy imbalance (Foken et al., 2006; Foken, 2008; Laubach and Teichmann, 1999; Schmid, 1997; Twine et al., 2000; Wilson et al., 2002).

Perhaps the most advisable paradigm is to compute net radiation as the sum of the incoming and outgoing longwave and shortwave components (Halldin, 2004; Kohsiek et al., 2007). This study used the CNR2 (Kipp & Zonen), which is a radiometer that measures net radiation from the four components. These measurements were placed 30 m into the prevailing direction of the EC footprint to align the source area of the radiation measurements with the EC source area. At the same time, a Q*7.1 net radiometer (REBS, Inc.) was positioned in a more traditional deployment in a chosen representative area approximately 10 m lateral to the EC footprint. Comparisons between the CNR2 and the Q*7.1 match observations made during EBEX-2000 between a CNR1 (a highly regarded model similar to the CNR2, also a Kipp & Zonen) and the Q*7.1 (Kohsiek et al., 2007) (data not shown). Recall from section 4.2.2 that CNR2 measurements of shortwave and longwave radiation in the prairie had excellent agreement with data from a CNR1 running simultaneously within an adjacent watershed. On the basis of these results, the CNR2 was determined to be the more accurate measure of net radiation at the two EC sites and hence was used solely for radiation measurements within the EC source area (and thus, the only R_n data used for EB calculations). In addition to using measurement of R_n by the four components, incorporating these measurements from within the footprint adequately tests the R_n part of the second factor mentioned by Foken et al. (2006) regarding mismatched source areas and produces a high quality dataset of net radiation for this study.

Soil heat flux calculations were an average of two separate soil instrumentation suites. The first grouping of instruments was positioned in the vicinity of the CNR2 net radiometer within the EC footprint. A replication of the soil instrumentation was also installed 3 m south of the tower in a more traditional deployment configuration (i.e., along the prevailing wind). Figure 4.8 shows the average difference between the traditional deployment and the footprint soil measurements. Some spatial variability exists between the two installments, but these slight inconsistencies are still small in regard to the available energy. The largest average diurnal deviations in G between the tower and footprint deployments were ±15 W m^{-2} at the upland site and ±8 W m^{-2} at the lowland site. Smith et al. (1992) showed that available energy for annually burned, ungrazed watersheds within the Konza prairie (similar to the watershed in this study) tended to depend more on the magnitude of incoming net radiation than on variations in soil heat flux. By using the mean soil heat flux of the location near the tower and the position within the EC prevailing sampling area, we obtained a more representative estimation of soil heat flux for closure analyses.

As described in section 4.2.2, the energy represented by ΔS (the change in heat storage within the canopy and the 0-3 m air column as well as the energy storage from photosynthesis) was included in all calculations involving the available energy term and thus any quantification of closure. Note that including ΔS increased calculations of overall closure. This increase, however, was 2.8% on average with a range of 1.4 to 4.4% for the three periods throughout the summer over both years. The composite average ΔS diurnal trend for each year is shown in Fig. 4.8 for the upland and lowland sites. Diurnal differences between the two sites were largest during midday, and from the beginning to the end of each summer, a consistent decrease in daily total ΔS occurred. This was similar between the sites within each summer; total ΔS declined by 105 and 79% in 2007 and 2008, respectively (data not shown). Such decreases in ΔS are expected because of the decline in photosynthesis as biomass matures and senescence sets in during the latter (and often the most stressed) portion of each summer. The lowland site had greater ΔS than the upland site in both years, and ΔS was higher at both sites in 2008 because of the lack of stress on the canopy, which again allowed for more energy storage by photosynthesis.

Although our data did not reveal the recondite nature of the systematic energy imbalance using EC, we did make improvements in regard to maximizing closure within this particular watershed. As stated previously, Ham and Heilman (2003) reported a closure coefficient of 0.79 at the same KPBS upland site used in this study, whereas in the present study, the estimated closure across 2 summers for the upland site was about 0.91 (see section 4.3.4). Given the high quality dataset of available energy, it appears that possible spatial variation between traditional R_n and G source areas and the EC footprint have little effect on overall closure within the tallgrass ecosystem.

Many studies have considered the contribution of low-frequency fluctuations to this systematic 20% energy imbalance (Foken and Wichura, 1996; Gao et al., 2017; Oncley et al., 1990). To evaluate whether the tallgrass prairie environment elicits energy exchanges at lower frequencies, we performed Ogive analysis to test if the sampling frequency and averaging interval of EC data adequately capture these exchanges (Foken and Wichura, 1996). Eddy covariance data in this study were collected at 20 Hz with integration periods of 30 min. The Ogive analysis provided no evidence that pointed to loss of flux through low-frequency transport (data not shown). Results from this analysis also suggest that averaging intervals of 20 min would also have been acceptable. Half-hourly fluxes are more than sufficient to describe H and λE in this system. Eder et al. (2014) tried to correct EB data using different parameterizations which included large-scale circulations from the literature. They suggested that both parameterizations failing suggests that the influence of mesoscale structures is not sufficient to explain the residual energy when using EC.

4.3.4 Latent and sensible heat flux and energy balance closure

Fluxes of latent and sensible heat are often used to quantify the evaporative demand of an environment by evaluating the ratio of H / λE, which is called the Bowen ratio (BR). Typically, BR < 1 indicates a more mesic environment, whereas BR > 1 points to an arid environment. In northeastern Kansas, BR usually increases throughout the latter portion of the growing season, when precipitation input tends to slow in correspondence with seasonal temperature maxima. As the summer progressed in 2007 and 2008, closure seemed to improve (closure is represented by the energy balance ratio, EBR, derived from eq. 4; Fig. 4.9). This development corresponded with increasing BR as the environment tended to dry, but correlation between closure and BR was low for both years (R^2 = 0.015 and 0.075 in 2007 and 2008, respectively, data not shown). Other studies have found no discernible correlation between closure and BR (Moderow et al., 2009; Oladosu and Sunmonu, 2011; Wilson et al., 2002). But despite the lack of regression correlation, many studies have obtained excellent closure in environments with high BR (Ham and Heilman, 2003; Heusinkveld et al., 2004; Hunt et al., 2002; Mauder et al., 2007b; Oladosu and Sunmonu, 2011). Visual assessment of increased closure over time was more apparent at both sites in 2007 when a late season dry spell portended higher BR, than in 2008 when only the upland site showed a perceptible increase in closure throughout the summer. Any visually observed correlation could be an artifact of less R_n and λE (i.e., less overall energy) in the environment during late summer, both of which dominate the energy exchange of the prairie system.

The total measure of closure at each site was determined using the methods of Wilson et al. (2002) to calculate the EBR:

$$\text{EBR} = \frac{\sum(H + \lambda E)}{\sum(R_n - G - \Delta S)} \qquad (4.4)$$

This equation was used to compile Fig. 4.9 and Table 4.3. The total EBR in 2007 was 0.882 and 0.901 at the upland and lowland sites, respectively (0.891 for both sites combined, Table 4.3). The degree of closure was greater in 2008, when higher λE fluxes at the lowland may have contributed slightly more outgoing energy to the overall budget. In 2008, the lowland site effectively closed the EB at an astounding 97.9% of the available energy (EBR = 0.979); upland closure was 88.3% (EBR = 0.883), and EBR of the total watershed was 0.932 (Table 4.3).

The 2007 study period coincided with deployment of an LAS that spanned a 500-m transect south of both EC towers. Integrated fluxes of H were recorded along the 500-m-long optical path (see end of section 4.3.2 for description). The LAS sensible heat flux data were compared with those of both towers (Fig. 4.10a). Sensible heat flux derived from the LAS (H_{LAS}) was marginally greater than lowland H and slightly less than upland H. Data presented in Fig. 4.10 are comparable to the findings of Liu et al. (2011) which also compared LAS and EC measurements of H. Considering the differences in scales and techniques, the agreement is good.

4.3.4.1 Accuracy of measuring the vertical wind speed

Recent studies by Kochendorfer et al. (2012), Horst et al. (2015), and Frank et al. (2016) have highlighted the significance of scrutinizing measurements of the vertical wind speed (*w*) made by non-orthogonal sonic anemometers. In these articles, the authors went to extreme care to ascertain the veracity of sonic anemometers (widely used in nearly all micrometeorological studies within the planetary boundary layer) to measure *w*, upon which the magnitude and direction of all turbulent flux data relies. The team that performed these studies concluded that transducer shadowing in non-orthogonal sonic anemometers typically results in underestimates of turbulent fluxes by 10-15%, with the full range of flux underestimates varying from -5 to +37% (Kochendorfer et al., 2012), 10 ± 2% (Frank et al., 2016) and 4-5% (Horst et al., 2015). Taking this important finding into account, EB closure variables derived from our data were recalculated with an assumed error of 10% (Frank et al., 2016) in H and λE for comparison. Table 4.4 shows how the “new” EBR calculated from the results of Frank et al. (2016) (EBR_{10}, second column) is affected when H and λE are adjusted to the value they would have had if their current value is 10% less than the “true flux” (see footnote for Table 4.4). The EBR calculated at the beginning of section 4.3.4 is displayed again for reference in the first (shaded) column of Table 4.4. The result of this calculation shows that closure increases for both sites and both years, ranging from 0.980 (upland, 2007) to 1.094 (lowland, 2008). Including this change in turbulent energy causes each period throughout the summers of 2007 and 2008 to approximate unity, with the exception of the lowland site in 2008 (which already had extremely high λE fluxes). The overall average closure across sites and years for EBR_{10} is 1.014. Kochendorfer et al. (2012) point out that the error in turbulent fluxes varies in an inconsistent fashion between manufacturers and even between instruments of the same make and model. They suggest that each non-orthogonal sonic anemometer may require its own calibration coefficient or correction, but further research will need to be accomplished to examine the ability of those implementing these anemometers to “back-correct” their flux data, if possible. However, Frank et al. (2016) applied a Bayesian correction algorithm to EC data and obtained excellent closure after doing so. Applying a rough correction to the H and λE data from our study seems to support the idea that the systemic lack of closure may indeed lie within making measurements of *w* that are corrected for transducer shadowing Based upon data from this study, it certainly appears that the “missing” energy is imbedded within the measurement of turbulent fluxes. Latent heat is definitely the driver of energy within the tallgrass prairie ecosystem, and the ratio of calculating λE_{res} with λE if it were underestimated by 10% (λE_{10}) appear to be very close to 1 (Table 4.4). This may indicate that measurements of λE in our study were relatively consistent with the mean error suggested by Frank et al. (2016) throughout both years and both summers. However, the ratio of H_{res} to H_{10} shows a marked difference from the beginning of each summer at each site to the end of the summer, but this is likely more related to how H changes throughout a growing season. Further research efforts will need to focus on the accuracy with which we measure *w*. If the residual energy is a result of errors in the vertical velocity, then forcing closure by using the BR (Twine et al., 2000) could be a reasonable way to resolve underestimation of H and λE terms.

4.4 Conclusions

Much discussion has taken place regarding the “ideal” landscape in which to perform EC measurements. Many would agree that tallgrass prairie can provide the ingredients known to make EC more viable: highly uniform vegetation is generally found within annually burned watersheds, upland and lowland terrains are often level enough for sufficient sampling range, and the windy environment encourages turbulent transport. In this study, every effort was exacted to minimize any effect of measurement and processing errors. Additionally, available energy measurements (R_n and G) were positioned within the prevailing footprint of each EC tower to resolve spatial mismatch in the component source areas of the energy budget observations. To further increase the accuracy of the available energy term, the change in heat storage within the canopy/air column along with the energy from photosynthesis (ΔS) was integrated into EB calculations. Nevertheless, the EBR was 0.882 and 0.901 at the upland and lowland sites, respectively, in 2007 and 0.883 and 0.979 at the upload and lowland sites, respectively, in 2008. Across both years, EC measurements at the watershed scale accounted for 89.1 and 93.1% of the total EB.

Despite differences between uplands and lowlands, neither surface energy budget nor degree of closure was strongly affected by landscape position within the watershed or across years. The largest difference between the two sites was that the lowland site had, on average, 8% higher λE than the upland site.

Only marginal improvement in closure was seen by resolving the scale mismatch, which some researchers have suggested as a possible hindrance to closing the energy budget with

EC (Foken et al., 2006; Kohsiek et al., 2007). The available energy dataset obtained in this study is representative of the EC footprint and is of extremely high quality. There is no indication that any of the R_n and G data had errors on the order of the energy imbalance (i.e., up to 20%). Given the location of the R_n and G measurements in near the center of the EC source area, and the spatial uniformity of the source area in general, it is highly unlikely that a scale mismatch between R_n + G and the EC measurements was a factor.

Sensible heat flux barely varied between sites and contributed only a small amount to the overall system energy exchange. In 2007, simultaneous data acquisition by an LAS upwind of the upland and lowland towers helped to verify the magnitude of H measurements at each EC tower. There was no clear evidence of any errors in EC estimates of H at either site.

The EB within a tallgrass prairie ecosystem is highly dependent on R_n and λE. Available energy in this environment is largely influenced by the input from R_n (Smith et al., 1992), and for a typical summer in northeast Kansas, sensible heat flux tends to contribute less to the total energy output than λE. Given the high degree of confidence in measurements of available energy (particularly R_n) and the lack of evidence pointing to large errors in H, it seems pertinent to take a closer look at possible correlations between λE and the lack of closure within a system. The data presented in this paper do not support the rationale for lack of closure that are often detailed in the literature (i.e., mismatched source areas of available and turbulent energy measurements, overlooked low-frequency energy transport, poor instrument quality/calibration or post-processing procedures, nonhomogeneous vegetation within the sampling area, or highly irregular topography). Given the lack of data suggesting that H is in error, these observations point to a possible systemic error in λE, leaving one to ponder if λE is somehow the culprit responsible for the overall energy imbalance when using EC. This may be the direct result of the sonic anemometer underestimating velocity and the subsequent EC calculation of turbulent fluxes of H and λE (Frank et al., 2016; Horst et al., 2015; Kochendorfer et al., 2012). From this, using a general correction of +10% for turbulent fluxes in this study results in near-perfect closure. Unfortunately, until the important issue of the EB closure problem is fully resolved, researchers are likely to underestimate field-scale evapotranspiration and possibly other scalars (CO_2 fluxes) when using EC.

4.5 Tables

Table 4.1. Green leaf area index and aboveground biomass for each site ± standard error for the summers of 2007 and 2008.

	Leaf Area Index (cm^2 cm^{-2})		Biomass (g m^{-2})	
Date	Upland	Lowland	Upland	Lowland
22 May 2007	1.6 ± 0.3	1.5 ± 0.3	137 ± 23	137 ± 25
24 Jul 2007	3.0 ± 0.9	3.6 ± 1.3	482 ± 65	595 ± 124
30 May 2008	1.0 ± 0.2[a]	1.5 ± 0.3[a]	107 ± 9	147 ± 52
03 Jul 2008	3.0 ± 1.2	3.6 ± 0.7	336 ± 62	464 ± 108
21 Aug 2008	2.8 ± 1.1	3.8 ± 1.3	539 ± 117	773 ± 168

[a] $p > 0.05$

Table 4.2. Composite mean 24-hr energy balance components.
(a) Average daily flux calculated by integrating under the curves in Figs. 4.2 and 4.3 (first four columns for each site). Right column under each site heading is the average 24-hour cumulative λE-derived ET. Data in Table 4.2a are unfiltered.

	Upland					Lowland				
	λE	H	R_n	G + ΔS	λE	λE	H	R_n	G + ΔS	λE
Date	-------- (MJ m^{-2} d^{-1})--------				(mm d^{-1})	-------- (MJ m^{-2} d^{-1})--------				(mm d^{-1})
21 Jun – 24 Jul, 2007	9.3	0.5	12.9	-0.8	3.4	9.7	0.1	12.2	-0.9	3.4
25 Jul – 27 Aug, 2007	10.0	1.3	12.7	-0.7	3.6	9.8	0.3	11.7	-0.6	3.8
28 Aug – 30 Sep, 2007	6.2	1.7	8.2	0.1	2.4	7.1	1.2	8.3	0.0	2.8
2007 Average	**8.5**	**1.2**	**11.3**	**-0.5**	**3.1**	**8.9**	**0.5**	**10.7**	**-0.5**	**3.3**
21 Jun – 24 Jul, 2008	12.2	-1.1	13.8	-1.1	4.7	13.0	-0.8	13.8	-1.3	5.0
25 Jul – 27 Aug, 2008	9.8	-0.2	11.3	-0.5	4.0	9.5	0.0	10.6	-0.6	4.0
28 Aug – 30 Sep, 2008	7.1	0.5	8.0	0.0	2.8	7.4	0.6	8.2	-0.1	2.9
2008 Average	**9.7**	**-0.3**	**11.0**	**-0.5**	**3.8**	**10.0**	**-0.1**	**10.9**	**-0.7**	**4.0**

(b) Difference between upland and lowland values for total daytime integrated flux calculated from the full filter data from Figs. 4.4 and 4.5. % Difference = (100%) × ($Flux_{UP}$ – $Flux_{LOW}$) / $Flux_{UP}$

	λE	H	R_n	G + ΔS
Date	------------% Difference------------			
21 Jun – 24 Jul, 2007	-5.8	—	2.2	-6.7
25 Jul – 27 Aug, 2007	-5.3	—	4.3	6.3
28 Aug – 30 Sep, 2007	-13.3	—	-0.3	0.7
2007 Average	**-8.1**	[a]—	**2.1**	**0.1**
21 Jun – 24 Jul, 2008	-9.9	—	2.9	14.5
25 Jul – 27 Aug, 2008	-7.3	—	1.4	11.3
28 Aug – 30 Sep, 2008	-5.9	—	1.8	6.0
2008 Average	**-7.7**	[a]—	**2.1**	**10.6**

[a] H data are not presented because daytime integrated H varied near zero and resulted in a spurious ratio

Table 4.3. Slopes from the ordinary least squares (OLS), reduced major axis (RMA), and the energy balance ratio (EBR). Average OLS and RMA are from data used in Figs. 4.4 and 4.5, and total EBR was calculated using data from Fig. 4.9.

	Upland			Lowland		
Date	OLS	[a] RMA	EBR	OLS	[a] RMA	EBR
21 Jun – 24 Jul, 2007	0.803	0.841	0.839	0.811	0.884	0.868
25 Jul – 27 Aug, 2007	0.846	0.871	0.893	0.883	0.925	0.896
28 Aug – 30 Sep, 2007	0.856	0.880	0.914	0.854	0.893	0.945
Entire Summer 2007	**0.828**	**0.859**	**0.882**	**0.844**	**0.897**	**0.901**
21 Jun – 24 Jul, 2008	0.775	0.809	0.844	0.876	0.946	0.979
25 Jul – 27 Aug, 2008	0.887	0.910	0.895	0.886	0.934	0.991
28 Aug – 30 Sep, 2008	0.854	0.881	0.935	0.891	0.929	0.970
Entire Summer 2008	**0.809**	**0.844**	**0.883**	**0.885**	**0.942**	**0.979**

[a] To perform RMA, regression statistics were found for the reverse axes of corresponding OLS plots. For example, in Figs. 4.4 and 4.5, the ordinate would be available energy (R_n – G – ΔS), and the abscissa would be the turbulent fluxes (H + λE). The RMA coefficient was calculated as the square root of the OLS slope (left columns, above) and the new slope of the reversed OLS. $RMA = \sqrt{slope_{OLS} / slope_{reverse\ OLS}}$

Table 4.4. Comparison of EBR from this dataset (shaded) to EBR_{10} (where the turbulent data is assumed to be underestimated by 10%) as well as an additional comparison of λE_{res} and H_{res} to corresponding hypothesized errors in λE and H (Frank et al., 2016).

	Upland				Lowland			
Date	EBR	[a] EBR_{10}	$\frac{\lambda E_{res}}{\lambda E_{10}}$	$\frac{H_{res}}{H_{10}}$	EBR	[a] EBR_{10}	$\frac{\lambda E_{res}}{\lambda E_{10}}$	$\frac{H_{res}}{H_{10}}$
21 Jun – 24 Jul, 2007	0.839	0.933	1.10	2.30	0.868	0.964	1.05	2.63
25 Jul – 27 Aug, 2007	0.893	0.993	1.05	1.31	0.896	0.996	1.03	1.46
28 Aug – 30 Sep, 2007	0.914	1.016	1.03	1.13	0.945	1.050	0.98	1.08
2007 Average	**0.882**	**0.980**	**1.06**	**1.39**	**0.901**	**1.001**	**1.02**	**1.43**
21 Jun – 24 Jul, 2008	0.844	0.938	1.07	[b]-36.5	0.979	1.158	0.92	1.83
25 Jul – 27 Aug, 2008	0.895	0.994	1.01	9.17	0.991	1.138	0.91	1.17
28 Aug – 30 Sep, 2008	0.935	1.038	0.99	1.15	0.970	1.038	0.94	1.02
2008 Average	**0.883**	**0.981**	**1.03**	**2.34**	**0.979**	**1.094**	**0.92**	**1.14**

[a] If our measured λE (and likewise, H) is underestimated by 10%, then the new flux (λE_{10}) is related to λE by: $\lambda E = \lambda E_{10} - 0.1\lambda E_{10}$ and solved for λE_{10} takes the form: $\lambda E_{10} = \frac{\lambda E}{1-error\ in\ \lambda E} = \frac{\lambda E}{1-0.10}$.

[b] Daily fluxes were close to zero and resulted in spurious ratios.

4.6 Figures

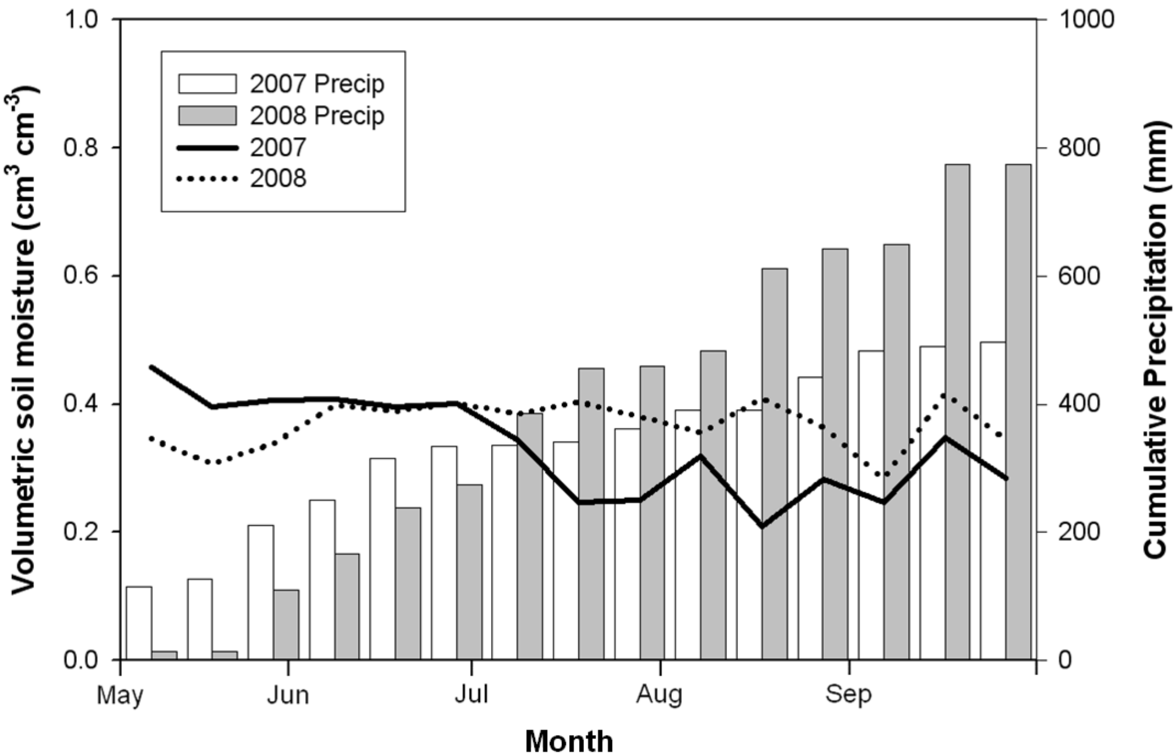

Figure 4.1. Growing season 10-d cumulative precipitation and average volumetric soil moisture at a 3.5-cm depth.

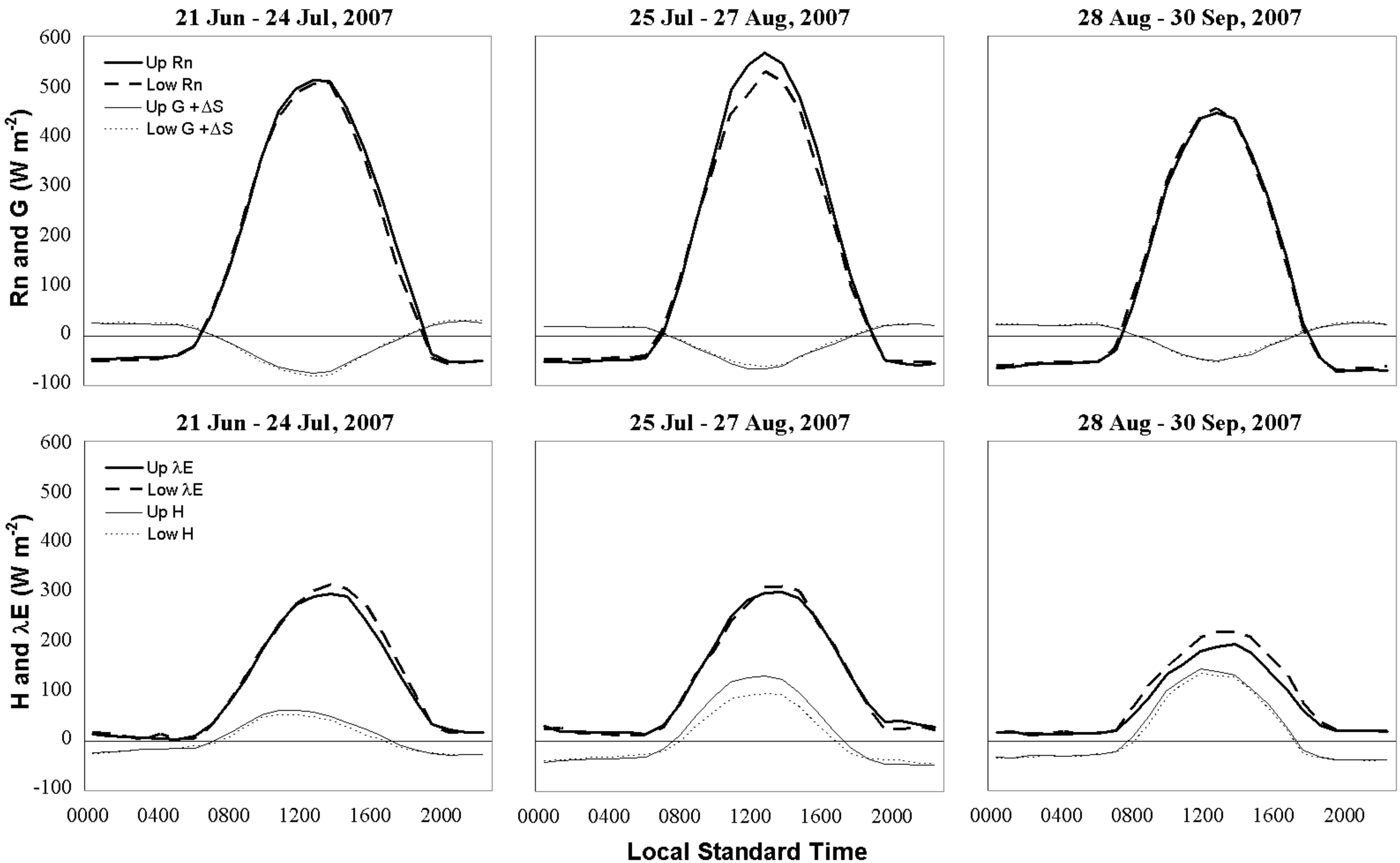

Figure 4.2. Comparison of upland and lowland diurnal energy balance in early and later summer, 2007.

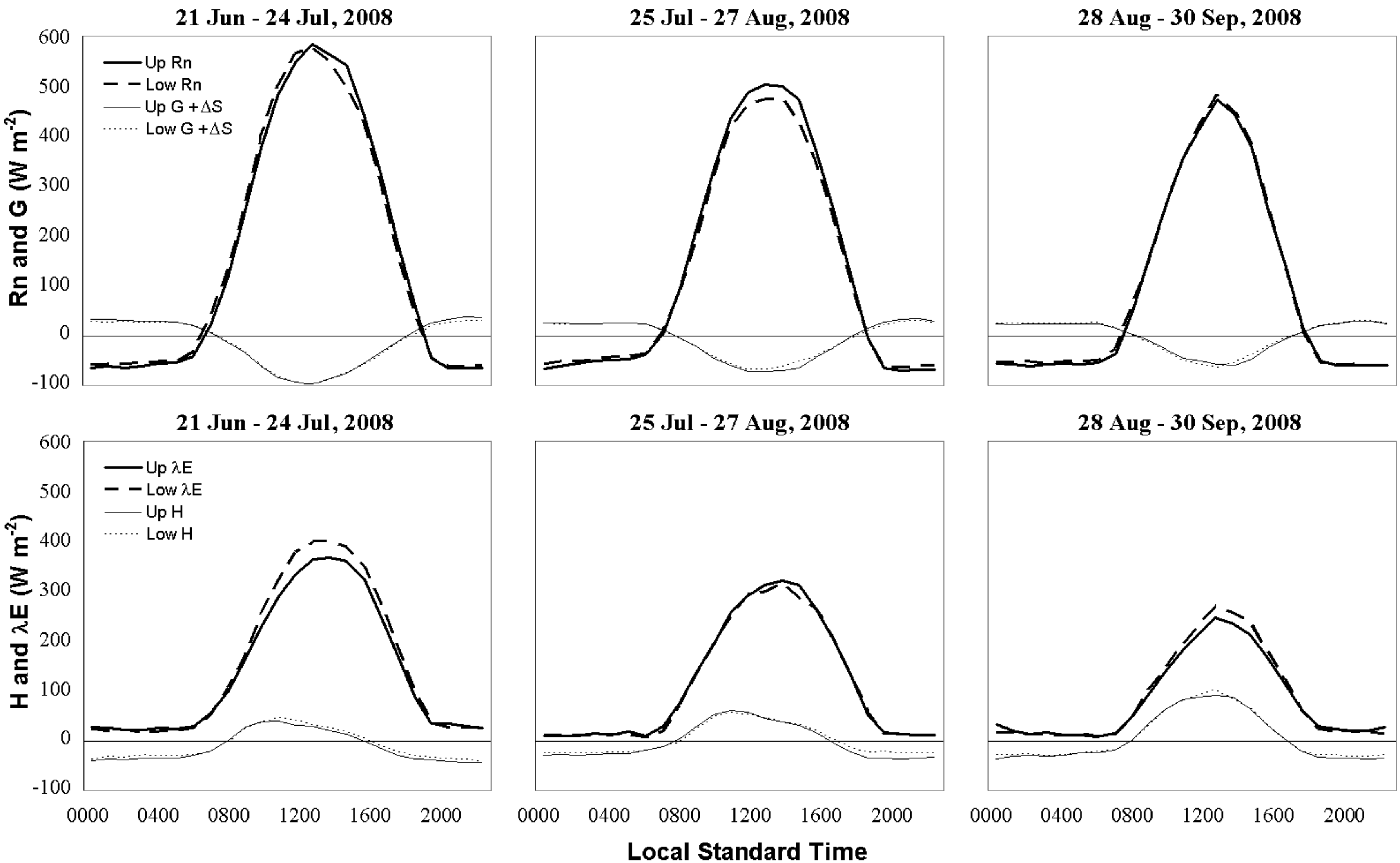

Figure 4.3. Comparison of upland and lowland diurnal energy balance in early and later summer, 2008.

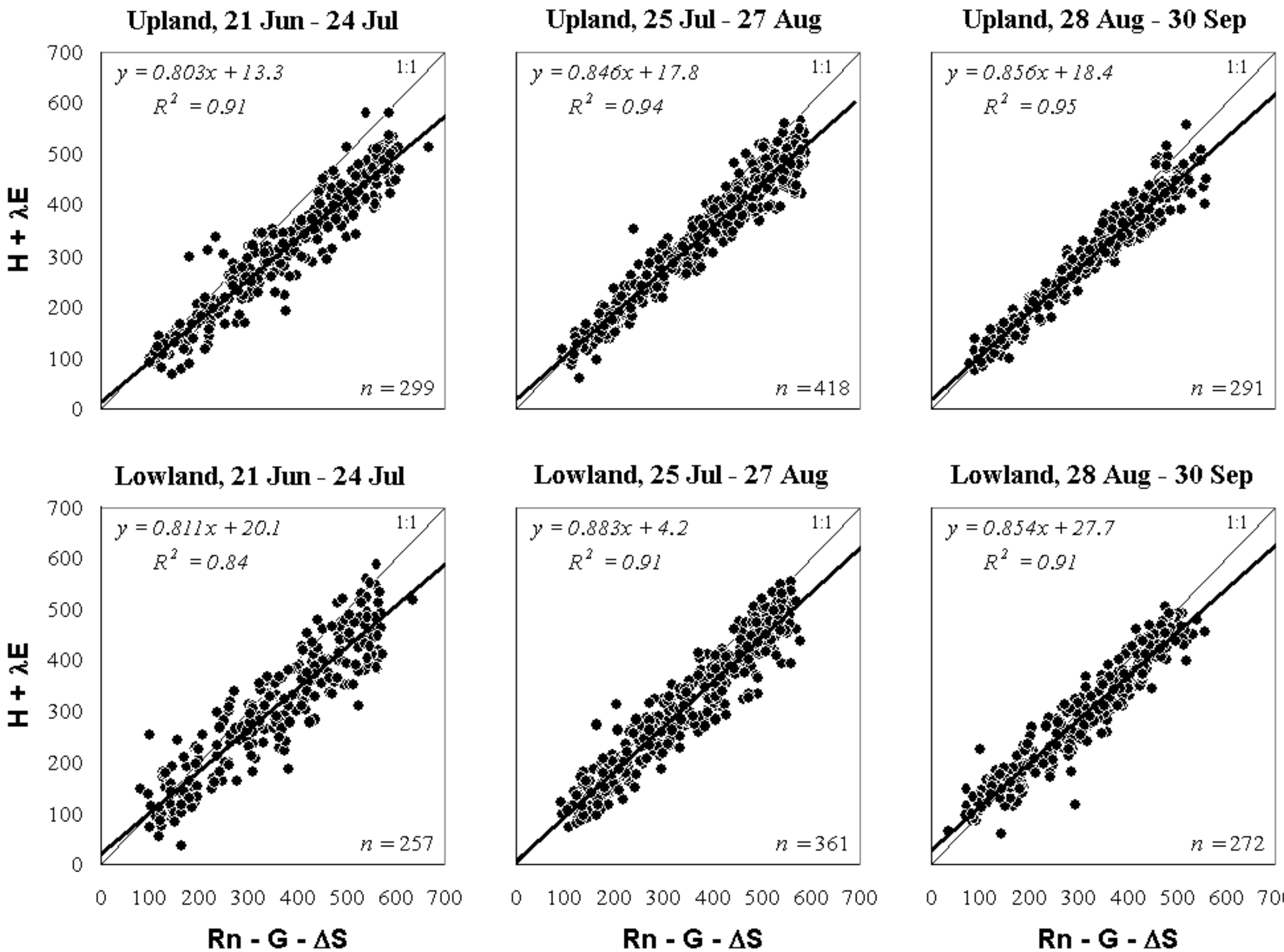

Figure 4.4. Analysis of energy balance closure at the upland and lowland sites during early, mid, and late summer, 2007. All units in W m^{-2}. Closure was plotted from 30-min fluxes of H, λE, R_n, and storage (G and ΔS).

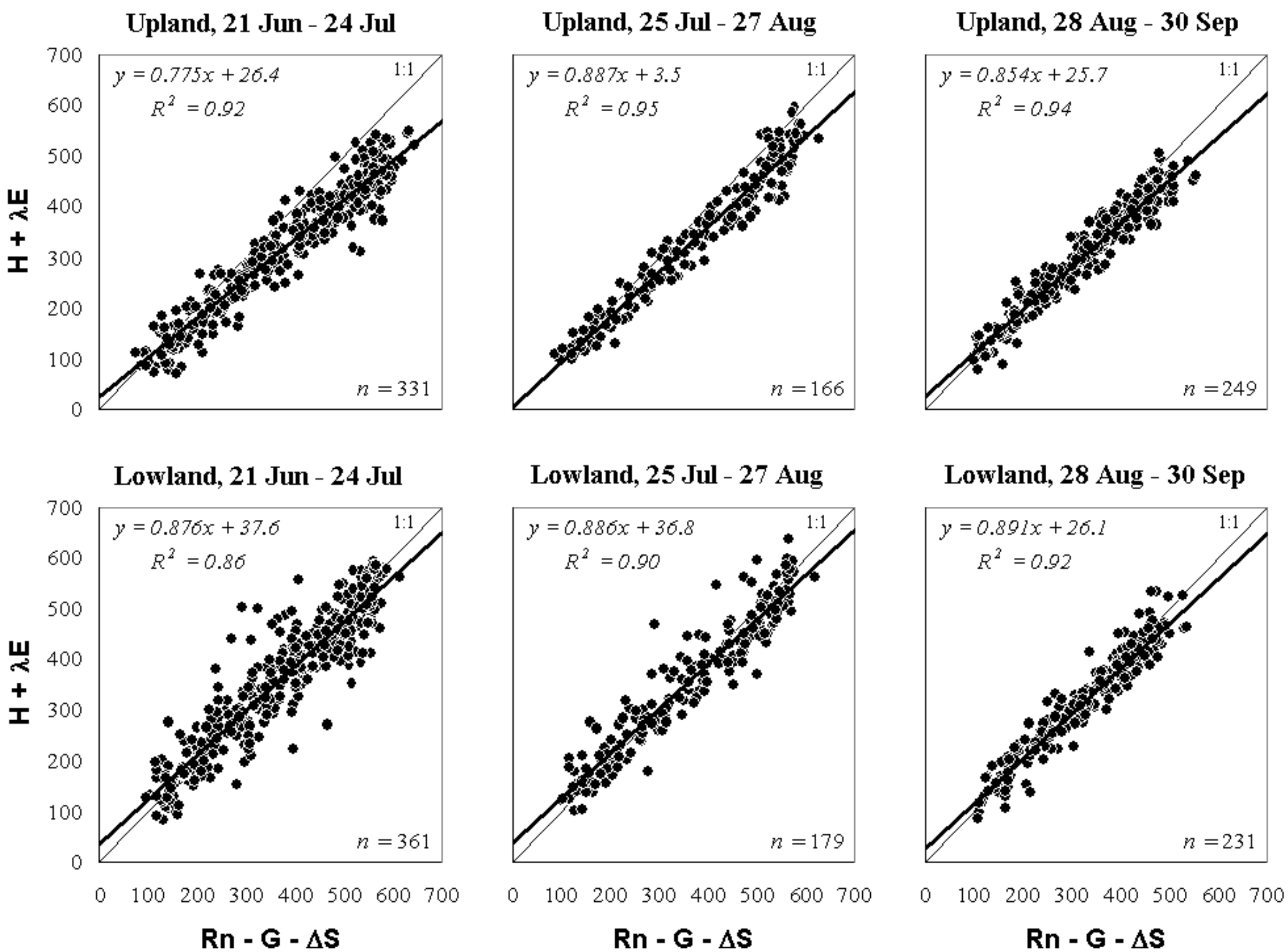

Figure 4.5. Analysis of energy balance closure at the upland and lowland sites during early, mid, and late summer, 2008. All units in W m^{-2}. Closure was plotted from 30-min fluxes of H, λE, R_n, and storage (G and ΔS).

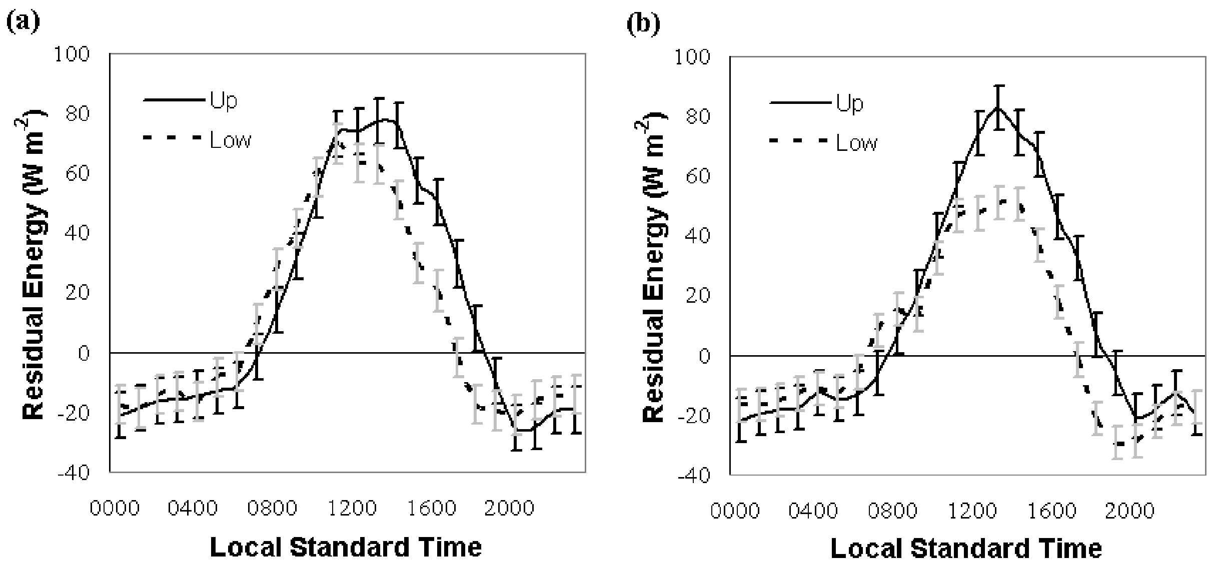

Figure 4.6. Composite of average diurnal residual energy and standard error by local standard time, 21 Jun to 30 Sep (a) 2007 and (b) 2008. This graph uses unfiltered data; E_{res} is calculated from eq. 4.3.

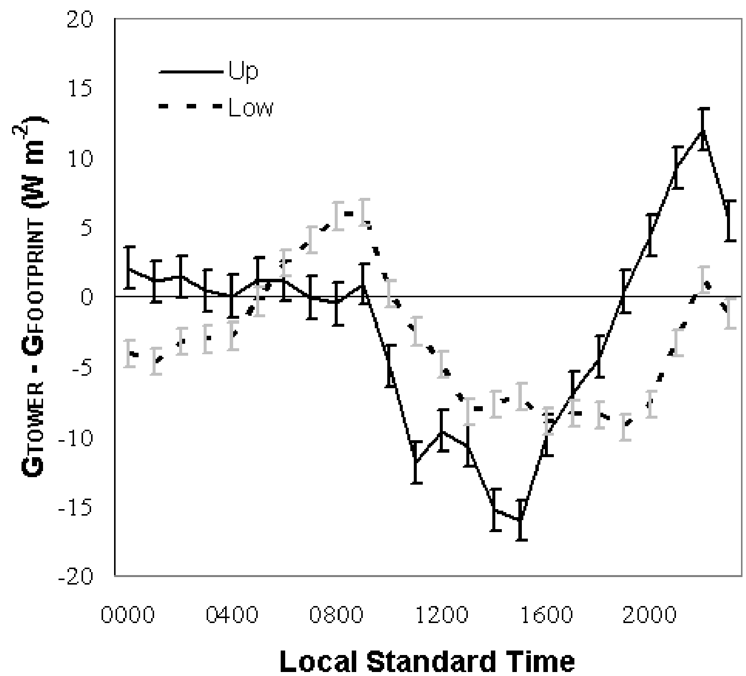

Figure 4.7. Average diurnal difference between G calculated near the EC tower (G_{TOWER}) and in the EC footprint near net radiation measurements ($G_{FOOTPRINT}$). Data shown include standard error and are averaged over both years. Difference = $G_{TOWER} - G_{FOOTPRINT}$

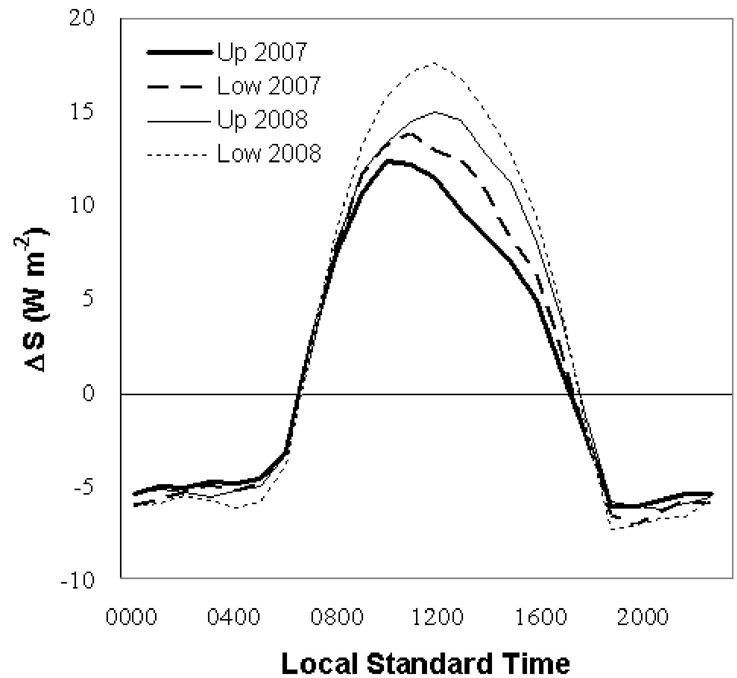

Figure 4.8. Average diurnal change in total heat storage within the canopy (ΔS) for the upland and lowland sites. Data shown are averaged by year.

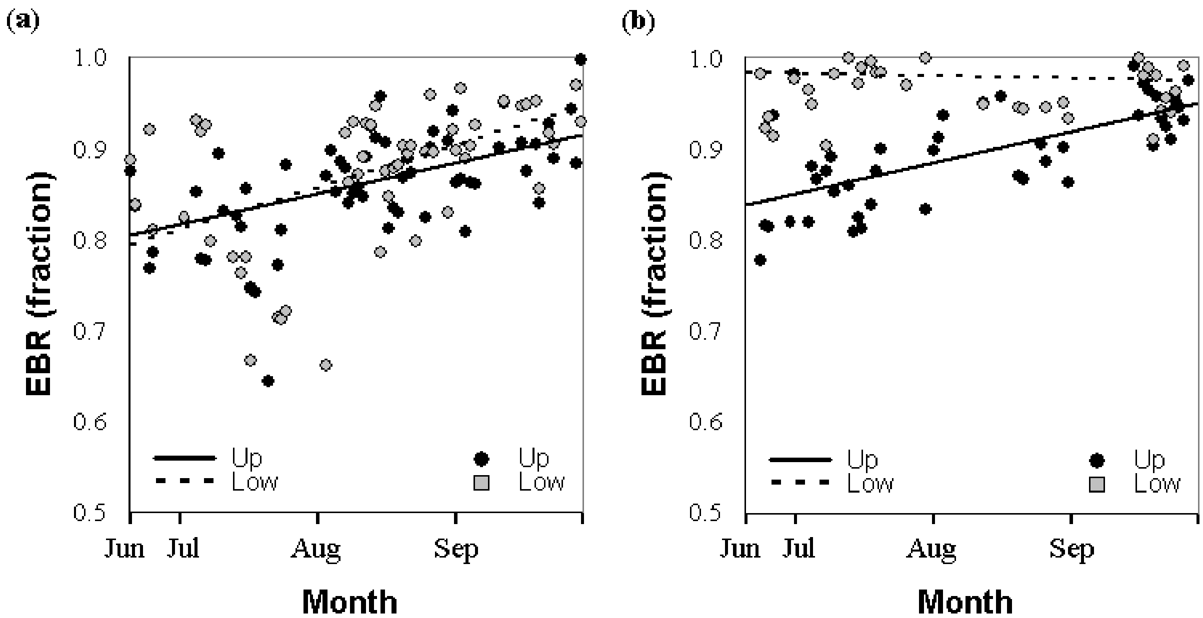

Figure 4.9. Energy balance ratio (EBR) as a function of calendar day in (a) 2007 and (b) 2008. Total EBR was 0.891 (0.882, upland; 0.901, lowland) and 0.932 (0.883, upland; 0.979, lowland) in 2007 and 2008, respectively. The EBR was computed with eq. 4, for which total daily H, λE, R_n, and storage (G and ΔS) were used as input.

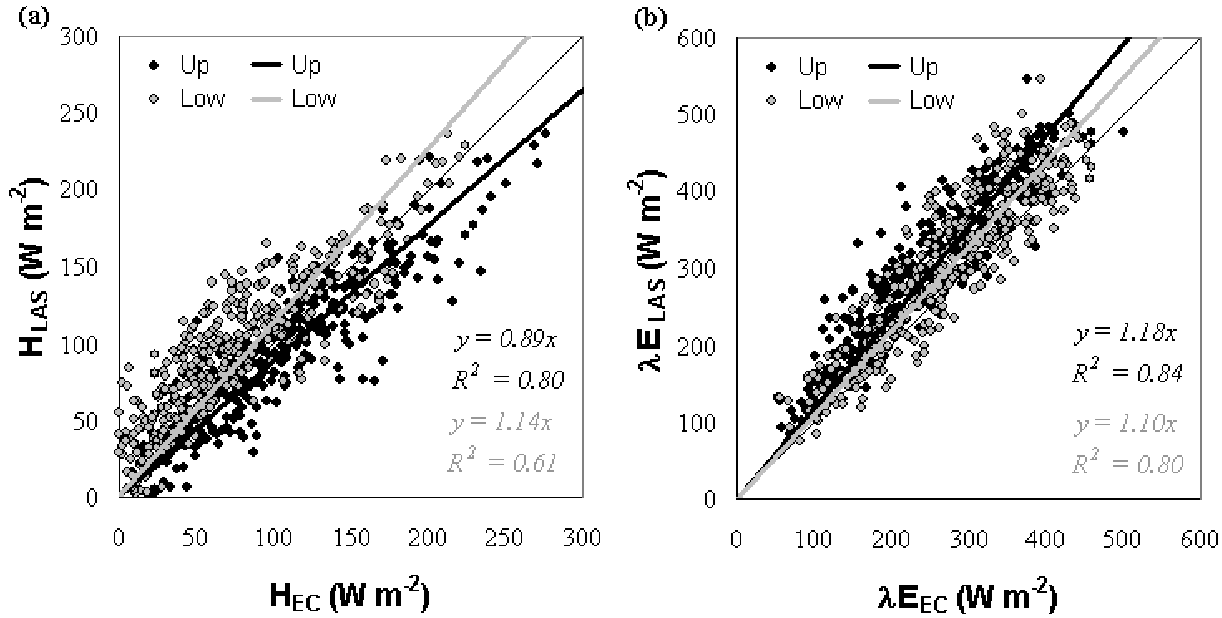

Figure 4.10. Comparison of sensible (a) and latent (b) turbulent heat fluxes measured by the LAS with those from the EC towers, 2007. $\lambda E_{LAS} = R_{n\ avg,U\&L} - H_{LAS} - G_{avg,U\&L} - \Delta S_{U\&L}$. Data are valid for 17 Jul to 4 Sep.

CHAPTER 5 – CONCLUSIONS

The work presented in this dissertation shows three micrometeorological studies of mass and energy fluxes in the surface boundary layer. The first two studies involved emissions of ammonia (NH_3) from a beef feedlot and methane (CH_4) from a large anaerobic dairy lagoon. The third involved using eddy covariance (EC) in ideal terrain to evaluate the "energy balance closure problem" at flux measurement towers.

Summertime data from a beef feedlot in Colorado showed that strong emissions of NH_3 occur directly downwind of a dense grouping of cattle pens. Emissions estimates were compared using two inverse models: one called FIDES (an inverse analytical model selected for its ease of use and applicability to real-time monitoring systems) and the other called WindTrax (WT; a backward Lagrangian stochastic model selected for its scientific accuracy and common use in livestock emissions literature). Emissions were also compared using concentration data from two different instruments: a single-point closed-path cavity ring-down spectroscopy (CRDS) analyzer and a long-open-path (LP) laser sensor typically integrates over a path several 100 meters long. Regardless of model or sensor, estimated emissions had a diurnal pattern, mostly owing to temperature-based processes dominating volatilization of NH_3 from pen surfaces and turbulent processes being more active during the day to transport any volatilized NH_3 from the surface to the ambient air. Unseasonable wind directions caused large amounts of data to be gap-filled (up to 90%), but this was addressed with a modified, iterative mean diurnal variation (MDV) approach. There was little difference between CRDS and LP datasets except that the CRDS had higher data retention and the LP had better spatial representation. This mostly confirms the hypotheses related to the sensor comparison: 1) concentrations should be similar, 2) CRDS will have more samples, and 3) LP data will have less variability. The variability component is more visually apparent in the emissions dataset (i.e., the CRDS emissions had higher peaks than LP) than concentration data. Ultimately, data show that a central downwind single-point sensor produces similar results to a well-placed LP laser. FIDES gap-filled emissions estimates were 25% less than WT. A prior study (see sections 2.2.3 and 2.3.3.1), had compared FIDES and WT for a slurry application over a field in Italy in a similar regional setup to the Front Range. The authors showed that FIDES and WT actually compared well during neutral stability and then tended towards FIDES underestimating WT emissions up to 32% for stable and unstable conditions. Most of the conditions at the feedlot that were retained after gap-filling were categorized at unstable or stable, with unstable being the majority occurrence (i.e., from daytime conditions when solar insolation caused increased surface winds and thus mixing). The difference between FIDES and WT in this study is similar to that seen in the Italian study for the same WT run configuration (i.e., using component statistics (e.g., σ_u/u^*) rather than the other option of direct raw input), confirming the initial hypothesis. Mean emission factor (EF) for the feedlot during the summer was 80 ± 39 g NH_3 hd^{-1} d^{-1}. This confirms the hypothesis that EFs from a feedlot in Colorado will have lower values than EFs from a similar practice feedlot in Texas. This is expected because NH_3 emissions are dependent on surface characteristics where the strongest drivers of emissions are temperature (i.e., amount of incident sunlight or climate) and turbulent transport (i.e., amount of winds blowing NH_3 emissions from the cattle pens). There is no way to determine which model is more accurate without comparing to direct emissions measurement (like EC). While FIDES is a far-field solution and thus has a higher uncertainty, WT is likely the better solution to the feedlot scenario as its emissions are based on near-field physics rather than the far field.

Methane emissions were determined for a large anaerobic dairy lagoon in Colorado using eddy covariance and inverse dispersion modeling (WindTrax) across nearly 20 months. Data show large CH_4 emissions in the summer and early autumn (Jun-Oct) with a tenfold decrease in emissions during the cool months (Nov-May). This confirms the initial hypothesis that most of the emissions will occur when sludge layer temperatures were above 10°C. Further inspection shows that on average 80.7% of emissions occurred in a 150-day period from late

May to late Oct. Methane emissions had a diurnal pattern (mostly owing to turbulent transport associated with daytime conditions). This also confirms a hypothesis of a diel pattern to emissions, predictably by the main drivers of emissions: rising surface temperatures due to increased solar radiation after sunrise, and increased wind speeds promoting turbulent transport of emissions associated with daytime temperature gradients. Mean 24-hour composite EC data were lower than 24-hr mean WT estimates of CH_4 emissions from the lagoon (ratio of WT:EC of 1.5). This confirms the hypothesis that EC might underestimate WT because of the difference in sampling footprints (i.e., EC sampled more edge emissions than WT which probably more accurately estimated larger emissions in the center of the lagoon). Due to lack of consistent wind conditions, about 77% of EC data and 85% of WT data had to be gap-filled using MDV. Mean annual emissions from the lagoon based on EC were 29.3 ± 25.5 g CH_4 m^{-2} d^{-1}, while yearly CH_4 emissions estimates from WT averaged 41.6 ± 36.7 g CH_4 m^{-2} d^{-1}. Mean lagoon annual EFs were 819 ± 774 and 1163 ± 1049 g CH_4 hd^{-1} d^{-1} for EC and WT, respectively, and were very close to molded IPCC Tier 2 estimates and means of field-based studies.

Data from the energy balance (EB) closure study provide evidence that many of the well-cited reasons for lack of closure do not contribute to the overall energy imbalance for EC measurements in tallgrass prairie. First, post-processing procedures were applied to data utilizing standard micrometeorological methods. The EC sites were well-maintained, and Ogive analyses precluded low frequency flux contributions from the ecosystem. Also, R_n and G measurements were aligned with the main EC source area. This configuration addresses arguments that surface heterogeneities between R_n – G and H + λE source areas hinders closure. Based on recent literature and data analysis, there is little reason to assume errors from R_n – G account for the “missing” energy. Topography (upland versus lowland) slightly influenced closure but seemed mostly connected to λE which comprises more of the outgoing EB component in lowlands, correlating with higher closures there. This confirms the hypothesis that uplands would have lower closures than lowlands, due to the larger component λE should play in the EB at the lowland. Deployment of a large-aperture scintillometer (LAS, a measure of watershed-integrated H) within the study watershed gives good agreement in H between LAS and EC (given scale and technique differences). There is no confounding evidence suggesting EC estimates of H are inaccurate. Lack of closure might be attributed to recent work that shows transducer shadowing in sonic anemometers may cause a systematic underestimate of vertical wind speed. The overall lack of closure after all the effort and extra computation still leads one to suspect that the globally-reported systematic lack of closure (in all ecosystems, on all continents, at all times of year) may be a result of a commonly-deployed setup. Though this study did not achieve 100% closure, and none of the typically-accepted reasons for lack of closure were responsible, this result still confirms the hypothesis that there would still be a general lack of closure after all was taken into account. This is because the author feels there is good evidence founded in her many years of field experiences and professional correspondence supporting the vertical velocity measurement notion.

It should further be stressed that there is a major need for more emissions research of all species from hotspots like livestock operations, especially in regions where weather conditions may preclude high retention of data. These studies open the window for long-term, near-continuous real-time monitoring at CAFOs, especially as lower-cost instrumentation for important pollutants like NH_3 and CH_4 become available.

Future work is recommended regarding ammonia emissions from feedlots. Particularly, to utilize a direct measurement such as EC against which to compare FIDES and WT. This would provide validation for these models in the livestock sector. Additionally, future studies should focus on a feedlot-centric approach (i.e., placing instrumentation in the feedlot interior to capture more emissions from more wind directions).

Data retention was impeded by the unique environmental conditions of the region (i.e., winds and stability). The lack of data retention (mostly due to filtering for undesirable winds) did not allow for a more refined analysis of the data such as during high wind events or detailed measurement of changing conditions. To address this, future work in this topic should focus on multiple measurement systems, especially as more affordable CH_4 sensors are starting to become commercially available, to capture the dynamics of these complex processes. More so, intensive co-sampling of ebullition, manure chemistry, and dairy operation effects (such as pumping, removal, irregular flushing, etc.) will allow for a plethora of analyses, hopefully enough for confident correlations to be determined. Additionally, multiple EC systems, especially if in a profile setup, could be used to establish a temporary springtime (when winds are highest) exploratory study look at advection and examine EC theory, as strong surface emissions gradients can cause EC theory (stationarity) to fail.

The energy balance closure problem study, in the author's mind, highlights the need for the micrometeorological community to come together and work towards a compromise in solving the EB closure problem. From initial beginnings of this study prior to 2007, it is being published as a doctoral work, nearly 10 years later, when it was the hopes of the author and advisors that more would have been decided by now in order to properly guide us how to better interpret it. With that in mind, more research is needed into the nature of the sonic anemometer vertical velocity error and back-correction schemes in order to finally resolve the energy balance closure problem. Determining the best correction algorithms should involve further research and funding to facilitate a more widely-accepted and distributable way of implementing the resolution to all major flux networks. Such research could result in greater data certainty worldwide and would properly update all EC datasets to their most accurate version possible.

REFERENCES

Allen, R.G., Pereira, L. S., Raes, D., Smith, M., 1998. Crop evapotranspiration. Irrigation and Drainage Paper No. 56. Food and Agriculture Organization of the United Nations, Rome, Italy.

Aneja VP, Blunden J, James K, Schlesinger WH, Knighton R, Gilliam W, Jennings G, Niyogi D, Cole S. 2008. Ammonia assessment from agriculture: U.S. status and needs. J. Environ. Qual. 37, 515-520, doi:10.2134/jeq2007.0002in.

Arogo J, Westerman PW, Heber AJ, Robarge WP, Classen JJ. 2006. Ammonia emissions from animal feeding operations. In: Rice JM, Caldwell DF, Humenik FJ (Eds.), Animal Agriculture and the Environment: National Center for Manure and Animal Waste Management White Papers. ASABE. St. Joseph, MI. pp. 41-88.

Aubinet M, Grelle A, Ibrom A, Rannik Ü, Moncrieff J, Foken T, Kowalski AS, Martin PH, Berbigier P, Bernhofer C, Clement R, Elbers J, Granier A, Grünwald T, Morgenstern K, Pilegaard K, Rebmann C, Snijders W, Valentini R, Vesala T. 2000. Estimates of the annual net carbon and water exchange of forests: the EUROFLUX methodology. Adv. Ecol. Res. 30, 113–175, doi: 10.1016/S0065-2504(08)60018-5.

Baek BH, Todd R, Cole NA, Koziel JA. 2006. Ammonia and Hydrogen Sulfide flux and dry deposition velocity estimates using vertical gradient method at a commercial beef cattle feedlot. Int. J. Global Environ. Issues. 6, 189-203.

Baldocchi D, Falge E, Gu L, Olson R, Hollinger D, Running S, Anthoni P, Bernhofer C, Davis K, Evans R, Fuentes J, Goldstein A, Katul G, Law B, Lee X, Malhi Y, Meyers T, Munger W, Oechel W, Paw U KT, Pilegaard K, Schmid HP, Valentini R, Verma S, Vesala T, Wilson K, Wofsy S. 2001. FLUXNET: a new tool to study the temporal and spatial variability of ecosystem-scale carbon dioxide, water vapor and energy flux densities. Bull. Am. Meteor. Soc. 82, 2415–2434, doi: 10.1175/1520-0477(2001)082<2415:FANTTS>2.3.CO;2.

Baldocchi DD, Hicks BB, Meyers TP. 1988. Measuring biosphere-atmosphere exchanges of biologically related gases with micrometeorological methods. Ecology. 69, 1331–1340, doi: 10.2307/1941631.

Baron JS, Rueth HM, Wolfe AM, Nydick KR, Allstott EJ, Minear JT, Moraska B. 2000. Ecosystem response to nitrogen deposition in the Colorado Front Range. Ecosys. 3, 352-368, doi: 10.1007/s100210000032.

Barr AG, Morgenstern K, Black TA, McCaughey JH, Nesic Z. 2006. Surface energy balance closure by the eddy-covariance method above three boreal forest stands and implications for the measurement of the CO_2 flux. Agric. Forest Meteor. 140, 322–337, doi: 10.1016/j.agrformet.2006.08.007.

Battye R, Battye W, Overcash C, Fudge S. 1994. Development and selection of ammonia emission factors. EPA/600/R-94/190, Final Report Prepared for US Environmental Protection Agency, Office of Research and Development, EPA Contract No. 68-D3-0034, Work Assignment 0–3.

Bauer SE, Tsigaridis K, Miller R. 2016. Significant atmospheric aerosol pollution caused by world food cultivation. Geophys. Res. Let. 43, 5394-5400, doi:10.1002/2016GL068354.

Baum KA, Ham JM, Brunsell NA, Coyne PI. 2008. Surface boundary layer of cattle feedlots: implications for air emissions measurement. Agric. Forest Meteor. 148, 1882–1893, doi: 10.1016/j.agrformet.2008.06.017.

Baum KA, Ham JM. 2009. Adaptation of a speciation sampling cartridge for measuring ammonia flux from cattle feedlots using relaxed eddy accumulation. Atmos. Environ. 43,1753-1759, doi: 10.1016/j.atmosenv.2008.12.021.

Behara SN, Sharma M, Aneja VP, Balasubramanian R. 2013. Ammonia in the atmosphere: a review on emission sources, atmospheric chemistry and deposition on terrestrial bodies. Environ. Sci. Pollut. Res. 20, 8092-8131, doi: 10.1007/s11356-013-2051-9.

Berkhout AJC, Swat DPJ, Volten H, Gast LFL, Haaima M, Verboom H, Stefess G, Hafkenscheid T, Hoogerbrugge R. 2017. Replacing the AMOR by the miniDOAS in the ammonia monitoring network in the Netherlands. Atmos. Meas. Tech. In review, doi:10.5194/amt-2016-348.

Bossert JE, Cotton WR. 1994. Regional-scale flows in mountain terrain. Part I: A numerical and observational comparison. Mon. Wea. Rev. 122, 1449–1471, doi: 10.1175/1520-0493(1994)122<1449:RSFIMT>2.0.CO;2.

Bowman WD, Murgel J, Blett T, Porter E. 2012. Nitrogen critical loads for alpine vegetation and soils in Rocky Mountain National Park. J. Environ. Manag. 103, 165-171, doi: 10.1016/j.jenvman.2012.03.002.

Bremer DJ, Ham JM. 1999. Effect of spring burning on the surface energy balance in a tallgrass prairie. Agric. Forest Meteor. 97, 43–54, doi: 10.1016/S0168-1923(99)00034-9.

Bremer DJ, Ham JM. 2010. Carbon fluxes over burned and unburned native tallgrass prairie. Rangeland Ecol. Manag. 63, 72-81, doi: 10.2111/REM-D-09-00010.1.

Briggs JM, Knapp AK. 1995. Interannual variability in primary production in tallgrass prairie: climate, soil moisture, topographic position, and fire as determinants of aboveground biomass. Am. J. Bot. 82, 1024–1030.

Brunsell NA, Ham JM, Owensby CE. 2008. Assessing the multi-resolution information content of remotely sensed variables and elevation for evapotranspiration in a tallgrass prairie environment. Remote Sens. Environ. 112, 2977–2987, doi: 10.1016/j.rse.2008.02.002.

Burns DA. 2004. The effects of atmospheric nitrogen deposition in the Rocky Mountains of Colorado and southern Wyoming, USA—a critical review. Environ. Pollut. 127, 257-269, doi: 10.1016/S0269-7491(03)00264-1.

Campbell GS, Norman JM. 1998. An Introduction to Environmental Biophysics, second ed. Springer-Verlag, New York.

Carozzi M, Loubet B, Acutis M, Rana G, Ferrara RM. 2013. Inverse dispersion modelling highlights the efficiency of slurry injection to reduce ammonia losses by agriculture in the Po Valley (Italy). Ag. Forest Meteor. 171-172, 306-318, doi: 10.1016/j.agrformet.2012.

Castellví F, Snyder RL, Baldocchi DD. 2008. Surface energy-balance closure over rangeland grass using the eddy covariance method and surface renewal analysis. Agric. Forest Meteor. 148, 1147–1160, doi: 10.1016/j.agrformet.2008.02.012.

CDPHE. 2014. Permitted confined animal operations database. Colorado Department of Public Health and the Environment. 4300 Cherry Creek Dr South, Denver, CO, USA.

Cole NA, Defoor PJ, Galyean ML, Duff GC, Gleghorn JF. 2006. Effects of phase-feeding of crude protein on performance, carcass characteristics, serum urea Nitrogen concentrations, and manure Nitrogen of finishing beef steers. J. Anim. Sci. 84, 3421-3432, doi: 10.2527/jas.2006-150.

Crenna B. 2006. An introduction to WindTrax. Thunder Beach Scientific, Inc. <www.thunderbeachscientific.com/downloads/introduction.pdf> Retrieved: 03 Feb 2017.

Denmead OT, Chen D, Griffith DWT, Loh ZM, Bai M, Naylor T. 2008. Emissions of the indirect greenhouse gases NH3 and NOx from Australian beef cattle feedlots. Aust. J. Exp. Agric. 48, 213-218, doi: 10.1071/EA07276.

Denmead OT, Chen D, Rowell D, Loh Z, Hill J, Muir S, Griffith DWT, Naylor T, Bai M, Phillips F, McGinn S. 2014. Gaseous nitrogen emissions from Australian cattle feedlots. In: Sutton MA, Mason KE, Sheppard LJ, Sverdrup H, Haeuber R, Hicks W (Eds.), Nitrogen Deposition, Critical Loads and Biodiversity. Dordrecht: Springer. pp. 23-30, doi: 10.1007/978-94-007-7939-6_3.

deVries DA. 1963. Thermal properties of soils, in: van Wijk, W.R. (Ed.), Physics of the Plant Environment. North-Holland, Amsterdam, The Netherlands, pp. 210–235.

DeWees JM. 2015. Refinery fenceline monitoring & method 325A/B. National Air Toxics Monitoring and Data Analysis Workshop. Research Triangle Park, NC. 28 Oct.

Directive 2001/81/EC of the European parliament and of the council of 23 October 2001 on national emission ceilings for certain atmospheric pollutants. 2001. Off. J. European Comm. L309, 22-30.

Doesken, N. 2014. Colorado water year 2014: a review. Annual meeting, Rocky Mountain Hydrologic Research Center. Allenspark, CO. 24 Oct.

Eder F, De Roo F, Kohnert K, Desjardins RL, Schmid HP, Mauder M. 2014. Evaluation of two energy balance closure parametrizations. Bound-Lay Meteorol. 151, 195-219, doi: 10.1007/s10546-013-9904-0.

Eilerman SJ, Peischl J, Neuman JA, Ryerson TB, Aikin KC, Holloway MW, Zondlo MA, Golston LM, Pan D, Floerchinger C, Herndon S. 2016. Characterization of ammonia, methane, and nitrous oxide emissions from concentrated animal feeding operations in Northeastern Colorado. Env. Sci. Tech. 50, 10885-10893, doi: 10.1021/acs.est.6b02851.

Erickson GE, Klopfenstein TJ, Milton CT. 2000. Dietary protein effects on nitrogen excretion and volatilization in open-dirt feedlots. In: Moore JA (Ed.), Proceedings, 8th International Symposium on Animal, Agricultural and Food Processing Wastes. Des Moines, IA. 12-15 Oct. ASAE Publications, St. Joseph, MI, pp 297-304.

Erisman JW, Galloway J, Seitzinger S, Bleeker A, Butterbach-Bahl K. 2011. Reactive nitrogen in the environment and its effects on climate change. Curr. Opin. Environ. Sustain. 3, 281-290, doi: 10.1016/j.cosust.2011.08.012.

Falge E, Baldocchi D, Olson R, Anthoni P, Aubinet M, Bernhofer C, Burba G, Ceulemans R, Clement R, Dolman H, Granier A, Gross P, Grünwald T, Hollinger D, Jenson N-O, Katul G, Keronen P, Kowalski A, Lai CT, Law BE, Meyers T, Moncrieff J, Moors E, Munger JW, Pilegaard K, Rannik Ü, Rebmann C, Suyker A, Tenhunen J, Tu K, Verma S, Vesala T, Wilson K, Wofsy S. 2001. Gap filling strategies for defensible annual sums of net ecosystem exchange. Agric. Forest Meteor. 107, 43-69, doi: 10.1016/S0168-1923(00)00225-2.

FAO. 2006. Livestock's long shadow: environmental issues and options. Livestock, Environment, and Development Initiative. Food and Agriculture Organization of the United Nations, Rome, Italy.

FAO. 2009. Grasslands: enabling their potential to contribute to greenhouse gas mitigation. <www.fao.org/forestry/foris/data/nrc/UNFCCCgrassland25.pdf> Retrieved 25 Nov 2009.

Faulkner WB, Shaw BW. 2008. Review of ammonia emission factors for United States animal agriculture. Atmos. Environ. 42, 6567-6574, doi: 10.1016/j.atmosenv.2008.04.021.

Felber R, Münger A, Neftel A, Ammann C. 2015. Eddy covariance methane flux measurements over a grazed pasture: effect of cows as moving point sources. Biogeosci., 12, 3925-3940, doi: 10.5194/bg-12-3925-2015.

Flesch TK, Wilson JD, Harper LA, Todd RW, Cole NA. 2007. Determining ammonia emissions from a cattle feedlot with an inverse dispersion technique. Agric. Forest Meteor. 144, 139-155, doi: 10.1016/j.agrformet.2007.02.006.

Flesch TK, Wilson JD. 2005. Estimating tracer emissions with a backward Lagrangian stochastic technique. In: Hatfield JL, Baker JM (Eds.), Micrometeorological measurements in agricultural systems. Agron. Monogr. 47. ASA, CSSA, and SSSA, Madison WI, pp. 513-531, doi: 10.2134/agronmonogr47.c22.

Foken T, Aubinet M, Finnigan JJ, Leclerc MY, Mauder M, Paw U KT. 2011. Results of a panel discussion about the energy balance closure correction for trace gases. B. Am. Meteorol. Soc. 92, ES13-ES18, doi: 10.1175/2011BAMS3130.1.

Foken T, Wichura B. 1996. Tools for quality assessment of surface-based flux measurements. Agric. Forest Meteor. 78, 83–105, doi: 10.1016/0168-1923(95)02248-1.

Foken T, Wimmer F, Mauder M, Thomas C, Liebethal C. 2006. Some aspects of the energy balance closure problem. Atmos. Chem. Phys. 6, 4395–4402, doi: 10.5194/acp-6-4395-2006.

Foken T. 2008. The energy balance closure problem: an overview. Ecol. Appl. 18, 1351–1367, doi: 10.1890/06-0922.1.

Frank JM, Massman WJ, Ewers BE. 2016. A Bayesian model to correct underestimated 3-D wind speeds from sonic anemometers increases turbulent components of the surface energy balance. Atmos. Meas. Tech. 9, 5933-5953, doi: 10.5194/amt-9-5933-2016.

Franssen HJH, Stöckli R, Lehner I, Rotenberg E, Seneviratne SI. 2010. Energy balance closure of eddy-covariance data: A multisite analysis for European FLUXNET stations. Agric. Forest Meteor. 150, 1553-1567, doi: 10.1016/j.agrformet.2010.08.005.

Fuchs M, Tanner CB. 1968. Calibration and field test of soil heat flux plates. Soil Sci. Soc. Am. Proc. 32, 326–328, doi: 10.2136/sssaj1968.03615995003200030021x.

Galloway JN, Dentener FJ, Capone DG, Boyer EW, Howarth RW, Seitzinger SP, Asner GP, Cleveland CC, Green PA, Holland EA, Karl DM, Michaels AF, Porter JH, Townsend AR, Vorosmarty CJ. 2004. Nitrogen cycles: past, present, and future. Biogeochem. 70, 153-226, doi: 10.1007/s10533-004-0370-0.

Gao Z, Liu H, Katul GG, Foken T. 2017. Non-closure of the surface energy balance explained by phase difference between vertical velocity and scalars of large atmospheric eddies. Environ. Res. Lett. 12, 034025, doi: 10.1088/1748–9326/aa625b.

Gebhart KA, Schichtel BA, Malm WC, Barna MG, Rodriguez MA, Collett Jr JL. 2011. Back-trajectory-based source apportionment of airborne sulfur and nitrogen concentrations at Rocky Mountain National Park, Colorado, USA. Atmos. Environ. 45, 621-633, doi: 10.1016/j.atmosenv.2010.10.035.

Gibson DJ, Hulbert LC. 1987. Effects of fire, topography and year-to-year climatic variation on species composition in tallgrass prairie. Vegetatio. 72, 175–185, doi: 10.1007/BF00039839.

Goulden ML, Munger JW, Fan S-M, Daube BC, Wofsy SC. 1996. Measurements of carbon sequestration by long-term eddy covariance: methods and critical evaluation of accuracy. Global Change Biol. 2, 169–182, doi: 10.1111/j.1365-2486.1996.tb00070.x.

Guo XF, Cai XH, Kang L, Zhu T, Zhang HS. 2009. Effects of vegetative heterogeneity and patch-scale harvest on energy balance closure and flux measurements. Theor. Appl. Climatol. 96, 281–290, doi: 10.1007/s00704-008-0031-7.

Halldin S. 2004. Radiation measurements in integrated terrestrial experiments, in: Kabat et al. (Eds.), Vegetation, Water, Humans and the Climate. Springer-Verlag, Berlin, Germany, pp. 167–171, doi: 10.1007/978-3-642-18948-7_14.

Ham JM, Heilman JL. 2003. Experimental test of density and energy-balance corrections on carbon dioxide flux as measured using open-path eddy covariance. Agron. J. 95, 1393–1403, doi: 10.2134/agronj2003.1393.

Ham JM, Knapp AK. 1998. Fluxes of CO 2, water vapor, and energy from a prairie ecosystem during the seasonal transition from carbon sink to carbon source. Agric. Forest Meteor. 89, 1–14, doi: 10.1016/S0168-1923(97)00062-2.

Hammerle A, Haslwanter A, Schmitt M, Bahn M, Tappeiner U, Cernusca A, Wohlfahrt G. 2007. Eddy covariance measurements of carbon dioxide, latent and sensible energy fluxes above a meadow on a mountain slope. Bound-Lay. Meteor. 122, 397–416, doi: 10.1007/s10546-006-9109-x.

Harper LA, Flesch TK, Todd RW, Cole NA. 2007. Air quality and global-change gas emissions in a beef feeding operation. In: Agronomy Abstracts, 2004 Annual Meetings. American Society of Agronomy. Seattle, WA. 31 Oct-4 Nov.

Harper LA. 2005. Ammonia: measurement issues. In: Hatfield JL, Baker JM (Eds.), Micrometeorological measurements in agricultural systems. Agron. Monogr. 47. ASA, CSSA, and SSSA, Madison WI, pp. 345–379.

Heald CL, Collett Jr JL, Lee T, Benedict KB, Schwandner FM, Li Y, Clarisse L, Hurtmans DR, Van Damme M, Clerbaux C, Coheur P-F, Philip S, Martin RV, Pye HOT. 2012. Atmospheric ammonia and particulate inorganic nitrogen over the United States. Atmos. Chem. Phys. 12, 10295-10312, doi: 10.5194/acp-12-10295-2012.

Heisler JL, Knapp AK. 2008. Temporal coherence of aboveground net primary productivity in mesic grasslands. Ecography. 31, 408–416, doi: 10.1111/j.0906-7590.2008.05351.x.

Hernandez-Ramirez G, Hatfield J, Prueger J, Sauer T. 2010. Energy balance and turbulent flux partitioning in a corn–soybean rotation in the Midwestern US. Theor. Appl. Climatol. 100, 79-92, doi: 10.1007/s00704-009-0169-y.

Heusinkveld BG, Jacobs AFG, Holtslag AAM, Berkowicz SM. 2004. Surface energy balance closure in an arid region: role of soil heat flux. Agric. Forest Meteor. 122, 21–37, doi: 10.1016/j.agrformet.2003.09.005.

Horst TW, Semmer SR, Maclean G. 2015. Correction of a non-orthogonal, three-component sonic anemometer for flow distortion by transducer shadowing. Bound-Lay Meteor. 155, 371-395, doi: 10.1007/s10546-015-0010-3.

Hristov AN, Hanigan M, Cole A, Todd, R, McAllister TA, Ndegwa PM, Rotz A. 2011. Review: ammonia emissions from dairy farms and beef feedlots. Can. J. Anim. Sci. 91, 1-35, doi: 10.4141/CJAS10034.

Huang CH. 1979. A theory of dispersion in turbulent shear flow. Atmos. Environ. 13, 453-463, doi: 10.1016/0004-6981(79)90139-2.

Hunt JE, Kelliher FM, McSeveny TM, Byers JN. 2002. Evaporation and carbon dioxide exchange between the atmosphere and a tussock grassland during a summer drought. Agric. Forest Meteor. 111, 65–82, doi: 10.1016/S0168-1923(02)00006-0.

Hutchinson GL, Mosier AR, Andre CE. 1982. Ammonia and amine emissions from a large cattle feedlot. J. Environ. Qual. 11, 288-293, doi: 10.2134/jeq1982.00472425001100020028x.

IEM. 2017. Site wind roses. <mesonet.agron.iastate.edu/sites/windrose.phtml?station=FMM&network=CO_ASOS> Retrieved: 27 May 2017.

Jacobs AFG, Heusinkveld BG, Holtslag A. 2008. Towards closing the surface energy budget of a mid-latitude grassland. Bound-Lay. Meteor. 126, 125-136, doi: 10.1007/s10546-007-9209-2.

Kanda M, Inagaki A, Letzel MO, Raasch S, Watanabe T. 2004. LES study of the energy imbalance problem with eddy covariance fluxes. Bound-Lay. Meteor. 110, 381–404, doi: 10.1023/B:BOUN.0000007225.45548.7a.

Kimball BA, Jackson RD. 1979. Soil heat flux, in: Barfield, B.J., Gerber, J.F. (Eds.), Modification of the Aerial Environment of Crops, Monograph No. 2. ASAE, St. Joseph, MI, pp. 211–229.

Kochendorfer J, Meyers TP, Frank J, Massman WJ, Heuer MW. 2012. How well can we measure the vertical wind speed? Implications for fluxes of energy and mass. Bound-Lay Meteorol. 145, 383-398, doi: 10.1007/s10546-012-9738-1.

Kohsiek W, Liebethal C, Foken T, Vogt R, Oncley SP, Bernhofer C, DeBruin HAR. 2007. The Energy Balance Experiment EBEX-2000. Part III: behaviour and quality of the radiation measurements. Bound-Lay. Meteor. 123, 55–75, doi: 10.1007/s10546-006-9135-8.

Kucharik CJ, Barford CC, Maayar ME, Wofsy SC, Monson RK, Baldocchi DD. 2006. A multiyear evaluation of a Dynamic Global Vegetation Model at three AmeriFlux forest sites: vegetation structure, phenology, soil temperature, and CO2 and H2O vapor exchange. Ecol. Model. 196, 1–31, doi: 10.1016/j.ecolmodel.2005.11.031.

Laubach J, Teichmann U. 1999. Surface energy budget variability: a case study over grass with special regard to minor inhomogeneities in the source area. Theor. Appl. Climatol. 62, 9–24, doi: 10.1007/s007040050070.

Lee X, Massman W, Law B. 2004. Handbook of Micrometeorology: a Guide for Surface Flux Measurement and Analysis. Kluwer Academic Publishers, Dordrecht, The Netherlands.

Lieb AM, Darrouzet-Nardi A, Bowman WD. 2011. Nitrogen deposition decreases acid buffering capacity of alpine soils in the southern Rocky Mountains. Geoderma. 164, 220-224, doi: 10.1016/j.geoderma.2011.06.013.

Liu SM, Xu ZW, Wang WZ, Jia ZZ, Zhu MJ, Bai J, Wang JM. 2011. A comparison of eddy-covariance and large aperture scintillometer measurements with respect to the energy balance closure problem. Hydrol. Earth Syst. Sci. 15, 1291-1306, doi: 10.5194/hess-15-1291-2011.

Loh Z, Chen D, Bai M, Naylor T, Griffith D, Hill J, Denmead T, McGinn S, Edis R. 2008. Measurement of greenhouse gas emissions from Australian feedlot beef production using open-path spectroscopy and atmospheric dispersion modelling. Aust. J. Exp. Agric. 48, 244-247, doi: 10.1071/EA07244.

Loubet B, Asman WA, Theobald MR, Hertel O, Tang YS, Robin P, Hassouna M, Dämmgen U, Genermont S, Cellier P. 2009. Ammonia deposition near hot spots: processes, models and monitoring methods. Sutton MA, Reis S, Baker SMH, eds. In: Atmospheric ammonia. Springer: Netherlands. pp. 205-267, doi: 10.1007/978-1-4020-9121-6_15.

Loubet B, Génermont S, Ferrara R, Bedos C, Decuq C, Personne E, Fanucci O, Durand B, Rana G, Cellier P. 2010. An inverse model to estimate ammonia emissions from fields. Eur. J. Soil Sci. 61, 793-805, doi: 10.1111/j.1365-2389.2010.01268.x.

Loubet B, Milford C, Sutton MA, Cellier P. 2001. Investigation of the interaction between sources and sinks of atmospheric ammonia in an upland landscape using a simplified dispersion-exchange model. J. Geophys. Res. 106, 24183-24195, doi: 10.1029/2001JD900238.

Malm WC, Schichtel BA, Barna MG, Gebhart KA, Rodriguez MA, Collett Jr JL, Carrico CM, Benedict KB, Prenni AJ, Kreidenweis SM. 2013. Aerosol species concentrations and source apportionment of ammonia at Rocky Mountain National Park. J. Air Waste Manage. Assoc. 63, 1245-1263, doi: 10.1080/10962247.2013.804466.

Masseroni D, Corbari C, Mancini M. 2014. Limitations and improvements of the energy balance closure with reference to experimental data measured over a maize field. Atmós. 27, 335-352, doi: 10.1016/S0187-6236(14)70033-5.

Massman WJ, Lee X. 2002. Eddy covariance flux corrections and uncertainties in long-term studies of carbon and energy exchanges. Agric. Forest Meteor. 113, 121–144, doi: 10.1016/S0168-1923(02)00105-3.

Massman WJ. 2000. A simple method for estimating frequency response corrections for eddy covariance systems. Agric. Forest Meteor. 104, 185-198, doi: 10.1016/S0168-1923(00)00164-7.

Mauder M, Jegede OO, Okogbue EC, Wimmer F, Foken T. 2007b. Surface energy balance measurements at a tropical site in West Africa during the transition from dry to wet season. Theor. Appl. Climatol. 89, 171–183, doi: 10.1007/s00704-006-0252-6.

Mauder M, Oncley SP, Vogt R, Weidinger T, Ribeiro L, Bernhofer C, Foken T, Kohsiek W, DeBruin HAR, Liu H. 2007a. The Energy Balance Experiment EBEX-2000. Part II: intercomparison of eddy-covariance sensors and post-field data processing methods. Bound-Lay. Meteor. 123, 29–54, doi: 10.1007/s10546-006-9139-4.

McGinn SM, Flesch TK, Crenna BP, Beauchemin KA, Coates T. 2007. Quantifying ammonia emissions from a cattle feedlot using a dispersion model. J. Environ. Qual. 36, 1585-1590, doi: 10.2134/jeq2007.0167.

McGinn SM, Janzen HH, Coates TW, Beauchemin KA, Flesch TK. 2016. Ammonia emission from a beef cattle feedlot and its local dry deposition and re-emission. J. Environ. Qual. 45, 1178-1185, doi: 10.2134/jeq2016.01.0009.

McGloin R, Šigut L, Havránková K, Dušek J, Pavelka M, Sedlák P. 2018. Energy balance closure at a variety of ecosystems in Central Europe with contrasting topographies. Agr. Forest Meteorol. 248, 418-431, doi: 10.1016/j.agrformet.2017.10.0003.

Meek DW, Prueger JH, Sauer TJ. 1998. Solutions for three regression problems commonly found in meteorological data analysis, in: Proceedings of the 23rd Conference on Agricultural Forest Meteorology. American Meteorological Society, Albuquerque, NM, Nov 2–6, 1998, pp. 141–145.

Meyers TP, Hollinger SE. 2004. An assessment of storage terms in the surface energy balance of maize and soybean. Agric. Forest Meteor. 125, 105–116, doi: 10.1016/j.agrformet.2004.03.001.

Meyers TP. 2001. A comparison of summertime water and CO2 fluxes over rangeland for well watered and drought conditions. Agric. Forest Meteor. 106, 205–214, doi: 10.1016/S0168-1923(00)00213-6.

Miller DJ, Sun K, Tao L, Pan D, Zondlo MA, Nowak JB, Liu Z, Diskin G, Sachse G, Beyersdorf A, Ferrare R, Scarino AJ. 2015. Ammonia and methane dairy emission plumes in the San Joaquin Valley of California from individual feedlot to regional scales. J. Geophys. Res. Atmos. 120: 9718-9738, doi: 10.1002/2015JD023241.

Moderow U, Aubinet M, Feigenwinter C, Kolle O, Lindroth A, Mölder M, Montagnani L, Rebmann C, Bernhofer C. 2009. Available energy and energy balance closure at four coniferous forest sites across Europe. Theor. Appl. Climatol. 98, 397–412, doi: 10.1007/s00704-009-0175-0.

Moore C. 1986. Frequency response corrections for eddy correlation systems. Bound-Lay. Meteor. 37, 17-35, doi: 10.1007/BF00122754.

NRC. 2003. Air emissions from animal feeding operations: current knowledge, future needs. The National Academies Press: Washington DC.

Oladosu OR, Sunmonu LA. 2011. Investigation of surface energy budget over a humid tropical site at Ile-Ife, Nigeria: A comparison of eddy covariance and Bowen ratio methods. Indian J. Radio Space. 40, 37-44.

Oncley SP, Businger JA, Itsweire EC, Friehe CA, LaRue JC, Chang SS. 1990. Surface layer profiles and turbulence measurements over uniform land under near-neutral conditions.

Proceedings, Ninth Symposium on Turbulence and Diffusion, 30 Apr–3 May 1990, RISO, Roskikle, Denmark. Am. Met. Soc. pp. 237–240.

Oncley SP, Foken T, Vogt R, Kohsiek W, DeBruin HAR, Bernhofer C, Christen A, van Gorsel E, Grantz D, Feigenwinter C, Lehner I, Liebethal C, Liu H, Mauder M, Pitacco A, Ribeiro L, Weidinger T. 2007. The Energy Balance Experiment EBEX-2000. Part I: overview and energy balance. Bound-Lay. Meteor. 123, 1–28, doi: 10.1007/s10546-007-9161-1.

Owen JJ, Silver WL. 2015. Greenhouse gas emissions from dairy manure management: A review of field-based studies. Global Change Biol. 21: 550-565, doi: 10.1111/gcb.12687.

Owensby CE, Ham JM, Auen L. 2006. Fluxes of CO2 from grazed and ungrazed tallgrass prairie. Rangeland Ecol. Manag. 59, 111–127, doi: 10.2111/05-116R2.1.

Paulot F, Jacob DJ, Pinder RW, Bash JO, Travis K, Henze DK. 2014. Ammonia emissions in the United States, European Union, and China derived by high-resolution inversion of ammonium wet deposition data: interpretation with a new agricultural emissions inventory (MASAGE_NH3). J. Geophys. Res. Atmos. 119, 4343-4364, doi: 10.1002/2013JD021130.

Paw U KT, Baldocchi DD, Meyers TP, Wilson KB. 2000. Correction of eddy covariance measurements incorporating both the future advective effects and density fluxes. Bound-Lay. Meteor. 97, 487–511, doi: 10.1023/A:1002786702909.

Philip JR. 1959. The theory of local advection: 1. J. Meteor. 16, 535-547, doi: 10.1175/1520-0469(1959)016<0535:TTOLAI>2.0.CO;2.

Raupach MR. 1989. Stand overstorey processes. Philos. Trans. R. Soc. London Ser. B. 324, 175-190, doi: 10.1098/rstb.1989.0043.

Rhoades MB, Parker DB, Cole NA, Todd RW, Caraway EA, Auvermann BW, Topliff DR, Schuster GL. 2010. Continuous ammonia emission measurements from a commercial beef feedyard in Texas. Trans. ASABE. 53, 1823-1831, doi: 10.13031/2013.35808.

Rodriguez MA, Barna MG, Gebhart KA, Hand JL, Adelman ZE, Schichtel BA, Collett Jr JL, Malm WC. 2011. Modeling the fate of atmospheric reduced nitrogen during the Rocky Mountain Atmospheric Nitrogen and Sulfur Study (RoMANS): Performance evaluation and diagnosis using integrated processes rate analysis. Atmos. Environ. 45, 223-234, doi: 10.1016/j.atmosenv.2010.09.011.

Schmid HP. 1997. Experimental design for flux measurements: matching the scales of observations and fluxes. Agric. Forest Meteor. 87, 179–200, doi: 10.1016/S0168-1923(97)00011-7.

Schotanus P, Nieuwstadt FTM, De Bruin HAR. 1983. Temperature measurement with a sonic anemometer and its application to heat and moisture fluxes. Bound-Lay. Meteor. 26, 81-93, doi: 10.1007/BF00164332.

Shen J, Chen D, Bai M, Sun J, Coates T, Lam SK, Li Y. 2016. Ammonia deposition in the neighbourhood of an intensive cattle feedlot in Victoria, Australia. Sci. Reports 6, 32793, doi: 10.1038/srep32793.

Shonkwiler KB, Ham JM. 2017. Ammonia emissions from a beef feedlot: Comparison of inverse modeling techniques using long-path and point measurements of fenceline NH3. Agric. Forest Meteor. (in press) doi: 10.1016/j.agrformet.2017.10.031.

Sintermann J, Dietrich K, Häni C, Bell M, Jocher M, Neftel A. 2016. A miniDOAS instrument optimized for ammonia field measurements. Atmos. Meas. Tech. 9, 2721-2734, doi: 10.5194/amt-9-2721-2016.

Smith EA, Hsy AY, Crosson WI, Field RT, Fritschen LJ, Gurney RJ, Kanemasu ET, Kustas WP, Nie D, Shuttleworth WJ, Stewart JB, Verma SB, Weaver HL, Wesely ML. 1992. Area-averaged surface fluxes and their time-space variability over the FIFE experimental domain. J. Geophys. Res. 97 (D17), 18,599–18,622, doi: 10.1029/91JD03060.

Soltani M, Mauder M, Laux P, Kuntsmann H. 2017. Turbulent flux variability and energy balance closure in the TERENO prealpine observatory: a hydrometeorological data analysis. Theoret. Appl. Climatol. doi: 10.1007/s00704-017-2235-1.

Staebler RM, McGinn SM, Crenna BP, Flesch TK, Hayden KL, Li S-M. 2009. Three-dimensional characterization of the ammonia plume from a beef cattle feedlot. Atmos. Environ. 43, 6091-6099, doi: 10.1016/j.atmosenv.2009.08.045.

Stoy PC, Mauder M, Foken T, Marcolla B, Boegh E, Ibrom A, Arain MA, Arneth A, Aurela M, Bernhofer C, Cescatti A, Dellwik E, Duce P, Gianelle D, van Gorsel E, Kiely G, Knohl A, Margolis H, McCaughey H, Merbold L, Montagnani L, Papale D, Reichstein M, Saunders M, Serrano-Ortiz P, Sottocornola M, Spano D, Vaccari F, Varlagin A. 2013. A data-driven analysis of energy balance closure across FLUXNET research sites: the role of landscape scale heterogeneity. Agr. Forest Meteorol. 171-172, 137-152, doi: 10.1016/j.agrformet.2012.11.004.

Sun K, Tao L, Miller DJ, Zondlo MA, Shonkwiler KB, Nash C, Ham JM. 2015. Open-path eddy covariance measurements of ammonia fluxes from a beef cattle feedlot. Agric. Forest Meteor. 213, 193-202, doi: 10.1016/j.agrformet.2015.06.007.

Suttie JM, Reynolds SG, Batello C. 2005. Grasslands of the World. FAO Plant Production and Protection Series No. 34. Food and Agriculture Organization of the United Nations, Rome, Italy.

Suyker AE, Verma SB. 2001. Year-round observations of the net ecosystem exchange of carbon dioxide in a native tallgrass prairie. Global Change Biol. 7, 279–289, doi: 10.1046/j.1365-2486.2001.00407.x.

Taylor AM, Amiro BD, Tenuta M, Gervais M. 2017. Whole-farm greenhouse gas flux measurements for a beef cattle operation. Agr. Ecosyst. Environ., 239, 65-79, doi: 10.1016/j.agee.2017.01.011.

Thompson TM, Rodriguez MA, Barna MG, Gebhart KA, Hand JL, Day DE, Malm WC, Benedict KB, Collett Jr JL, Schichtel BA. 2015. Rocky Mountain National Park reduced nitrogen source apportionment. J. Geophys. Res. Atmos., 120, 4370-4384, doi: 10.1002/2014JD022675.

Thomson DJ. 1987. Criteria for the selection stochastic models of particle trajectories in turbulent flows. J. Fluid Mech. 180, 529-556.

Todd RW, Cole NA, Harper LA, Flesch TK, Baek BH. 2005. Ammonia and gaseous nitrogen emissions from a commercial beef cattle feedyard estimated using the flux gradient method and N:P ratio analysis. In: Proceedings of the State of the Science: Animal Manure and Waste Management, CD-ROM. San Antonio, TX. 5-7 Jan.

Todd RW, Cole NA, Nolan Clark R, Flesch TK, Harper LA, Baek BH. 2008. Ammonia emissions from a beef cattle feedyard on the southern High Plains. Atmos. Environ. 42, 6797-6805, doi: 10.1016/j.atmosenv.2008.05.013.

Todd RW, Cole NA, Parker DB, Rhoades M, Casey K. 2009. Effect of feeding distiller's grain on dietary crude protein and ammonia emissions from beef cattle feedyards. In: E. Jordan (Ed.), Proceedings, Texas Animal Manure Management Issues Conference, Round Rock, TX. 29-30 Sep. pp. 37-44.

Todd RW, Cole NA, Rhoades MB, Parker DB, Casey KD. 2011. Daily, monthly, seasonal, and annual ammonia emissions from Southern High Plains Cattle Feedyards. J. Environ. Qual. 40, 1090-1095, doi: 10.2134/jeq2010.0307.

Todd RW, Cole NA, Waldrip HM, Aiken RM. 2013. Arrhenius equation for modeling feedyard ammonia emissions using temperature and crude protein. J. Environ. Qual. 42, 666-671, doi: 10.2134/jeq2012.0371.

Turner DP, Ritts WD, Cohen WB, Gower ST, Running SW, Zhao M, Costa MH, Kirschbaum A, Ham J, Saleska S, Ahl DE. 2006. Evaluation of MODIS NPP and GPP products across multiple biomes. Remote Sens. Environ. 102, 282–292, doi: 10.1016/j.rse.2006.02.017.

Twine TE, Kustas WP, Norman JM, Cook DR, Houser PR, Meyers TP, Prueger JH, Starks PJ, Welely M. 2000. Correcting eddy-covariance flux underestimates over a grassland. Agric. Forest Meteor. 102, 279–300, doi: 10.1016/S0168-1923(00)00123-4.

USDA. 2017a. Cattle on feed. <http://usda.mannlib.cornell.edu/usda/current/CattOnFe/CattOnFe-11-17-2017.pdf> Retrieved: 12 Dec 2017.

USDA. 2017b. Milk cows and production by state and region (annual). <www.ers.usda.gov/webdocs/DataFiles/48685/milkcowsandprod_1_.xlsx?v=42866> Retrieved: 12 Dec 2017.

USEPA. 2004. National emission inventory ammonia emissions from animal husbandry, draft report. US Environmental Protection Agency, Washington, D.C. 30 Jan 2004.

USEPA. 2014. Draft other test method 33A: geospatial measurement of air pollution, remote emissions quantification – direct assessment (GMAP-REQ-DA). <https://www3.epa.gov/ttnemc01/prelim/otm33a.pdf> Retrieved: 10 Sep 2017.

USEPA. 2016. Agriculture. In: Inventory of U.S. greenhouse gas emissions and sinks: 1990-2014. <https://www3.epa.gov/climatechange/Downloads/ghgemissions/US-GHG-Inventory-2016-Chapter-5-Agriculture.pdf> Retrieved: 02 Aug 2016.

USGS. 2017. Land cover data viewer. <https://gis1.usgs.gov/csas/gap/viewer/land_cover/Map.aspx> Retrieved: 10 Mar 2017.

van Haarlem RP, Desjardins RL, Gao Z, Flesch TK, Li X. 2008. Methane and ammonia emissions from a beef feedlot in western Canada for a twelve-day period in the fall. Can. J. Anim. Sci. 88, 641-649, doi: 10.4141/CJAS08034.

Verma SB, Kim J, Clement RJ. 1992. Momentum, water vapor, and carbon dioxide exchange at a centrally located prairie site during FIFE. J. Geophys. Res. 97 (D17), 18,629–18,640, doi: 10.1029/91JD03045.

Vitousek PM, Aber J, Howarth RW, Likens GE, Matson PA, Schindler DW, Schlesinger WH, Tilman GD. 1997. Human alteration of the global nitrogen cycle: causes and consequences. Issues Ecol. 1, 1-16, doi: 10.1890/1051-0761(1997)007[0737:HAOTGN]2.0.CO;2.

Webb E, Pearman G, Leuning R. 1980. Correction of flux measurements for density effects due to heat and water vapour transfer. Quart. J. Roy. Meteor. Soc. 106, 85-100, doi: 10.1002/qj.49710644707.

Wilczak JM, Oncley SP, Stage SA. 2001. Sonic anemometer tilt correction algorithms. Bound-Lay. Meteor. 99, 127–150, doi: 10.1023/A:1018966204465.

Wilson JD, Flesch TK, Crenna BP. 2013. Estimating surface-air gas fluxes by inverse dispersion using a backward Lagrangian stochastic trajectory model. In: Lin J, Brunner D, Gerbig C, Stohl A, Luhar A, Webley P (Eds.), Lagrangian Modeling of the Atmosphere. pp. 149-162, doi: 10.1029/2012GM001269.

Wilson K, Goldstein A, Falge E, Aubinet M, Baldocchi D, Berbigier P, Bernhofer C, Ceulemans R, Dolmanh H, Field C, Grelle A, Ibrom A, Law BE, Kowalski A, Meyers T, Moncrieff J, Monsonn R, Oechel W, Tenhunen J, Valentini R, Verma S. 2002. Energy balance closure at FLUXNET sites. Agric. Forest Meteor. 113, 223–243, doi: 10.1016/S0168-1923(02)00109-0.

Wohlfahrt G, Hammerle A, Georg N, Katharina S, Enrico T, Peng Z. 2016. On the energy balance closure and net radiation in complex terrain. Agric. Forest Meteor. 226-227, 37-49, doi: 10.1016/j.agrformet.2016.05.012.

Wohlfahrt G, Haslwanter A, Hörtnagl L, Jasoni RL, Fenstermaker LF, Arnone III JA, Hammerle A. 2009. On the consequences of the energy imbalance for calculating surface conductance to water vapour. Agric. Forest Meteor. 149, 1556-1559, doi: 10.1016/j.agrformet.2009.03.015.

Wohlfahrt G, Irschick C, Thalinger B, Hörtnagl L, Obojes N, Hammerle A. 2010. Insights from independent evapotranspiration estimates for closing the energy balance: a grassland case study. Vadose Zone J. 9, 1025-1033, doi: 10.2136/vzj2009.0158.

Wohlfahrt G, Widmoser P. 2013. Can an energy balance model provide additional constraints on how to close the energy imbalance? Agric. Forest Meteor. 169, 85-91, doi: 10.1016/j.agrformet.2012.10.006.

Wolfe AP, Baron JS, Cornett RJ. 2001. Anthropogenic nitrogen deposition induces rapid ecological changes in alpine lakes of the Colorado Front Range (USA). J. Paleolimnol. 25, 1-7, doi: 10.1023/A:1008129509322.

Wolfe AP, Van Gorp AC, Baron JS. 2003. Recent ecological and biogeochemical changes in alpine lakes of Rocky Mountain National Park (Colorado, USA): a response to anthropogenic nitrogen deposition. Geobiol. 1, 153-168, doi: 10.1046/j.1472-4669.2003.00012.x.

WRCC. 2011. Fort Morgan, Colorado NCDC 1981-2010 monthly normals. Western Regional Climate Center. <www.wrcc.dri.edu/cgi-bin/cliMAIN.pl?co3038> Retrieved: 27 Dec 2016.

Yang Y, Liao W, Wang X, Liu C, Xie Q, Gao Z, Ma W, He Y. 2016. Quantification of ammonia emissions from dairy and beef feedlots in the Jing-Jin-Ji district, China. Ag. Ecosys. Environ. 232, 29-37, doi: 10.1016/j.agee.2016.07.016.

Zhengquan L, Guirui Y, Xuefa W, Leiming Z, Chuanyou R, Yuling F. 2005. Energy balance closure at ChinaFLUX sites. Sci. China Earth Sci. 48, 51-62, doi: 10.1360/05zd0005.